The Reaction Kinetics of Neutral Free Radicals and Radical Ions Studied by Laser Flash Photolysis

Robert A. Friedline

Dissertation submitted to the Faculty of the
Virginia Polytechnic Institute and State University
in partial fulfillment of the requirements for the degree of

Doctor of Philosophy
in
Chemistry

James M. Tanko, Chair
Dr. Alan Esker
Dr. Timothy Long
Dr. James Mahaney
Dr. J. Paige Stevenson

April 21st, 2004
Blacksburg, Virginia

Keywords: Free radical, alkoxy, *t*-butoxyl, radical anion, laser flash photolysis

Copyright 2004, Robert A. Friedline

The Reaction Kinetics of Neutral Free Radicals and Radical Ions Studied by Laser Flash Photolysis

by

Robert A. Friedline

James M. Tanko, Chair
Chemistry

(Abstract)

t-Butoxyl radical has been used as a chemical model for hydrogen abstractions in many enzymatic and biological systems. However, the question has arisen as to how well this reactive intermediate mimics these systems. In addressing this concern, absolute rate constants and Arrhenius parameters for hydrogen abstraction by *t*-butoxyl radical were measured for a broad class of substrates including amines, hydrocarbons, and alcohols using laser flash photolysis. Initially, no obvious reactivity relationship between rate constant and substrate structure was observed for these homolytic reactions. However, by closely examining the Arrhenius parameters for hydrogen abstraction, a pattern was revealed. For substrates with C-H bond dissociation energy (BDE) > 92 kcal/mole, activation energy increases with increasing BDE (as expected). However, for substrates with a lower BDE, the activation energy levels out at approximately 2 kcal/mole, essentially independent of structure. Viscosity studies with various solvents were conducted, ruling out the possibility of diffusion-controlled reactions. Entropy rather than enthalpy appears to be the dominating factor at 25 °C, contributing to the free energy barrier for these reactions.

Laser flash photolysis was also used to study radical anions. Using an indirect photoexcitation method, the properties of radical anions, generated from aryl ketones, were investigated. These radical anions, such as *t*-butyl phenyl ketone and cyclopropyl phenyl ketone, measured to have decay rate constants of 1.0×10^6 s^{-1}, although they are known to be persistent when studied electrochemically. They also had measured activation energies around 6.0 kcal/mole and log A values close to 9.5. By extending the molecules's conjugation, the decay rate constants increased to greater than 10^7 s^{-1}, decreased their activation energy by half, and lowered the log A values to 8.0. This trend was observed in aryl ketones such as *trans*-1-benzoyl-3-phenyl cyclopropane. It is believed that the generation of a benzyl radical during the

decay that facilitates the enhancement of the unimolecular decays. These unimolecular decays were also observed with the previously studied hypersensitive SET probes, 5,7-di-*tert*-butylspiro[2.5]octa-4,7-dien-6-one and 1,1,-dimethyl-5,7-di-*tert*-butylspiro[2.5]octa-4,7-dien-6-one. The decay rate constants for these radical anions were measured to be greater than 10^8 s^{-1}, driven by the formation of an aromatic ring.

ACKNOWLEDGEMENTS

I would like to take a moment to offer an enormous thank you to Dr. James M. Tanko for his patience, leadership, friendship, advice, and understanding on all aspects of life throughout my graduate career. You are the only man I know who would have allowed me to obtain every one of my goals while I was here at Virginia Tech and complete my degree. I am also grateful to each one of my committee members for the donation of their precious time and efforts for the thorough reviews of my work and progress. I would also like to express my deepest appreciation to all the faculty, staff and students (past and present) in the Chemistry Department for helping me make Virginia Tech my home for the last five years.

A huge thank you must be sent out to the National Science Foundation for their funding of my projects, as well as the chemistry department at Virginia Tech for their financial support, as a TA and a recipient of an Alan Clifford Fellowship.

Finally, I cannot put an ending on my graduate career without thanking my family and friends who have been beside me through everything in my career. To my parents, thank you for always supporting me in every decision I have made in the first 26 years of my life. To Shawn Thomas, thank you for always helping me with all the changes in my life and picking me up when I make one of my traditional mistakes; and finally, to Michael Vadala, my best friend and other half in this pursuit of chemical education and enlightenment. May your journey through academics come to a closure soon and a wonderful career be opened for you. Thank you for keeping me sane and on track for the last four years.

TABLE OF CONTENTS

Page

LIST OF FIGURES

LIST OF TABLES

CHAPTER 1. HISTORICAL OVERVIEW OF *t*-BUTOXYL RADICAL

1.1 INTRODUCTION

In organic chemistry, free radicals are among the most reactive intermediates formed. They have become commonplace in discussions about many chemical reactions due to their involvement in halogenations and many polymerizations. In addition, a large number of the reactions in chemical and biological systems such as oxidations, reductions, compound degradation, and even the aging process, are believed to involve some sort of free radical process. The formation of aerosols and ground-level ozone in the atmosphere have been reported in recent years to be associated with free radical reactions in the atmosphere with compounds such as terpenes.[1] These compounds and other volatile organic compounds have been investigated for their roles in radical generation causing environmental problems, such as the conversion of NO into NO_2. Because of the reactivity of these intermediates, many carbon-centered radicals have been examined with regard to their structure and reactivity. Heteroatom radicals, such as oxygen or nitrogen-centered radicals, have been found to be extremely reactive and are often the precursor to carbon-centered radicals (i.e., reaction of a heteroatom-centered radical with an organic compound may lead to a carbon-centered radical). In addition, nitroxide radicals have become a significant influence in polymerization reactions,[2] in the study of antioxidant reactions,[3] and coupling reactions with other radicals.[4] It is believed that the chemistry involved with many of these heteroatom-centered radicals is well understood, allowing them to be used for more in-depth biological and even enzymatic studies of reactions where radical intermediates are believed to be formed.

For example, *tert*-butoxyl radical, $(CH_3)_3C\text{-}O\bullet$, is used as a chemical model for enzymatic oxidations in biological systems, like those catalyzed by cytochrome P-450.[5-7] It has also been used to model the chemistry for hydrogen abstractions by other enzymes, in which the active site is believed to be a radical, such as methane monooxygenase.[8] Because of its use as an

enzymatic oxidation model, *t*-butoxyl radical was used to investigate the mechanism involved in the oxidation of 1-methyl-4-phenyl-1,2,3,6-tetrahydropyridine (MPTP), a tertiary amine and neurotoxin found to be a direct cause of Parkinson disease-type symptoms in humans. With increased use of this radical, questions regarding the reactivity of this radical have surfaced. Earlier examinations of the chemistry of *t*-BuO• have involved product studies[9,10] and laser flash photolysis.[11,12]

1.2 *t*-BUTOXYL RADICAL

1.2.1 *Production*

Early studies of *t*-butoxyl radical generated the radical from hypohalite compounds, such as *t*-butyl hypochlorite.[13-16] The generation of $(CH_3)_3C$-O• (and sometimes Cl•) can be induced through photochemical or thermal initiation (Scheme 1). In-In represents a thermal initiator, such as azobisisobutyronitrile (AIBN). These radicals then react with other substrates in the solution through propagation reactions, as depicted in Scheme 2 for the reaction of a hydrocarbon.

Scheme 1

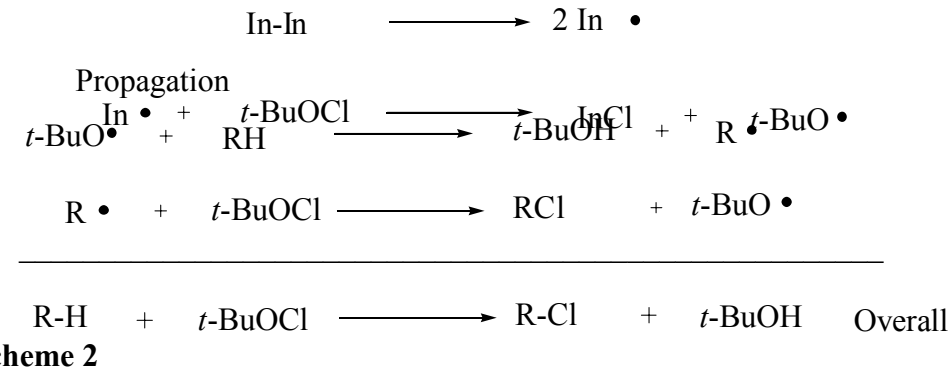

Scheme 2

This radical can also be produced photochemically. Irradiation of di-*tert*-butyl peroxide with UV light causes its excitation and decomposition into *t*-butoxyl radicals (Eq.1).[17]

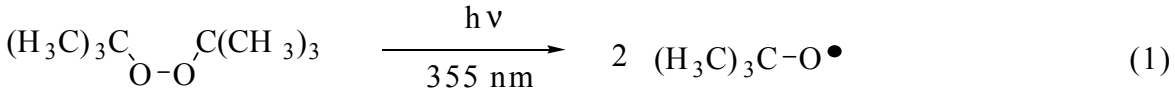

(1)

1.2.2 *Decomposition*

Once produced, the *t*-butoxyl radical decomposes in solution through a first-order process, generating methyl radical and acetone through β-scission (Eq. 2).[18,19]

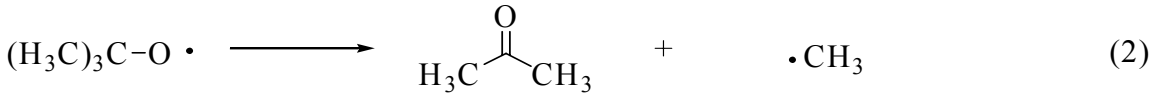

(2)

These methyl radicals, when produced in the gas phase, can terminate in a combination reaction, creating ethane (Eq. 3).

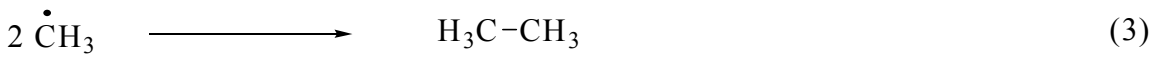

(3)

Different studies of the decomposition of *t*-butoxyl radical found this β-scission reaction to have extremely large Arrhenius parameters.[20,21] This decay process was observed in different solvents by Tsentalovich *et al.* The activation energy for this reaction in benzene was measured to be 12.4 ± 1.0 kcal/mol with a corresponding log A value of 13.4. With such high requirements, the studies suggest that the reaction occurs through a unimolecular process in the rate-determining step. It had been assumed that the A factors, activation energies, and the rate constants for decomposition were approximately equal in solution and in gas phase.[18,19] However, it was observed that the β-scission process of *t*-butoxyl radical is actually dependent on the solvent.[21-23] As seen in Table 1.1, the activation energy for β-scission actually varies slightly with solvent.

Table 1.1. Absolute rate constants and activation energies for the β-scission of the *t*-butoxyl radical at 298 K[23]

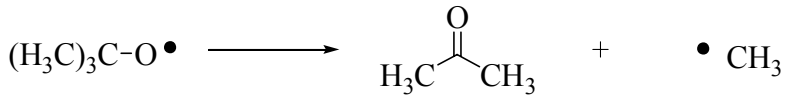

Solvent	T, K	k_β s^{-1}	E_a, kcal/mol
1,1,2-Trichloro-1,2,2-trifluoroethane	278-312	8050	12.6
Di-*tert*-butyl peroxide (neat)	283-323	12000	12.0
C_6H_6	284-318	20300	11.6
C_6H_5F	263-308	21400	11.3

These parameters for β-scission in solution are significantly lower than the rate constants and activation energies measured in the gas phase.[24] This phenomenon can be explained through the solvation of the transition state associated with the β-scission reaction. The solvation of the β-scission transition state has been argued to be more sterically feasible than solvating a hydrogen atom abstraction transition state,[10] due to the reaction being a bimolecular process. Additionally, evidence showed that the transition state for the β-scission to acetone and methyl radical is more polar than the *t*-butoxyl radical itself (shown in Eq. 4).

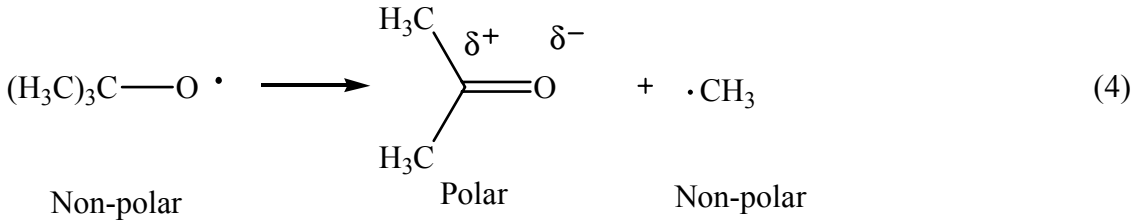

Non-polar Polar Non-polar (4)

Consequently, there is an increase in the rate constant for β-scission and a decrease in activation energy when conducted in more polar solvents. Using the solvents listed in Table 1 and using cyclohexane as a substrate, it was determined that there was no solvent dependence on the rate of hydrogen atom abstraction by *t*-butoxyl radical.[23]

1.2.3. *Influences on reactivity towards hydrogen atom abstraction*

Looking beyond hydrocarbons, changes in selectivity and reactivity of *t*-butoxyl radical towards hydrogen atom abstraction from other classes of substrates have been observed. When factors such as substituents and intermolecular forces are examined, the medium in which the reaction takes place becomes a major contributor towards the magnitude of the rate constant.[25] Hydrogen atom abstractions between oxygen atoms, such as H-atom abstraction from phenol by *t*-butoxyl radical, normally show rate constants that appear close to the diffusion-controlled limit ($\cong 1 \times 10^{10}$ M^{-1} s^{-1}).[26] However, using acetic acid as the solvent and hydrogen donor, intermolecular interactions, such as hydrogen bonding between the solvent and substrates, have been shown to decrease the rate constant of hydrogen atom abstraction, making the β-scission pathway more competitive. Additional evidence for solvent influence over radical reactivity was collected by allowing *t*-butoxyl radical to react with substituted thiols as depicted in Eq. 5,

$$(H_3C)_3C{-}O^{\cdot} + YC_6H_4SH \longrightarrow (H_3C)_3C{-}OH + YC_6H_4S^{\cdot} \qquad (5)$$

where Y equals *p*-OCH_3, *p*-CH_3, *p*-F, H, *p*-Cl, and *p*-Br.[25] With rate constants for these compounds and the Hammett equation, it was shown that the data correlated best to σ^+ with a $\rho^+ = -0.30$, suggesting a buildup of a positive charge in the transition state. The observed correlation suggests a polar transition state that is stabilized by the electron donating substituents. This correlation was also found to hold with derivatives of phenol (YC_6H_4OH), consistent with a

reactant-like, asymmetrical transition state (Eq. 6). Kinetic primary isotope effect studies for these compounds (Table 1.2) also agree with the notion of an non-symmetrical transition state.

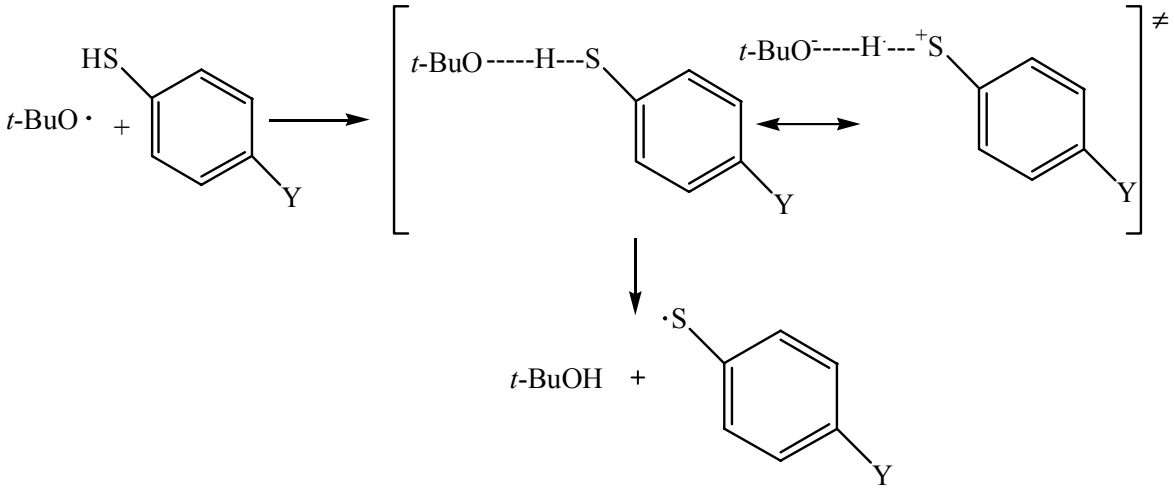

(6)

Table 1.2. Primary deuterium kinetic isotope effects in the hydrogen abstraction at 130 °C[25]

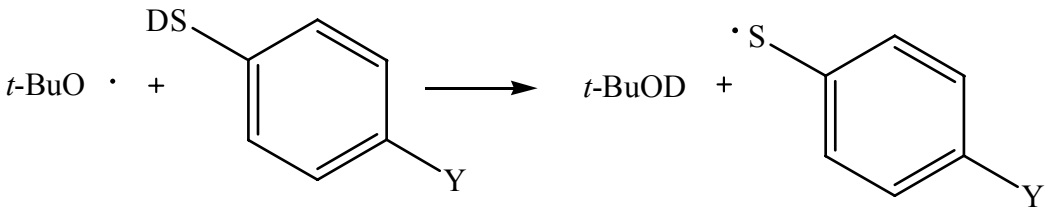

Substrates	k_H/k_D		
	CCl_4	C_6H_6	CH_3CN
C_6H_5O-H vs. C_6H_5O-D	1.33 ± 0.02	1.40 ± 0.19	2.79 ± 0.03
C_6H_5S-H vs. C_6H_5S-D	1.02 ± 0.04	1.05 ± 0.05	1.07 ± 0.03
$C_6H_5CH_3$ vs. $C_6H_5CD_3$	6.76 ± 0.06	4.40 ± 0.20	5.38 ± 0.20

Other compounds, such as benzaldehyde, N-benzylidene aniline, and anisole, were found to show the same effects and correlations; all produced negative ρ^+ values.[27] When polar and solvent effects were examined for substituted toluenes, once again, the best correlation was found with σ^+ parameters.[28] The data shown in Table 1.3 illustrates the better correlation to σ^+. In this study, di-*tert*-butyl peroxyoxalate was used as the radical source to produce *t*-butoxyl radical.

Table 1.3. Reaction constants (ρ values) and correlation factors (r) for the reaction of substituted toluenes with *t*-butoxyl radical[28]

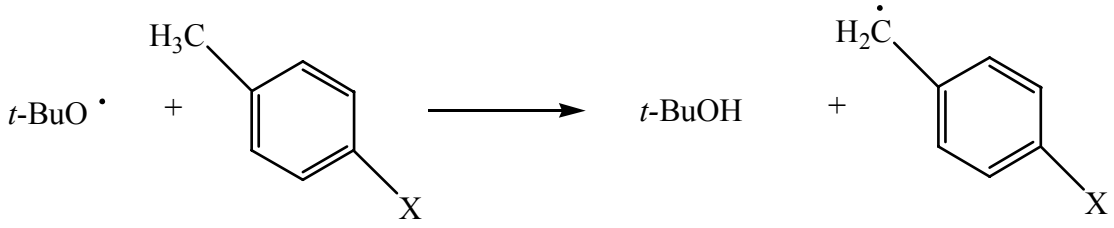

Solvent	With σ^+		With σ	
	ρ	r	ρ	r
Freon-113	-0.35	0.989	-0.40	0.977
Chlorobenzene	-0.32	0.973	-0.36	0.953
Acetonitrile	-0.39	0.994	-0.43	0.955

With a ρ^+ value equaling -1.81for the abstraction from the phenolic O-H bond, the small k_H/k_D value for CCl_4 provides evidence for an early transition state as mentioned above.[25] The increase in k_H/k_D in CH_3CN may result from the increased solvation of the transition state by the more polar solvent, allowing for easier bond breaking and making, with less hydrogen bonding.

1.3. TECHNIQUES USED TO OBSERVE *t*-BUTOXYL RADICAL REACTIONS

1.3.1. *Diphenylmethanol*

Although solvent and polarity effects on the reactivity of *t*-butoxyl radical have been examined to an extent, an in-depth study of absolute rate constants for hydrogen atom abstraction by the radical with different substrates has not been completed. When produced in solution or gas phase, the *t*-butoxyl radical is nearly invisible to UV/visible detection. The spectrum for *t*-butoxyl radical has been recorded to give a very weak signal below 300 nm, with an absorption maximum at approximately 277 nm.[21] It is more difficult to measure the appearance of this intermediate due to interference from other absorbing substrates in solution. In addition to this, many of the radical products generated from hydrogen atom abstraction are invisible to this detection system. However, other techniques have been used to measure rate constants for *t*-butoxyl radical. In some studies, diphenylmethanol has been used as a probe for the reaction.[29] When diphenylmethanol undergoes the reaction shown in Scheme 3, the resulting ketyl radical

produces a strong absorption maximum at 535 nm. The non-radical products form due to decomposition or other reactions that yield undetected products.

Scheme 3

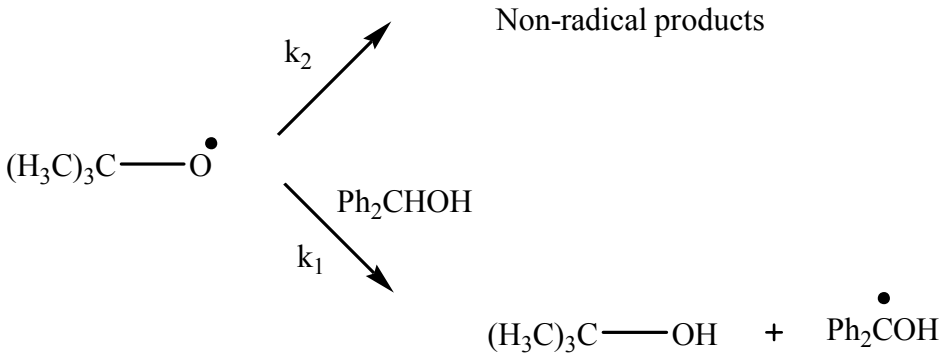

It is assumed that the *t*-butoxyl radical will decay in a normal pseudo-first order decay process. This assumption allows the rate of reaction to be determined by Eq. 7

$$k_{obs} = k_2 + k_1[Ph_2CHOH] \quad (7)$$

where k_2 is the first order (or pseudo-first order) rate constant for the decomposition of the *t*-butoxyl radical and k_1 (measured by LFP) is the rate constant for hydrogen atom abstraction from diphenylmethanol. By plotting k_{obs} vs. $[Ph_2CHOH]$, the rate constant for hydrogen atom abstraction was determined to be 6.9×10^6 M^{-1} s^{-1} at 21 ± 2 °C.

1.3.2. *Adding different substrates to the reaction mixture*

Once this rate constant was experimentally determined, the concentration of diphenylmethanol was held constant in the experiment, allowing for the addition of new substrates and adding a new reaction pathway (Scheme 4).

Scheme 4

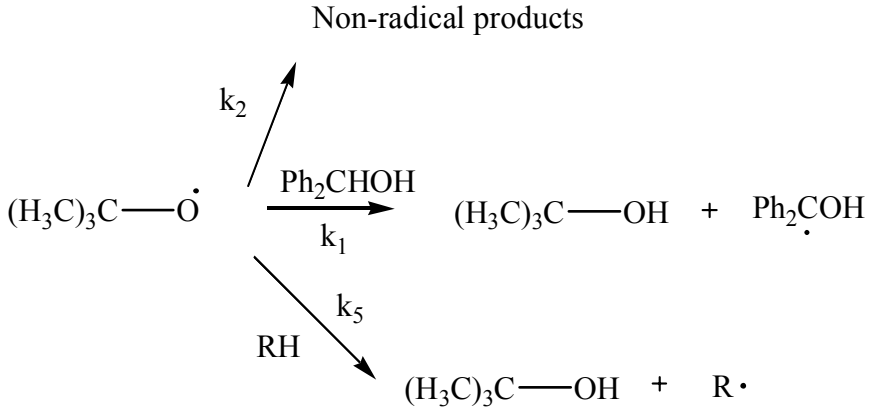

At constant [Ph_2CHOH], the rate law for the reaction with *t*-butoxyl radical is that shown in Eq. 8,

$$k_{obs} = (k_2 + k_1[Ph_2CHOH]) + k_5[RH] \quad (8)$$

which allows for plotting k_{obs} vs. [RH] to find the rate constant for hydrogen atom abstraction (k_5). The slope of this plot is equal to k_5. The appearance of the diphenylmethyl ketyl radical in the system is measured to find k_{obs}.

1.4. LITERATURE REVIEW

1.4.1. *Hydrogen atom abstractions*

With the number of absolute rate constants of hydrogen atom abstraction by *t*-butoxyl radical that have been recorded, only a handful of Arrhenius parameters have been measured. The rate constants, activation energies, and log A values for various organic compounds, found in Table 1.4, were determined in solution using flash photolysis electron spin resonance (FPESR).[30]

Table 1.4. Rate constants and Arrhenius parameters for hydrogen abstraction by *t*-butoxyl radical (per active hydrogen) at 293 K[30]

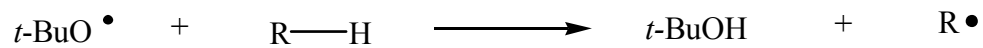

Substrate	k_1 ($M^{-1} s^{-1}$)	Log A	E_a (kcal/mol)	BDE (kcal/mol)[31]
Cyclopentane	3.4×10^4	9.1	6.1	96.1 ± .6
Anisole	2.4×10^4	8.8	5.9	
Methyl tert-butyl ether	8.1×10^4	8.8	5.2	95.8[a]
Methanol	4.3×10^4	8.6	5.3	95.7 ± .4

[a]Since this compound's BDE is unavailable, the BDE for the primary hydrogen on dimethyl ether can be compared.

The data above compares the reactivity of *t*-butoxyl radical towards primary hydrogen (i.e., breaking of the C-H bond of the methyl groups) in different structural environments. The exception in the table is cyclopentane, which only has secondary carbon-hydrogen bonds. Including cyclopentane in the study, all of the reactions appear to have similar rate constants, activation energies, and log A values. Only the methyl group's primary hydrogens was taken into account in the rate constant for methyl *tert*-butyl ether. These results coincided with the innate reasoning that the measured rate constant and Arrhenius parameters for hydrogen atom abstraction will be controlled by the bond dissociation energy from breaking the C-H bond.

The rate constant for hydrogen atom abstraction from cyclopentane and other compounds with secondary and tertiary hydrogen were also studied. However, this study was performed in the gas phase. These abstraction rate constants were found to be faster than those previously observed in solution.[32] When the methyl-substituted cyclohexanes were examined, it was found that primary hydrogen exhibited little or no reactivity. The *t*-butoxyl radical reacts preferentially with secondary and tertiary hydrogen because of lower activation energies and larger log A values (Table 1.5).

Table 1.5. Arrhenius parameters for abstraction of primary, secondary, and tertiary H atoms (per atom) at 410 K[32,33]

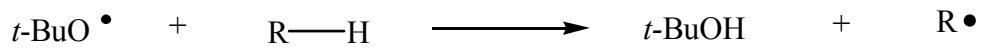

C-H Bond	Log A	E_a (kcal/mol)	BDE (kcal/mol)[34]	k_H (M^{-1} s^{-1})[a]
Primary[a]	9.25 ± 0.18	7.72 ± 0.3	98	3.72×10^3
Secondary	9.23 ± 0.12	6.05 ± 0.3	95	6.01×10^4
	9.44 ± 0.03[b]	6.43 ± 0.1[b]		
	9.56 ± 0.45[b]	6.88 ± 0.9[b]		
Tertiary	9.90 ± 0.15	5.29 ± 0.2	91	1.02×10^6
	9.97 ± 0.10[b]	5.48 ± 0.1[b]		

[a]Rate constants calculated from Arrhenius parameters at 25 °C [b]Values calculated from data found in Reference 25.

For the creation of carbon-centered radicals, the rate constant correlates nicely with the stability of the resulting radical (3°>2°>1°).

1.4.2. *Reaction with alkenes: Hydrogen atom abstraction or addition*

Taking the stability of the resulting radical further than only a secondary or tertiary carbon, simple alkenes were investigated for their ability to react with *t*-butoxyl radical. A competitive reaction to hydrogen atom abstraction from these compounds is the addition of the radical to the double bond (Scheme 5).[12]

Scheme 5

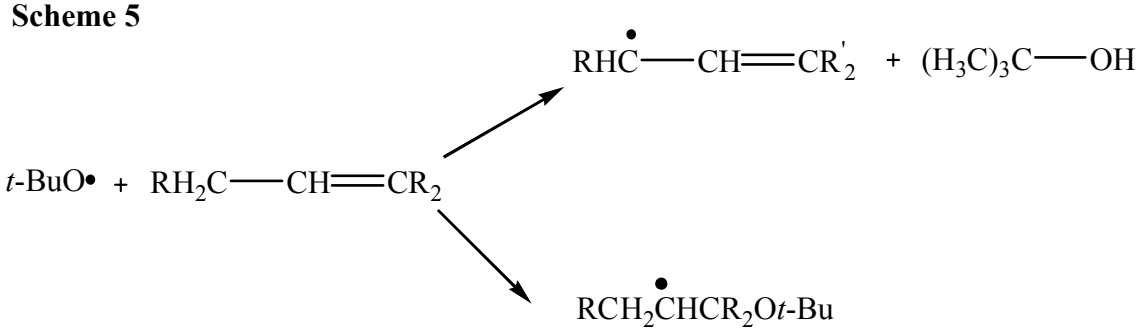

The simplest alkene with abstractable hydrogen atoms is propene. Electron spin resonance (EPR) showed that *t*-butoxyl radical only abstracts hydrogen to produce the allyl radical.[35] No products from the addition to the double bond were observed. In cyclic systems, the selectivity of the *t*-butoxyl radical changed slightly. For cyclopentene, most of the reaction went through the hydrogen atom abstraction pathway. However, with cyclopentadiene, over half of the reaction involves addition. The bicyclic compounds, norbornene and norbornadiene, underwent the addition reaction only.[12] In these latter compounds, stereoelectronic and geometrical factors became important issues. Although the hydrogen in the allylic positions could be abstracted, in principle, this radical derives little or no stability from the double bond since the orbitals are orthogonal (Scheme 6).

Scheme 6

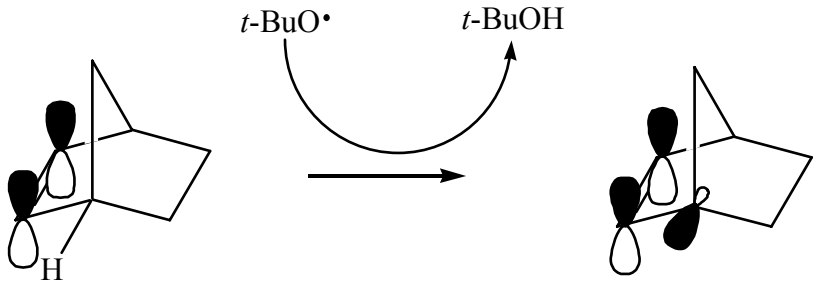

It has also been observed for different alkenes that hydrogen atom abstraction by *t*-butoxyl radical follows the sequence of primary < secondary < tertiary.[9,36] This reactivity trend illustrates again that the structure of the resulting radical determines the reaction pathway, overshadowing the stability of the double bond.

1.4.3. Reactions with aromatic compounds

Taking the examination of *t*-butoxyl radical further, the rate constants for hydrogen atom abstraction from substituted aromatic compounds were estimated. As mentioned before, the strength of the C-H bond being broken in the abstraction should play a major role in the absolute rate constant. Stabilization of the resulting radical weakens the C-H bond, causing an increase in the rate constant. Measuring the hydrogen atom abstraction rate constants for a set of alkyl-substituted aromatic compounds tested this reasoning.[37] Within each aromatic compound examined (i.e., naphthalene, anthracene, etc.), the rate constants of hydrogen atom abstraction from various alkyl groups in different positions on the rings were measured and shown in Table 1.6.

Table 1.6. Rate constants in benzene at 383 K[37]

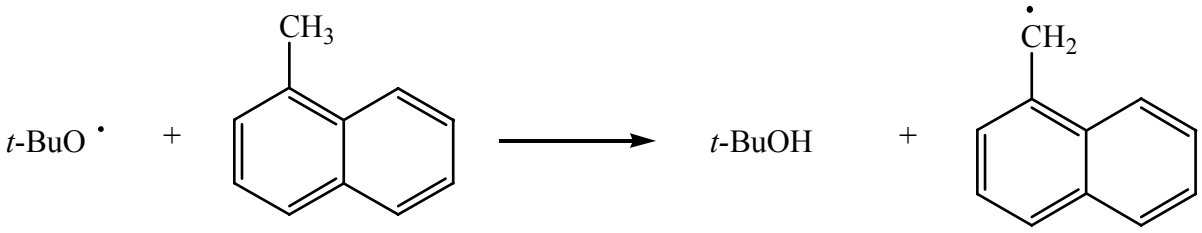

Compound	k_{RH} ($M^{-1} s^{-1}$)	($k_{RH}/k_{Toluene}$) per H
toluene	1.24×10^6	---
1-methylnaphthalene	2.7×10^6	2.2
2-methylnaphthalene	2.8×10^6	2.3
1-methylanthracene	8.1×10^6	6.6
2-methylanthracene	7.7×10^6	6.2

The values indicate that only the structure of the compound (i.e., the number of bonded aromatic rings) determined the stabilization of the radical, not the position of the allylic substituent on the ring. Though the methyl-substituent was moved from C-1 to C-2, the rate constant for hydrogen atom abstraction by *t*-butoxyl radical was not affected. This phenomenon has been seen in other free radical reactions with the same compounds.[38] It has been postulated that the reason for the similar reactivity and little selectivity of *t*-butoxyl radical towards these compounds is related to the large exothermicity of the reaction.[37] The BDE of *t*-BuOH is 105 kcal/mol. For toluene and 1-methylnaphthalene, BDE's are 88 and 85 kcal/mol, respectively.[39] Thus, because *t*-BuO• is highly reactive towards the substrate's C-H bonds, it exhibits little selectivity. Although these BDE's are highly exothermic, the reactions of the substrates with *t*-butoxyl radical are not diffusion-controlled, contrary to standard assumptions.

Di-substituted aromatic compounds, such as 1,2-dimethyl-naphthalene, showed similar reactivity within these series of compounds toward *t*-butoxyl radical, regardless of substituent placement. In addition, other substituted aromatics, such as ethyl or carboxylaldehyde derivatives, showed an even weaker dependence on the stabilization of the resulting free radical

than the compounds mentioned above, resulting once again from the reaction's exothermic nature.

Due to the extremely high estimated errors (± 15%) in Lissi's study of these aromatic compounds, a more expanded study of these compounds was conducted. Mahiou and Gleicher measured relative rates for the hydrogen atom abstraction from 13 different arylmethanes and heteroarylmethanes.[40] A representative sample of these compounds and their relative reaction rates can be found in Table 1.7.

Table 1.7. Relative reaction rates for the hydrogen atom abstraction by *t*-butoxyl radical from arylmethanes and heteroarylmethanes at 70 °C.[37]

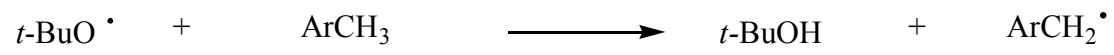

Substrate	Relative Reaction Rate
1-methylnaphthalene	1.654 ± 0.053
2-methylnaphthalene	1.210 ± 0.008
7-methylquinoline	0.835 ± 0.007
3-methylpyridine	0.635 ± 0.011
2-methylquinoline	0.290 ± 0.003
4-methylpyridine	0.228 ± 0.003

This study was conducted at a much lower temperature than the previous one and actually showed a difference, by a factor of 7, in the relative reaction rates for the different isomers. In addition to measuring the relative rates, they also employed HMO and SCF-PPP theory calculations to help in determining the charge on the intermediate for this reaction. These calculations allowed them to illustrate the charge development believed to occur in the transition state for these hydrogen atom abstractions. Correlations with these calculations could only be made towards the appearance of a carbocation intermediate. The difference in the relative rates for these compounds was believed to be controlled by the stability of this charge development in the transition state.

1.4.4 *Reactions with alcohols, aldehydes, and ketones*

Studies of hydrogen atom abstraction by *t*-butoxyl radical from hydrocarbons have been expanded to include reactions with alcohols, aldehydes, and ketones. On the basis of kinetic isotope effects, the rate-determining step for the reaction between an alcohol and the *t*-butoxyl radical has been suggested to be the actual hydrogen atom transfer between the two oxygen atoms.[41] Additionally, the activation energy for the H-atom abstraction have been found to be quite small, which agrees with the reaction being a hydrogen atom transfer between two of the same atoms. The breakage and creation of the two O-H bonds releases little energy. Furthermore, the organizational energy barriers are negligible. This hydrogen atom transfer was found to have a rate constant at least as great as the hydrogen atom abstraction from a primary hydrocarbon. Kinetic primary isotope experiments, conducted on formaldehyde, acetylaldehyde, and acetone, generated information on *t*-butoxyl radical's reactivity towards creating different carbon-centered radicals.[42] The aldehydes were found to have lower activation energies than ketones, due to the stability of the radical on the carbonyl carbon, instead of the carbon α to the carbonyl (Scheme 7). The second resonance structure drawn for the acetone radical species is insignificant in the stability of the radical.

Scheme 7

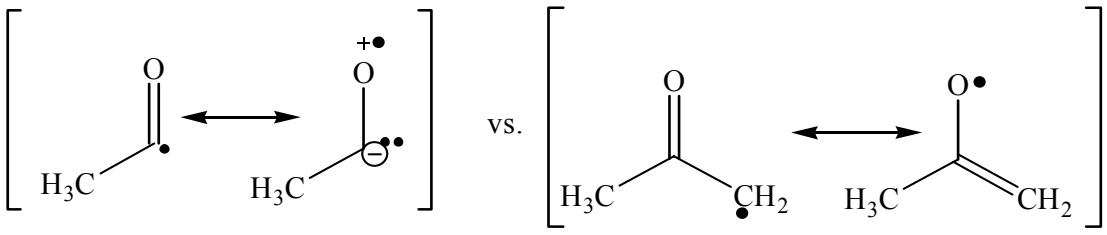

The *t*-butoxyl radical's reactivity towards ketones was examined further when the autooxidation of aliphatic esters was examined.[43] In this study, selectivity by alkoxyl radicals, such as *t*-butoxyl, towards the α-alykl, α-acyl, or β-acyl hydrogen (respectively) found within

these substrates was investigated. An example of this reaction is found in Eq. 9, illustrating the three reactive sites on these molecules.

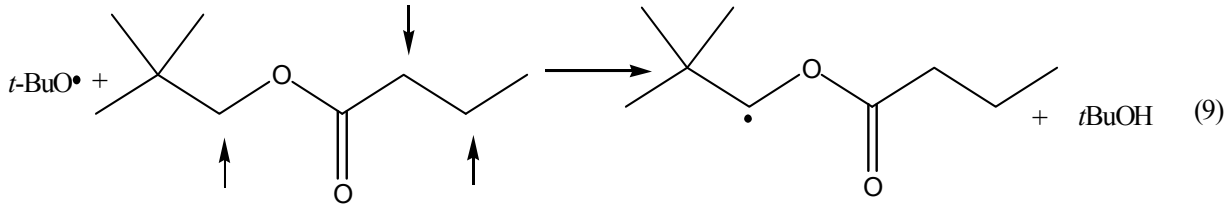

(9)

By comparing the rate constants measured for the hydrogen atom abstraction by *t*-butoxyl from structurally different esters, it was determined that the selectivity followed α-alkyl > β-acyl > α-acyl positions. These results could be explained due to polar arguments once again, due to the electrophilic nature of the alkoxyl radicals. The α-alkyl hydrogen is a more electron rich site in the esters, rather than the electron-deficient α-acyl due to the carbonyl.

1.4.5. *Reactivity of t-butoxyl radical vs. carbonyl triplets*

In early reaction studies of *t*-butoxyl radicals with compounds such as phenols and different alkenes, it was found that the *t*-butoxyl radical had similar reactivity properties compared to the benzophenone triplet (Eq. 10) and other π^* carbonyl triplets.[44]

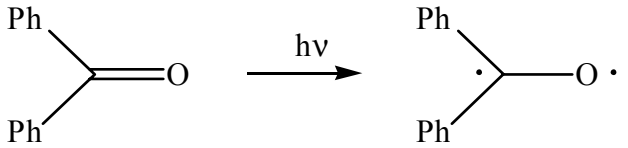

(10)

In the case of the benzophenone triplet, quenching of the excited state has been found to occur through a hydrogen atom abstraction process (Eq. 11).

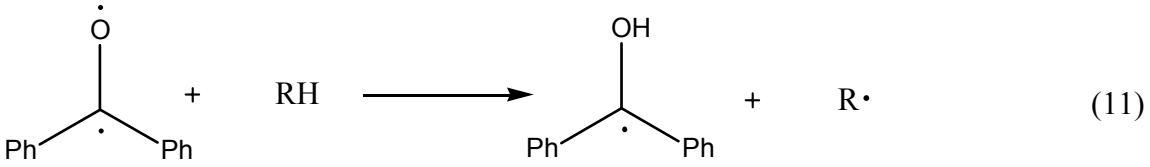

(11)

The rate constants for this hydrogen atom abstraction from different phenols by the benzophenone triplet appear to be very similar to *t*-butoxyl radical, although the *t*-butoxyl radical reaction tends to be controlled more by the bond dissociation energy of RH. This feature is not the case with the benzophenone triplet reaction. Analogous rate constants have been documented for reactions of this intermediate with allylic hydrogens, creating more allylic radicals than addition products.[45] Although these rate constants were found to be higher than those observed with the *t*-butoxyl radical, the *t*-butoxyl radical and benzophenone triplet reaction show a considerable amount of similarity.

Moving away from simple alkanes, alkenes, and phenols, other studies involving the reactivity of *t*-butoxyl radical towards amines have been conducted. In an earlier study, Encinas and Lissi measured the rate constants for hydrogen atom abstraction from primary, secondary, and tertiary amines.[29] Because of the similarity between the *t*-butoxyl radical and ketone triplets, these rate constants, shown in Table 1.8, were compared to the rate constant for the quenching of the acetone triplet.[46]

Table 1.8. Rate constants for hydrogen atom abstraction from amines by *t*-butoxyl radical and acetone triplet[29]

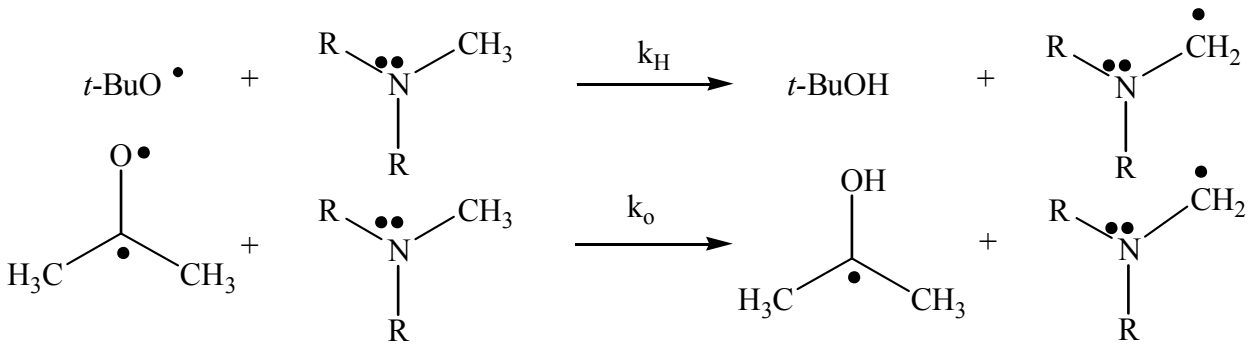

Compound	k_H ($M^{-1} s^{-1}$) at 388 K	k_O ($M^{-1} s^{-1}$) at 286 K[46]
N-methylaniline	2.5×10^7	1.0×10^9
Triethylamine	6.6×10^6	3.0×10^8
Diethylamine	3.8×10^6	5.0×10^7
n-Butylamine	2.2×10^6	1.8×10^7
t-Butylamine	2.0×10^5	2.0×10^6

1.4.6. *Hydrogen atom abstraction from amines*

Comparing the rates between primary, secondary, and tertiary amines, the rate constant for hydrogen atom abstraction from the tertiary amine, triethylamine, was estimated to be significantly faster than the others. The rate constants shown in the Table 8 have not been adjusted for the number of reactive hydrogen. Because of this fact and the greater rate constant found for triethylamine, a reaction pathway via abstraction from the α-carbon to the nitrogen can be deduced. The rate constants for all the amines were found to be larger than the rate constant for the abstraction of hydrogen atom from a C-H bond in a saturated hydrocarbon. It has been

proposed that this increased rate constant may be attributed to the stabilization of the radical that may occur with the lone pair of electrons on the nitrogen (Eq.12).[47,48,49]

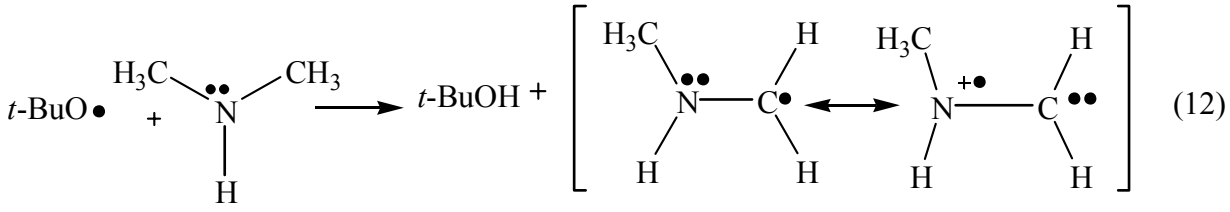

(12)

Although nitrogen's lone pair of electrons can give stabilization, this does not always determine which hydrogen is the most reactive towards the *t*-butoxyl radical, especially in secondary amines. With amines such as dimethylamine, there is a competition between producing radicals $Me_2N^{\bullet}$ and $MeNHCH_2^{\bullet}$ via hydrogen atom abstraction. The rate constants and Arrhenius parameters have been measured for both reactions.[48,49] Using ESR techniques, the energy of activation to transfer the hydrogen atom on the nitrogen to *t*-butoxyl radical was measured to be 4.6 kcal/mol less than the reaction with the α-carbon's hydrogen. However, the A-factor for abstraction of hydrogen from the methyl group was measured to be 3.4 times greater than the N-H abstraction.[49] The greater A value for the methyl group correlates to the number of abstractable hydrogens in that position. Although the C-H bond is weaker, due to the electron stabilization from the nitrogen, it is easier to complete an atom transfer between two electronegative atoms such as nitrogen and oxygen, which would lower the activation energy. However, Griller found that the rate constant for hydrogen atom abstraction at the α-carbon by a *t*-butoxyl radical is faster for all the amines studied in Table 1.9.[48]

Table 1.9. Rate constants for the reaction of *t*-butoxyl radicals with amines at 298 K[48]

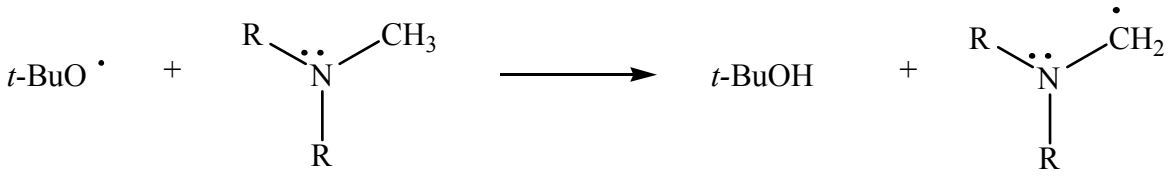

Amine	$k_{\alpha\ C\text{-}H}(M^{-1}\ s^{-1})$	$k_{N\text{-}H}(M^{-1}\ s^{-1})$
Me_2NH	6.5×10^7	1.1×10^7
Et_2NH	6.6×10^7	1.0×10^7
n-$PrNH_2$	1.3×10^7	3.3×10^6
n-$BuNH_2$	7.0×10^7	3.3×10^6

This stabilization of the resulting radical by the lone pair of electrons on the nitrogen has been studied in more detail. In studying the absolute rate constants for reactions of amines with alkoxy radicals and benzophenone triplets, it was observed that hydrogen atom abstraction occurred at the α-carbon to the nitrogen for all substrates. In addition, these rate constants were faster than ones measured for hydrocarbons and isostructural ethers.[11] Results for the small number of the amines examined are summarized in Table 1.10.

Table 1.10. Rate constants for the reaction of *t*-butoxyl radical with tertiary amines[11]

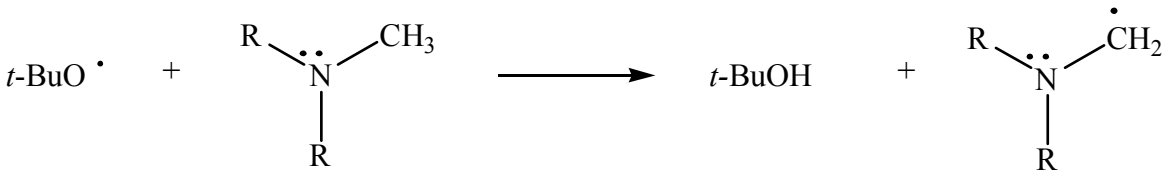

Compound	k ($M^{-1} s^{-1}$) at 295 K
Trimethylamine	1.1×10^8
Triethylamine	1.8×10^8
DABCO (Diaminebicyclooctane)	6.0×10^6
Quinuclidine	2.8×10^7
Diethylaniline	1.3×10^8

Once again, compared to the rate constants for different hydrocarbons given earlier, the rate constants shown above in Table 1.10 are faster. Comparing the straight chain amines to the cyclic amines such as DABCO and quinuclidine, the importance of stereoelectronic factors becomes apparent. Being cyclic structures, DABCO and quinuclidine are unable to rotate the nitrogen-carbon bonds to allow the C-H bond to line up with the lone pair of electrons. The bond angle between the nitrogen lone pair and the abstractable hydrogen is approximately 60°,[11] decreasing the amine's ability to obtain complete overlap and stabilization, and resulting in a significant decrease in the rate constant for abstraction by the *t*-butoxyl radical. An illustration of this inability to obtain orbital overlap can be seen below using the quinuclidine radical (Scheme 8).

Scheme 8

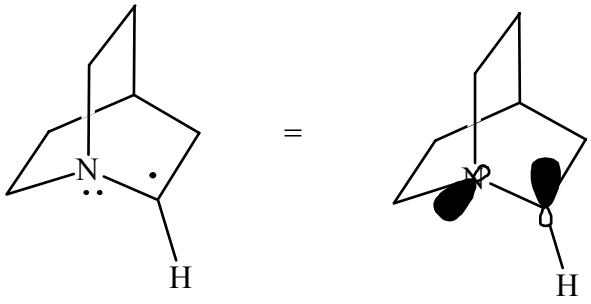

Investigating further into the radical stabilization obtained through the overlap of nitrogen's long pair of electrons, studies of the bond dissociation energy for the C-H bonds on the α-carbon have been conducted. Via photoacoustic calorimetry techniques using the triplet state of benzophenone as the hydrogen abstractor, bond dissociation energies were collected for a series of tertiary amines, ranging from alkyl to allyl to phenyl substituents.[50] Examples of these BDE's are found in Table 1.11.

Table 1.11. Experimental α-C-H bond dissociation energies (BDE's) for tertiary amines[50]

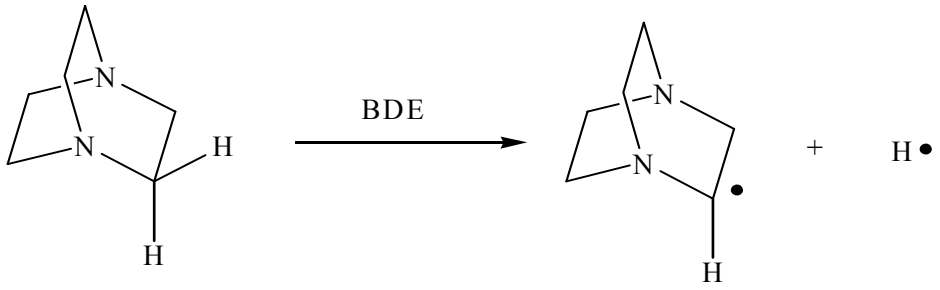

Amine	α-C-H BDE (kcal/mol)	Amine	α-C-H BDE (kcal/mol)
Ph_2NCH_3	90.7 ± 0.4	$N(CH_2CH{=}CH_2)_3$	82.6 ± 0.8
$(CH_3CH_2)_3N$	90.7 ± 0.4	$PhN(CH_2Ph)_2$	85.4 ± 2.1
$(CH_3CH_2)_3N$[51]	90.8	$N(CH_2Ph)_3$	89.1 ± 0.6
$(n\text{-}C_4H_9)_3N$[51]	90.8	$(CH_3)_3N$[51]	88.6
$PhN(CH_2CH_3)_2$	91.6 ± 1.0	*t*-$BuN(CH_3)_2$	90.0 ± 1.2
$PhN(CH_3)_2$	91.7 ± 1.3		

Looking at these different α-carbon hydrogen bond strengths, an understanding can be deduced for the contribution that amine structures have correlating the C-H BDE and reactivity towards *t*-butoxyl radical. In comparing triethylamine and *t*-$BuN(CH_3)_2$, a noticeable change in BDE was found between the two compounds, although it falls within experimental error. This difference can possibly be explained through the release of steric hinderance by the abstraction of the hydrogen atom. Another interesting comparison appears with $(Ph)_2NCH_3$ and triethylamine. Although it may be assumed that the phenyl rings would allow for more radical stabilization and decreasing the bond strength, both of these compounds have the same α-C-H BDE. When comparing aromatic amines, more stabilization of the radical and a lower BDE was found for amines with the phenyl rings on the alkyl substituent instead of bonded to the nitrogen (Scheme 9).

Scheme 9

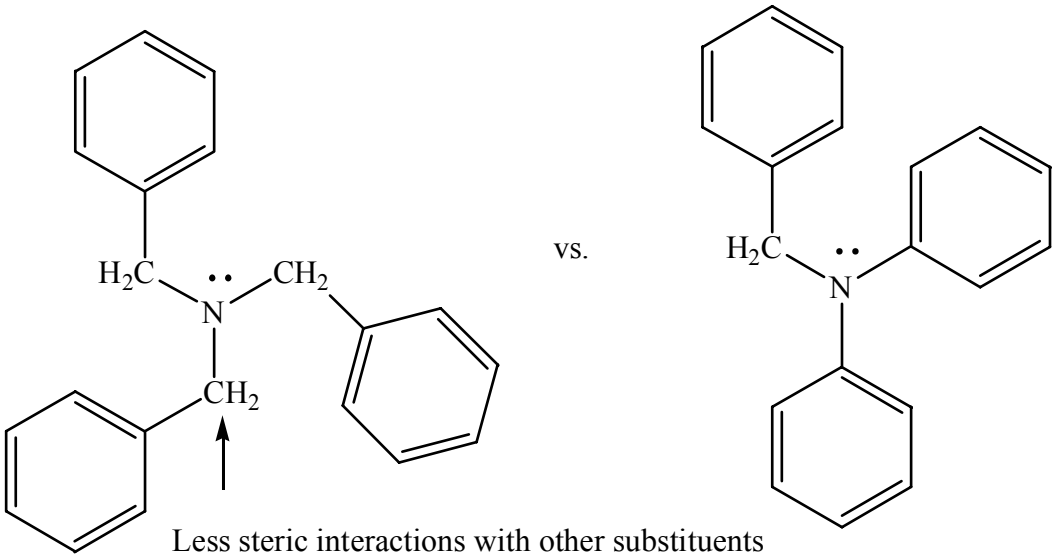

Since the lone pair on the nitrogen already stabilizes the radical, the resonance stabilization from the aromatic rings becomes a minor contributor to the radical's stability. Steric hinderance between the phenyl ring's ortho-hydrogens and the nitrogen's syn-substituent decreases the phenyl ring's ability to help in the radical stabilization.[50] The lowest C-H BDE in the amine series was triallylamine at 82.6 kcal/mol. With the double bonded substituent, overlap

with its π system becomes easier, allowing for more radical stabilization without excess bond rotation.

These findings were solidified in other studies using *t*-butoxyl radical and tertiary amines. Investigating deeper into the structure and bond angles needed for reactions with *t*-butoxyl radical, Wayner found that amines react the fastest when the abstractable hydrogen is anticoplanar to the lone pair of electrons.[51] The stabilization that occurs can be attributed to a three-electron, two-orbital π-like interaction which is maximized when the singly occupied sp^n orbital of C and the nonbonded doubly occupied sp^n orbital of N are anticoplanar to each other.[51] To obtain this structural geometry, the amine must overcome steric hinderance to rotate the bonds of the substituents. It is these obstacles to obtain the correct geometry that increase the amine's α-C-H BDE and decrease its reactivity towards the *t*-butoxyl radical. Similar results were obtained when absolute rate constants for the hydrogen atom abstraction by *t*-butoxyl radical from ethers were measured.[52] Compounds that allowed for more overlap from the π electrons on the oxygen adjacent to the point of attack had higher rate constants for abstraction. Ethers with large dihedral angles between atoms or poor overlap measured to have much slower rate constants for hydrogen atom abstraction from the α-C-H bonds.

To complete the comparison of *t*-butoxyl radical's reactivity towards hydrocarbons and amines, Encinas and Lissi investigated the effect that solvent had on the reactivity of different amines.[26] As before, the reaction in the gas phase gave the fastest rate constant for abstraction. However, they found that solvent polarity played a role in the reactivity of the amine and the *t*-butoxyl radical. It was discovered that as the dielectric constant of the solvent increased, from benzene to benzonitrile, the abstraction rate constant increased dramatically. Once again, the solvent stabilizes the polar transition state and the delocalization of the nitrogen lone pair in the α-hydrogen abstraction from the amine. Also, besides polarity, they examined this rate constant dependence via the ionization potential (I.P.) of the amine, shown in Table 1.12. The I.P. appears to play a significant role in the bond energy for different amines, corresponding to the change in the rate constant for hydrogen atom abstraction by *t*-butoxyl radical.

Table 1.12. Rates of α-hydrogen abstraction for several amines[26]

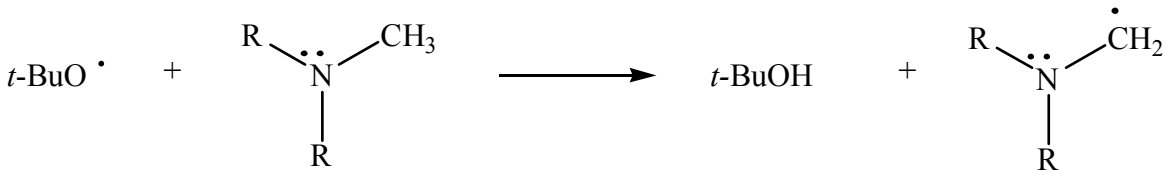

Amine	Bond Energy (kcal/mol)	I.P.[53] (eV)	k_{rel}[a]
Trimethylamine	94.2[54]	7.82	1
N,N-dimethylaniline	97.2[54]	7.10	4.3
Triethylamine	91.0[b]	7.50	3.5
Diisopropylamine	90.5[b]	7.73	1.4

[a]Value per α-hydrogen relative to a primary hydrogen in trimethylamine in benzene at 388 K
[b]Bond dissociation energy of the α(C-H) bond in the monoalkyl amines

1.4.7. *Biological pathways*

Because of its reactivity towards hydrogen in many types of compounds, *t*-butoxyl radical has been used to model hydrogen atom abstraction pathways in certain biological systems, such as the heme-containing proteins, generically named cytochrome P-450. These enzymes have been found to catalyze many aliphatic and aromatic hydroxylations, deaminations, and dehalogenations, as well as act as a reducing agent in reactions with azo and nitro groups.[55] This family of enzymes plays a significant role in the detoxification and excretion of xenobiotics.[6] This enzyme system also catalyzes the oxidation of many amines into carbinolamines. Two mechanisms have been proposed for this oxidation reaction (Scheme 10). One mechanism occurs via a single electron/proton transfer (SET) process (Reaction A). The other mechanism occurs via a simple hydrogen atom (HAT) abstraction (Reaction B).

Scheme 10

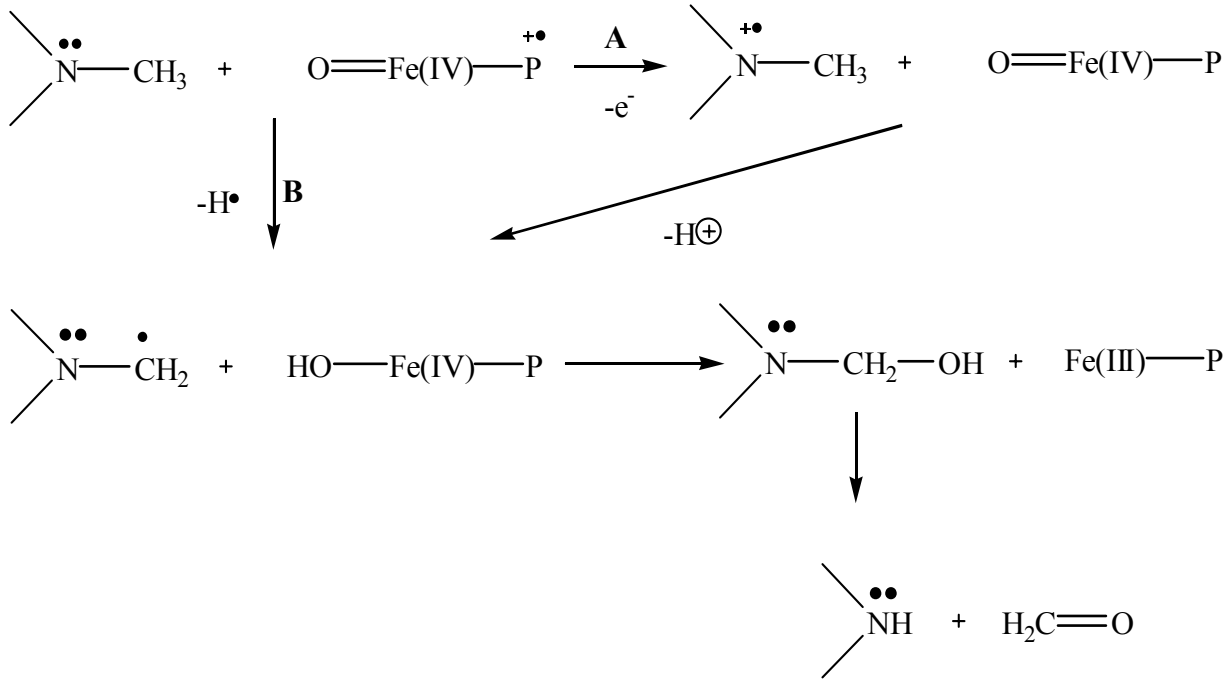

Until recently, it was believed that the reaction with cytochrome P-450 occurred via SET (Reaction A).[6] A study was developed to compare kinetic primary isotope effect profiles observed in the cytochrome P-450 reactions with amines, modeling the SET and HAT pathway conditions and finding a distinction between the two mechanisms. In the hydrogen atom abstraction mechanism, it has been discussed that a symmetrical transition state is involved in the reaction.[56] Although this type of transition state has not always been seen in *t*-butoxyl radical reactions, it is still considered to be a great model for the hydrogen atom abstraction pathway. In various papers, kinetic isotope effect profiles for the hydrogen atom abstraction from various substituted amines by *t*-butoxyl radical have been compared to those of cytochrome P-450.[5,6,55] Using different P-450 enzymes, it was shown that they all show the same reactivity trends, similar to *t*-butoxyl radical. The idea believed in these studies was that SET would show a small isotope effect, while HAT would show a large effect. The hydrogen atom abstraction by *t*-butoxyl radical was found to have an isotope effect of 2.5, smaller than expected.[56] The same kinetic isotope effect was observed for the cytochrome P-450 oxidation of the amines. These

studies suggest that cytochrome P-450 reacts via a hydrogen atom abstraction pathway for the oxidation of secondary amines. A comparison of these profiles is shown in Table 1.13.

Table 1.13. Kinetic deuterium isotope effects for reaction of various substrates with *t*-butoxyl and cytochrome P-450[6]

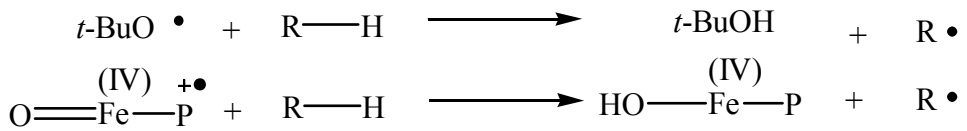

Substrate	k_H/k_D(·OBu^t)	k_H/k_D(P-450)
p-Xylene	6.3 ± 0.3	6.4 ± 0.9
Toluene	6.0 ± 0.2	5.9 ± 0.35
p-Nitro-N,N-dimethylaniline[55]	3.8 ± 0.1	4.0 ± 0.1
p-Cyano-N,N-dimethylaniline[55]	3.5 ± 0.1	3.6 ± 0.1
p-Chloro-N,N-dimethylaniline[55]	2.7 ± 0.1	2.8 ± 0.2
N,N-dimethylaniline[55]	2.5 ± 0.1	2.6 ± 0.1
Benzyl alcohol	3.6 ± 0.4	2.7 ± 0.1

As stated before, *t*-butoxyl radical was chosen as a model for cytochrome P-450 reactions on the basis that it would have a similar transition state to the enzyme's hydrogen atom abstraction during substrate oxidation. However, studying the reaction of methylcubane with *t*-butoxyl radical and the enzyme, it was discovered that the transition states were not as similar as first thought.[7] When the *t*-butoxyl radical reacted with methylcubane, abstraction of the hydrogen atom only occurred at the methyl C-H position, immediately causing the rearrangement illustrated in Eq.13, which then reacts further to form its alcohol product.

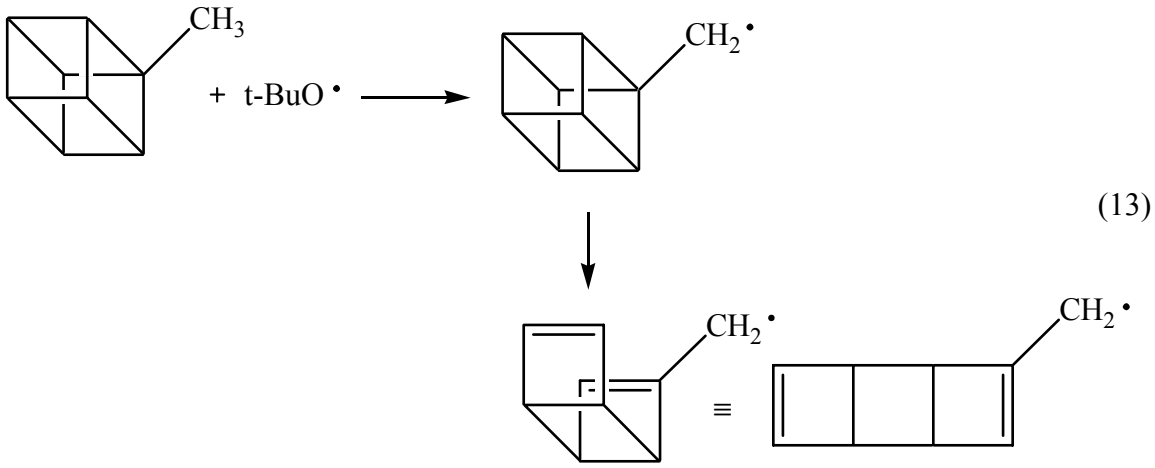

(13)

Conversely, a different reactivity towards methylcubane was found when it was reacted with cytochrome P-450 enzymes. The oxidation into the substrate's alcohol products by the enzyme was found to occur at all positions on the compound, showing a definite difference in regioselectivity compared to *t*-butoxyl radical. It was observed that the site of oxidation was determined after the enzyme binds to the substrate, not allowing any variation in the orientation of attack for the enzyme. The discrepancy between the enzyme and *t*-butoxyl radical found in this mechanistic probe study illustrates that insufficient work has been done with *t*-butoxyl radical to ensure its complete use as a biological model.

t-Butoxyl radical continues to be used in biological systems to determine antioxidant sites in different compounds, such curcumin and vitamin E analogues.[57-59] In both studies, *t*-butoxyl radical was used to determine rate constants for hydrogen atom abstraction at the compounds' most labile site. The rate constant for curcumin was measured at almost the diffusion-controlled limit, $7.5 \pm 0.8 \times 10^9$ M^{-1} s^{-1}. It has been suggested that the site of reaction produces a radical within a heptadienone linkage, between the two carbonyl groups.

Scheme 11

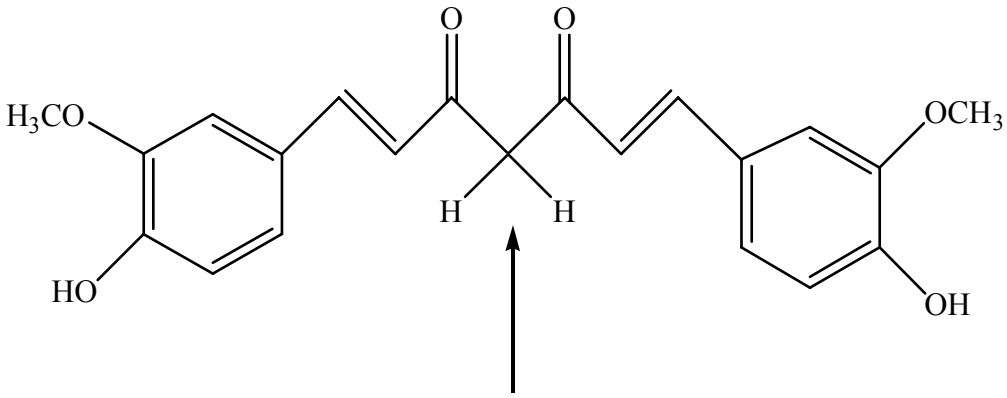

Since the reaction could also occur at the phenolic positions, the rate constant for curcumin was compared to constants measured for dehydrozingerone, a half-curcumin compound without the $–CH_2-$ linkage, allowing for only phenolic attack.

Scheme 12

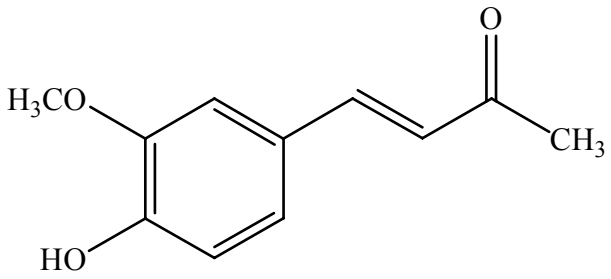

Reacting this compound with *t*-butoxyl radical showed complete abstraction at its phenolic positions with a rate constant equaling $1.1 \pm 0.1 \times 10^9$ M^{-1} s^{-1}, almost a full order of magnitude slower.[58] This dramatic decrease in the rate constant was hypothesized to be caused by the loss of the CH_2 group linkage. It was hypothesized that it was this site in which hydrogen atom abstraction occurs. However, after this study, more evidence was produced to contradict the thought that the $–CH_2-$ linkage was the main site for oxidation. In a study conducted by Barclay *et al.*, he determined that nonphenolic curcuminoid compounds lost their ability to

suppress oxidation, though they still had the assumed $-CH_2-$ active site present.[60] His study illustrates, using peroxyl radicals, that it is the phenolic site, not the $-CH_2-$ linkage that controls curcumin's antioxidant properties. Peroxyl radicals are much more selective due to the stabilization of their radical center. By using a less reactive oxygen centered radical, the most oxidative site in a molecule can be determined more precisely. The use of *t*-butoxyl radical in the previous study may have lead to skewed evidence due to the alkoxyl radical's reactivity. Barclay also proposes that the spectral data for the intermediate, an absorption band seen at approximately 500 nm., generated in this reaction points towards an oxygen centered radical, instead of a carbon-centered radical in the curcumin. In addition to this new evidence, he also states that conditions, such as solvent polarity, must be considered important factors when trying to understand biological oxidation processes. In an additional study with other antioxidants, the importance of solvent conditions was examined by measuring the rate constants for hydrogen atom abstraction from different vitamin E analogues in four different solvents by *t*-butoxyl radical.[58,59] Table 1.14 illustrates that as the polarity of the solvent increases, the rate constant for hydrogen atom abstraction by the alkoxyl radical decreases. In modeling biological systems, these conditions must be considered for the results from the model to be accurate.

Table 1.14. Absolute rate constants for hydrogen atom abstraction by *t*-butoxyl radical from vitamin E analogues[58,59]

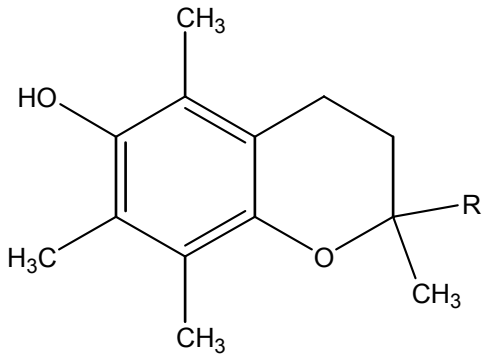

α-TOH, R = $C_{16}H_{33}$

Trolox, R = COOH

HCAA, R = CH_2COOH

Vitamin E analogue	**k_H (M^{-1} s^{-1}) 298 ± 2 K**			
	$C_6H_5OCH_3$	**CH_3CN**	**$CH_3C(O)OC_2H_5$**	**H_2O**
Trolox	1.6 x 10^9	5.2 x 10^8	2.0 x 10^8	1.75 x 10^9
HCAA	1.9 x 10^9	8.5 x 10^8	3.2 x 10^8	8.4 x 10^8
α-TOH	2.0 x 10^9	9.4 x 10^8	2.9 x 10^8	----------

In recent studies, a look into the flavoenzymes, the monoamine oxidases- MAO A and B, has opened a major discussion into how enzymes cause the degradation of biogenic amines through a SET or HAT reaction pathway, similar to the pathways illustrated for cytochrome P-450. For example, some investigations have given evidence that MAO B catalyzes amine oxidation via the deprotonation of the α-hydrogen of certain substrates via either of these two pathways. This oxidation reaction creates an intermediate that reacts further to complete the decarboxylation of these compounds.[61] Additional studies demonstrate this enzyme's ability to catalyze the oxidative deamination of brain neurotransmitters such as dopamine (DA) and serotonin.[62]

Classes of amines that have been found to react as good substrates towards MAO B are cyclic tertiary allylamines, including 1-methyl-3-pyrrolines and 2-methylisoindolines.[63-65] Within these classes, certain neurotoxins have been found, especially 1-methyl-4-phenyl-1,2,3,6-tetrahydropyridine (MPTP), an amine that produces Parkinson's disease-type symptoms. This compound was first reported in the 1950's, when it was being tested for its analgesic activity.[66] In later years, MPTP was found to be a side product in the production of "street heroin". MPTP is oxidized quite rapidly, via a dihydropyridinium intermediate to the neurotoxic pyridinium species that mediates its neurodegenerative properties. In studies with different animals such as primates and mice, MPTP causes the massive, selective damage of neurons in the *substantia nigra*, which leads to a depletion of DA levels in the brain.[66,67]

The known degradation by oxidation of MPTP, catalyzed by MAO B, into the intermediate MPDP+ and finally MPP+ is shown in Scheme 13. The oxidation of MPTP to MPDP+ has been seen in vivo, but since MPP+ does not cross the blood-brain barrier easily, it is not accessible to study.[66]

Scheme 13

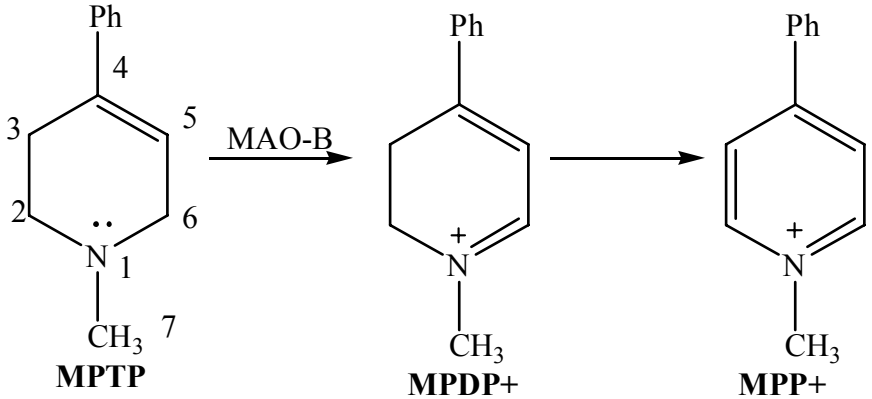

MPTP **MPDP+** **MPP+**

Hydrogen atom abstraction could occur theoretically at the C-2, C-6, or C-7 positions. Although other hydrogen abstractions are possible, the MAO B enzyme attacks regiospecifically at the C-6 allylic position. Through *in vitro* studies with MAO B inhibitors[68-70] and confirmed

with NMR, mass spectral data, and other methods, it has been determined that the MPP+ species causes the induced-Parkinson-type disease.[66,71]

Similar to the oxidation of amines by cytochrome P-450, the mechanism for MPTP oxidation into the MPDP+ intermediate has been proposed to follow either a SET or HAT mechanism. Both of these mechanisms occur in the C-6 position, which has the weakest C-H bond. The two mechanism pathways are shown in Scheme 14.

Scheme 14

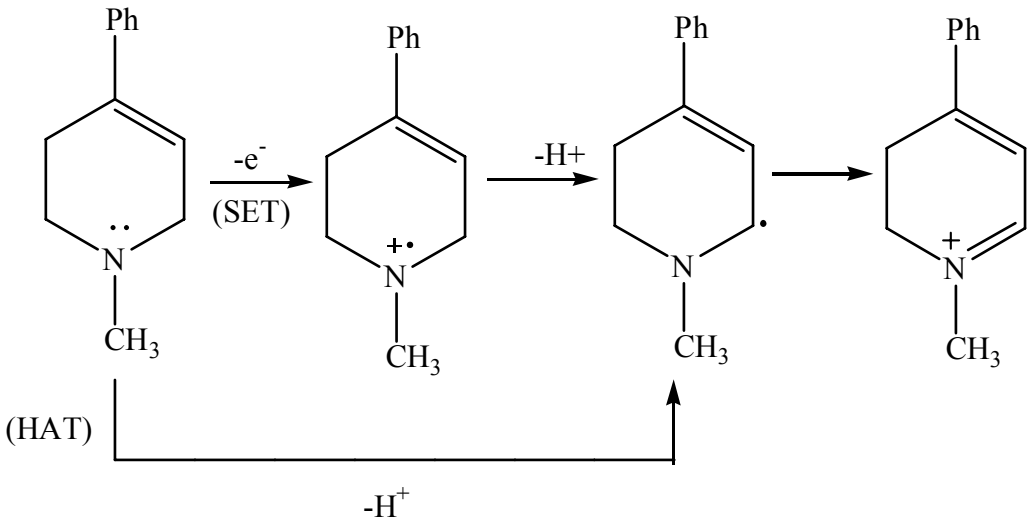

To gather evidence for the relevance of these pathways, studies were conducted on MAO B catalyzed oxidations of 4-phenyl-1-cyclopropyl-1,2,3,6-tetrahydropyridines and 4-phenyl-1-methyl-1,2,3,6-tetrahydropyridines.[64,65] These compounds were examined under chemical conditions that mimic the SET and HAT pathways. The data collected for the 1-methyl-1,2,3,6-tetrahydropyridines did not allow for any conclusions to be made about the pathways. However, the study of 4-phenyl-1-cyclopropyl-1,2,3,6-tetrahydropyridine gave a deeper insight into the more probable oxidation pathway. Under HAT conditions, these compounds underwent hydrogen atom abstraction at the C-6 position to yield, eventually, the MPDP+ intermediate and the MPP+ pyridinium compound. However, under SET conditions, the proposed reaction pathway creates a cyclopropylaminyl radical cation, illustrated in Scheme 15.

Scheme 15

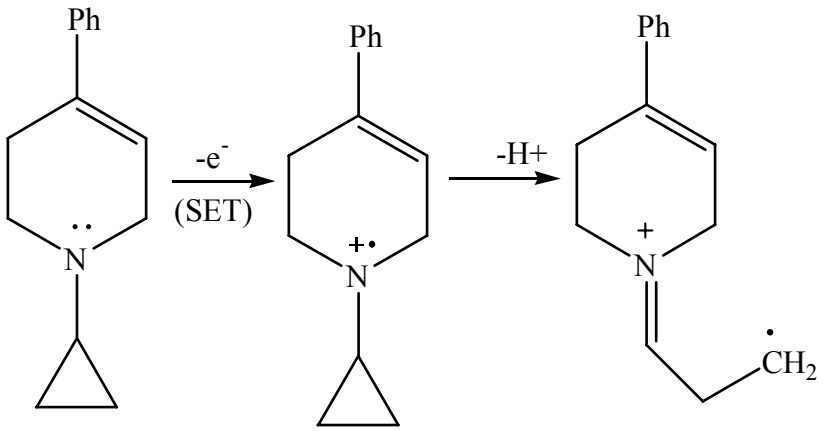

Under HAT conditions, no evidence was found for the formation of this radical cation. When the compounds were reacted under SET conditions, evidence supported the creation of the radical intermediate shown above, by observing the inactivation of MAO B. The intermediates formed during amine oxidation of MPTP by MAO B do not cause inactivation of the enzyme. With this evidence, it can be postulated that MAO B amine oxidation does not occur via a SET pathway.

To further study the production of MPDP+ in the oxidation of MPTP, deuterium kinetic primary isotope effect measurements were collected for the reaction with MAO B.[72] It has been proposed that attack on the amine could occur at the C-6 position or the C-2 position, followed by rearrangement, to achieve the radical. The mechanism for attack at these positions is shown in Scheme 16. Using LSI mass spectral analysis after reacting MAO B with the amine deuterated in the C-2 and C-6 positions, the pathway via the C-2 position was ruled out. No products by means of this attack pathway were found. These examinations show evidence for the attack at the C-6 position only.

Results from kinetic primary isotope effect studies added additional evidence for the deprotonation from this carbon. Deuterating the C-2 position did not cause a decrease in the rate constant for amine oxidation. These kinetic isotope effects are found in Table 1.15 and the deuterated MPTP structures examined are shown in Scheme 17.

Scheme 16

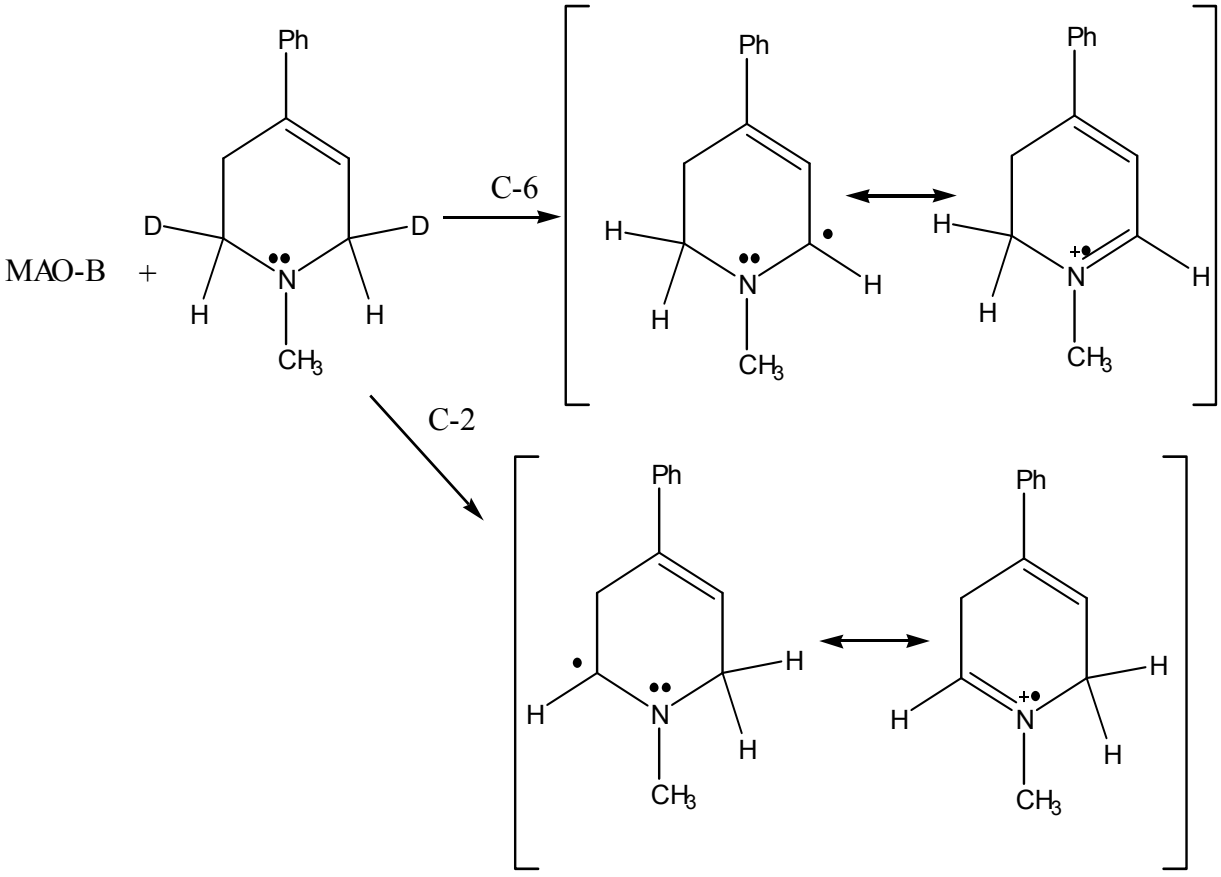

Table 1.15. Kinetic parameters and intermolecular effects for the MAO B catalyzed oxidation of MPTP[72]

Substrate	V_{max} (mmol/min)	K_m (mM)	$^{D}(V_{max})$	$^{D}(V_{max}/K_m)$
MPTP-d_o	18.2 ± 0.46	0.48 ± 0.02	------	------
MPTP-d_2	5.14 ± 0.55	1.07 ± 0.18	3.55 ± 0.39	8.01 ± 0.56
MPTP-d_4	5.72 ± 0.47	1.13 ± 0.19	3.19 ± 0.27	7.56 ± 0.69
MPTP-d_7	4.18 ± 0.19	1.02 ± 0.07	4.37 ± 0.23	9.35 ± 0.51

Scheme 17

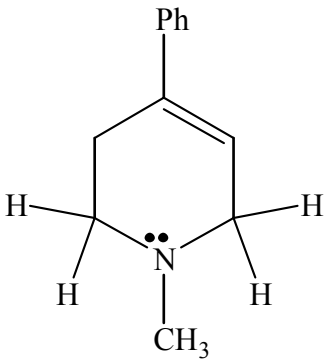

MPTP

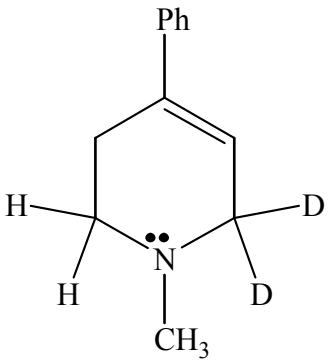

MPTP-d_2

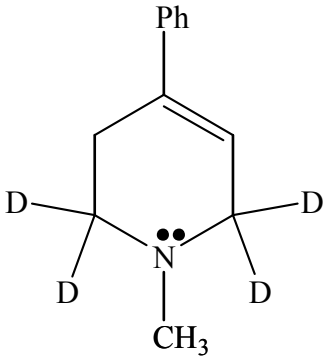

MPTP-d_4

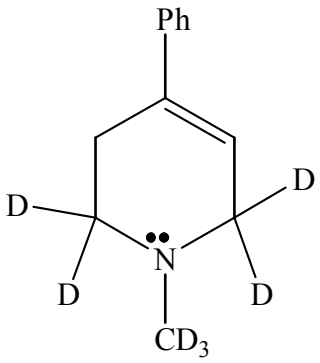

MPTP-d_7

Using these isotope effects, no real understanding of the mechanism can be achieved. As shown by the data in Table 1.15, all of the deuterated substrates show similar isotope effects

towards the MAO-B enzyme. These effects were expected for this reaction following the HAT pathway. However, they did not disprove any other mechanistic pathways. Newer methods and different oxidation models, like *t*-butoxyl radical, are now being used to solidify the true mechanism for causing this amine's degradation in the brain.

1.5. SUMMARY

The heteroatom radical, *t*-butoxyl radical, is a highly reactive intermediate that has begun to take on an important role in organic chemistry. Through the years, this radical has been generated by different techniques and from different types of compounds. Initially, it was produced through photochemical or thermal means from hypohalite compounds, such as *t*-butyl hypochlorite. However, as newer techniques have become available, the alkoxyl radical has been generated easily from di-*tert*-butyl peroxide through laser flash photolysis techniques.

Once the radical is created in solution or gas phase, decomposition of the highly unstable intermediate occurs rapidly. The radical can undergo β-scission into acetone and the methyl radical. Also, the radical can decompose by reacting with a solvent via hydrogen atom abstraction. It has been determined that this decomposition through β-scission increases with solvent polarity, due to stabilizing the transition state of the reaction.

t-Butoxyl radical has been examined for its ability to abstract hydrogen atoms from an assortment of different substrates. This alkoxyl radical has shown a very high reactivity towards all of the substrates studied, while illustrating a low selectivity towards the different hydrogen available for abstraction. In addition to observing the radical's high reactivity, it was also found that the rate constant for hydrogen atom abstraction from all the substrates, except for alkanes, was affected by the solvent polarity due to stabilization of the polar transition state. Using carboxylic acids and alcohols as substrates, studies have shown that rate constant for hydrogen atom abstraction may also be subject to change due to interactions such as hydrogen bonding. All of these studies were conducted to gain some understanding into this versatile organic intermediate.

Similar to radical reactivity found in the laboratory, free radicals have been found to be key intermediates in many oxidations, degradations, etc. in biological systems. However, since these intermediates are extremely energetic and, many times, invisible to many analytical techniques, studies of certain radicals have been inconclusive. *t*-Butoxyl radical is one of these highly reactive intermediates that may warrant further investigation before it can be used to model radical behavior in "unknown" systems such as an enzyme active site. Absolute rate constants have been collected for this radical from only a small range of substrates.

With little justification, the use of *t*-butoxyl radical in other studies, such as a biological model for enzymes, has begun to grow. It has been used to model systems catalyzed by cytochrome P-450 oxidations, making the assumption that both compounds follow similar transition states. In addition to this oxidation system, the *t*-butoxyl radical has been used to understand the mechanism for oxidation of the neurotoxin, 1-methyl-4-phenyl-1,2,3,6-tetrahydropyridine (MPTP). With this radical's potential uses, a complete assessment of how well *t*-butoxyl radical can model biological enzymes and reactions is long overdue.

CHAPTER 2. HYDROGEN ABSTRACTION BY *t*-BUTOXYL RADICAL

2.1. INTRODUCTION

To mimic enzymatic mechanisms believed to involve radical intermediates, the alkoxy radical, *tert*-butoxyl radical has often been utilized as a model for oxygen-centered radical hydrogen atom abstractions. However, the chemistry of the *t*-butoxyl radical itself is far from being completely understood. In using the radical to probe the correct mechanism for the enzymatic oxidation of the neurotoxin, 1-methyl-4-phenyl-1,2,3,6-tetrahydropyridine (MPTP), preliminary results suggested that *t*-butoxyl radical exhibited no selectivity in hydrogen atom abstraction.[73] Due to these unexpected results, the objective of this project is to investigate *t*-butoxyl radical's reactivity towards hydrogen atom abstraction from general tertiary amines, hydrocarbons and other substrates.

Different tertiary amines with varying α-C-H BDE's, such as triallylamine, diphenylmethyl amine, and quinuclidine, were examined by laser flash photolysis for their reactivity with *t*-butoxyl radical for abstraction of the α-hydrogen. Intuition would lead one to expect that the weaker the C-H BDE, the greater the rate constant for hydrogen atom abstraction. However, our results revealed no obvious correlation to BDE; in fact, the substrates with the weakest C-H bonds reacted the slowest. From the data collected, we theorized that this reaction with *t*-butoxyl radical may not be controlled by the enthalpic considerations, and that entropic influences may be important. To understand these results, Arrhenius experiments, as well as, viscosity studies and BDE calculations (B3LYP/6-31G*/CC-PVTZ(-F)), were conducted in order to truly comprehend the complexity of the reactivity for this small alkoxyl radical.

2.2. ABSOLUTE RATE CONSTANTS FOR HYDROGEN ATOM ABSTRACTION

To obtain the hydrogen atom abstraction rate constants, *t*-butoxyl radical was generated by flash photolysis of *tert*-butyl peroxide (Eq.1), following techniques used by Scaiano, which were already discussed.[17] Since this alkoxyl radical is spectroscopicly invisible at wavelengths greater than 300 nm, the observed rate constants were measured by observing the products of these hydrogen abstraction reactions. However, many of the radicals (R•) generated by this reaction do not give strong absorbing chromophores in the UV/visible region. To compensate for this, a spectroscopic "probe", at a fixed concentration, was added to the reactions. Diphenylmethanol was used as this probe and, after hydrogen abstraction, generates the diphenylhydroxymethyl radical that absorbs at 535 nm. This method was previously discussed in Chapter 1 and illustrated in Scheme 3.

Referring to Scheme 4 and Eq. 9 from Chapter 1 for an explanation of parallel pseudo first order kinetics, the second order rate constant for hydrogen atom abstraction by *t*-butoxyl radical from the substrates (k_H) could be obtained from the slope of a plot of the observed rate constant vs. the concentration of the substrates [RH]. For every substrate, at least five different concentrations of substrates, ranging over one full order of magnitude, were investigated. The second order rate constants measured in this study are shown in Table 2.1. A complete list of published rate constants for hydrogen abstraction by *t*-butoxyl for various substrates can be found in Table 1 in Appendix A.

Table 2.1. **Absolute rate constants for hydrogen abstraction by *t*-BuO• from a variety of substrates. (95 % confidence intervals in the last reported digits are shown in parentheses).**

Substrate	Log(k_H) at 25 °C[a]	C-H BDE (kcal/mol)
Amines[b]		
Tribenzylamine (3)	7.62	89.1(6)[c]
N,N-dibenzylaniline (2)	7.27	85(2)[c]
DABCO (2)	7.06	94(2)[d]
triallylamine (2)	7.95	82.6(8)[c]
triethylamine (3)	7.99	90.7(4)[c,e]
quinuclidine (2)	7.02	96(2)[d]
N-methylpyrrole (1)	6.86	91(2)[f]
N,N-dimethylaniline (2)	8.01	92(1)[c]
Hydrocarbons		
triphenylmethane (1)	6.31	81(1)[g]
diphenylmethane (2)	6.53	84(1)[g]
allylbenzene (1)	6.51	82(2)[f]
cyclohexane (4)	5.91	98.7(5)[h]
	5.92[i]	98.7(5)[h]
toluene (3)	5.28	90(1)[h]
Alcohols		
diphenylmethanol (1)	6.84	79(2)[f]
	6.91[j]	79(2)[f]

[a]Calculated from Arrhenius parameters. [b]Value in parentheses indicates number of times study was performed. [c]Reference 50. [d]Reference 74. [e]Reference 51. [f]Calculated (B3LYP/6-31G*/CC-PVTZ(-F)) as described herein. [g]Reference 39. [h]Reference 75. [i]Reference 23. [j]Reference 52.

When measuring rate constants for hydrogen atom abstractions, it is expected for the rate constants to increase with decreasing bond strength for the breaking C-H bond. The classic method for comprehending this relationship is based upon the Evans-Polanyi relationship which predicts a linear correlation between the log of the rate constant for hydrogen atom abstraction and the enthalpy of the reaction: $\log(k_H) = \alpha\Delta H^o + \text{constant}$. ΔH^o is directly related to the strength of the breaking bond; for H-abstractions by *t*-BuO•, ΔH^o = BDE(C-H) – BDE(OH). The proportionality constant α is believed to be a measure of transition state location: A value of $\alpha < 0.5$ implies an early, more reactant-like transition state, while $\alpha > 0.5$ implies a late, more product-like transition state.[76]

When no experimental values of C-H bond dissociation energies for the substrates pertinent to this study were available, they were estimated using density functional theory[77,78] as follows: Geometry optimizations at the B3LYP/6-31G* level followed by single point energy calculations (B3LYP/CC-PVTZ(-F)), were performed on the substrate and its corresponding free radical to obtain the difference in their energy (ΔE). Using 17 compounds with known C-H BDE's (ranging from 81 – 132 kcal/mol), a plot of BDE vs. ΔE was constructed and analyzed by linear least squares regression analysis. This calibration plot can be found in Figure 20 in Appendix A. Unknown C-H BDE's were estimated by calculating ΔE using density functional theory as described above, and using the results of the regression analysis. Literature and calculated values of pertinent C-H BDE's are summarized in Table 1. A summary of these calculated BDE's are shown in Table 2 in Appendix A.

Using values for k_H at 25 ^oC (Table 2.1), a plot of $\log(k_H/n)$ vs. BDE (where n is the number of abstractable hydrogens) is presented in Figure 2.1. Based upon the observed scatter, no simple relationship between $\log(k_H/n)$ and C-H BDE in the context of the Evans-Polanyi relationship is evident. Through the scatter, however, there appears to be a curvature in the plot. Looking closely, there appears to be two distinct regions that need to be addressed. For substrates with C-H BDE's greater than 92 kcal/mol, $\log(k_H/n)$ decreases with increasing bond strength as expected on the basis of the Evans-Polanyi equation. In the other region of the plot, for substrates with C-H BDEs less than 92 kcal/mol, $\log(k_H/n)$ seems to be leveling off at a value of approximately 6.6, independent of C-H BDE.

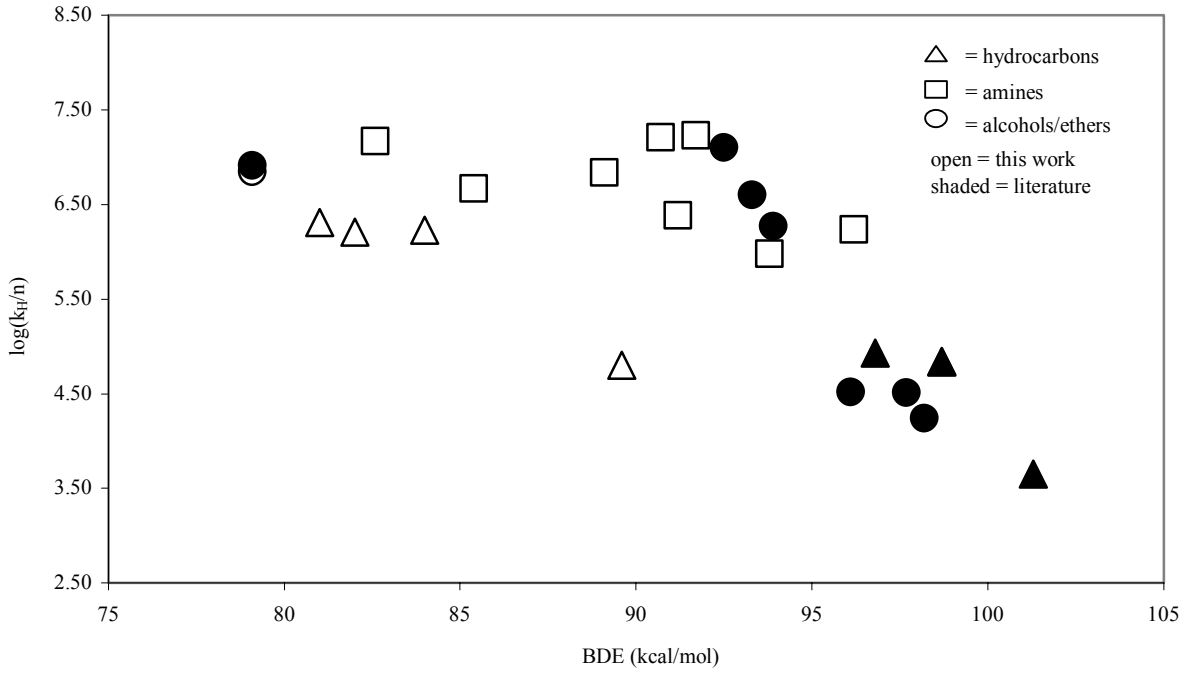

Figure 2.1. Plot of log(k_H/n) vs.C-H BDE for the hydrogen abstraction from substrates (RH) by *t*-butoxyl radical

Initially, these results may be explained on the basis of the reactivity-selectivity principle. The strength of the O-H bond in *t*-BuOH is 105 kcal/mol,[75] which means that all of these reactions are exothermic by 3 – 25 kcal/mol. Due to the alkoxyl radical's high reactivity, *t*-BuO• is expected to exhibit low selectivity. In the context of the Evans-Polanyi relationship, a low value of α would be expected, consistent with an early, reactant-like transition state. However, in comparing experimental results for different substrates, triallyl amine and triethyl amine react at nearly the same rate with *t*-BuO•, despite triallyl amine having a C-H bond which is weaker by 8 kcal/mol. Similarly, on a per hydrogen basis, the rate constant for hydrogen atom abstraction from cyclohexane and toluene are the same, despite the fact that the C-H bond in toluene is 10 kcal/mol weaker. From these comparisons, the high reactivity/low selectivity argument would appear to suggest that every encounter of *t*-BuO• would lead to reaction (*i.e.*, the onset of diffusion control), perhaps explaining why log(k_H/n) does not vary significantly with structure for substrates with low C-H BDEs. However, the observed bimolecular rate constants

reported in Table 16 are lower than values typically associated with a diffusion-controlled reactions in solution ($10^9 - 10^{10}$ $M^{-1}s^{-1}$).[79]

2.3. ARRHENIUS PARAMETERS

Arrhenius parameters for hydrogen abstraction were determined via non-linear regression analysis in accordance with the Arrhenius equation (Eq. 14).[80]

$$k = A\exp\left(\frac{-E_a}{RT}\right) \tag{14}$$

The experiments were conducted over a temperature range between 10 - 80 °C. Reported errors are based upon 95% confidence limits of the parameters. To verify reproducibility, several of the experiments were repeated over the course of the study. Averaged results are summarized in Table 2.2. In addition to the rate constants, published Arrhenius parameters for hydrogen abstraction by *t*-butoxyl for the various substrates can be found in Table 1 in Appendix A.

Table 2.2. Arrhenius parameters for hydrogen abstraction by *t*-BuO• from a variety of substrates. (95 % confidence intervals in the last reported digits are shown in parentheses).

Substrate	Temperature range (°C)	E_a. (kcal/mol)	log A (A in units of M^{-1} s^{-1})
Amines[b]			
tribenzylamine (3)	5 → 80	1.34(16)	8.60(10)
N,N-dibenzylaniline (2)	10 → 80	2.02(18)	8.75(15)
DABCO (2)	10 → 70	2.15(18)	8.63(11)
triallylamine (2)	10 → 80	2.20(21)	9.56(12)
triethylamine (3)	10 → 70	2.38(49)	9.73(25)
quinuclidine (2)	10 → 70	2.41(66)	8.78(31)
N-methylpyrrole (1)	10 → 80	2.42(70)	8.62(32)
N,N-dimethylaniline (2)	10 → 80	2.54(61)	9.87(29)
Hydrocarbons			
triphenylmethane (1)	10 → 70	1.86(36)	7.67(19)
diphenylmethane (2)	10 → 70	2.42(53)	8.30(26)
allylbenzene (1)	10 → 80	2.48(31)	8.15(18)
cyclohexane (4)	10 → 70	4.42(78) 3.11(24)[a]	9.15(35) 8.2(20)[a]
toluene (3)	10 → 80	3.46(49)	7.81(24)
Alcohols			
diphenylmethanol (1)	10 → 70	2.03(28)	8.33(16)
	-35 → 70	1.99(35)[b]	8.37(28)[b]

[a]Reference 23. [b]Reference 52.

In addition to expanding the scope of our earlier study,[81] some of the activation parameters have been revised and are considered more accurate than the previously reported values. Meticulous purification of the reactants and an extended temperature range for the Arrhenius studies have led to more reliable and reproducible values.

The motivation for measuring these Arrhenius parameters was to understand the reason for the apparent breakdown in normal activation/driving force relationships. To do so, , it was critical to go beyond the absolute rate constants and examine the activation parameters for hydrogen atom abstraction by *t*-BuO•. These parameters can be examined by recalling the relationships between log(A) and E_a of the Arrhenius equation and the enthalpy and entropy of activation of activated complex theory (Eqs. 15 and 16).[80]

$$\Delta H^{\neq} = E_a - RT \tag{15}$$

$$\Delta S^{\neq} = R\left(\ln(\frac{h}{k_B T}) + 2.303 \log A - 1 \right) \tag{16}$$

In Figure 2.2, a plot of $-T\Delta S^{\neq}$ vs. $\Delta H^{\neq}$ is presented which has been constructed from the results shown in Table 2.2 and data already reported in the literature. The diagonal line corresponds to $-T\Delta S^{\neq} = \Delta H^{\neq}$ (at 298 K). It should be noted that the derived $\Delta H^{\neq}$ and $\Delta S^{\neq}$ refer to a reference state where one mole of reactants, each at 1 M concentration, are converted to one mole of the transition state, also at 1 M concentration.

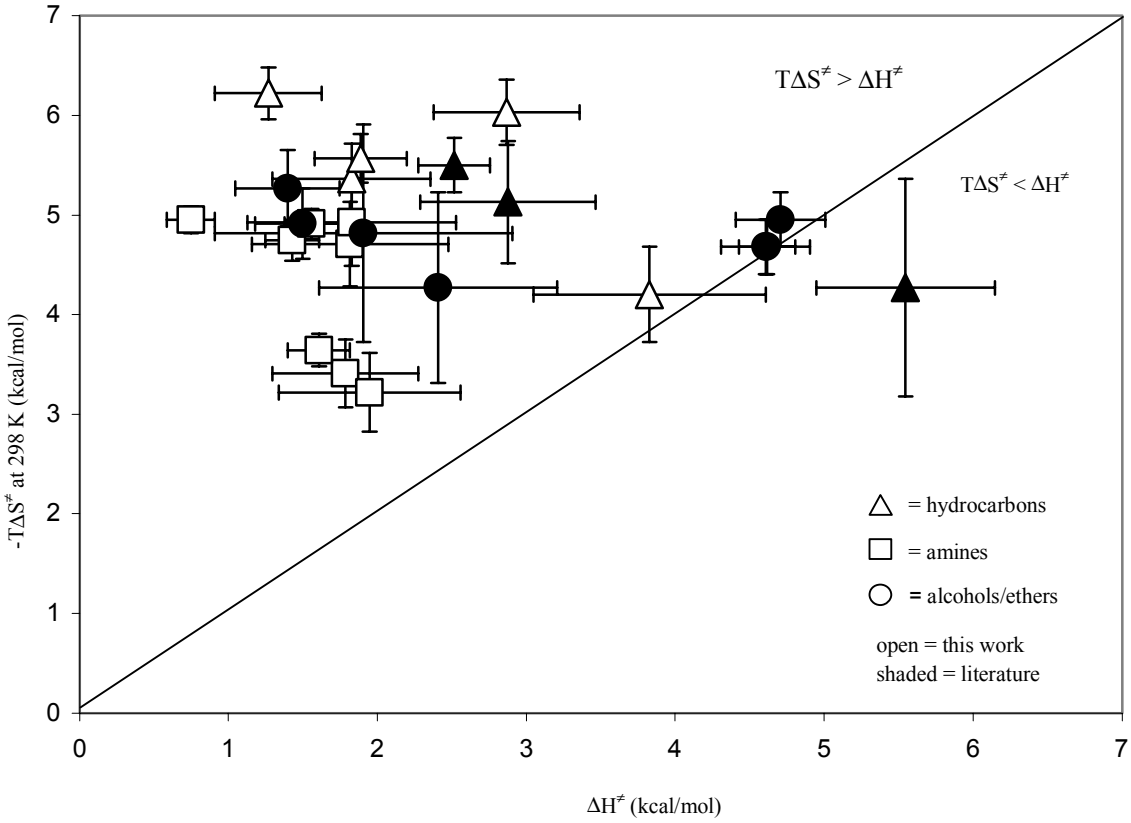

Figure 2.2. Plot of $-T\Delta S^{\neq}$ vs. $\Delta H^{\neq}$ for hydrogen abstractions by *t*-BuO• at room temperature

A critical feature about *t*-BuO• chemistry emerges from this analysis: *At room temperature, most hydrogen abstractions by t-BuO• in solution are entropy-controlled.* What does this plot mean? Well, in examining the free energy barrier ($\Delta G^{\neq} = \Delta H^{\neq} - T\Delta S^{\neq}$) for hydrogen atom abstraction, it appears that the entropy rather than the enthalpy of activation governs the reaction more. This point is illustrated graphically in Figure 2.2, which shows that for most substrates at room temperature, $-T\Delta S^{\neq} > \Delta H^{\neq}$ (*i.e.*, most of the points in Figure 2.2 fall *above* the line corresponding to $-T\Delta S^{\neq} = \Delta H^{\neq}$). This means that *t*-BuO• is *so* reactive that issues of orientation, trajectory, accessibility, etc. govern rate constants for hydrogen atom abstractions more, than by the strength of the breaking C-H bond. Entropy-controlled reactions are not common in organic chemistry and do not follow "normal" structure/reactivity and/or linear free energy relationships. Examples of reported entropy-controlled reactions include additions of carbenes to multiple bonds[82,83] and radical-radical recombination reactions.[4] Some of these reactions are characterized by very low activation energies, or in some cases, even negative

activation energies and/or curved Arrhenius plots, low A-factors, and rate constants below the diffusion-controlled limit. For all substrates examined in this study, "normal" Arrhenius behavior was observed.

The next question addressed examines if the activation energy (or $\Delta H^{\neq}$) varies sensibly with the strength of the breaking C-H bond? A plot of activation energies vs. BDE (Figure 2.3) once again reveals two distinct regions. For substrates with C-H BDE's greater than about 92 kcal/mol, the activation energy decreases as the C-H bond becomes weaker (expected behavior

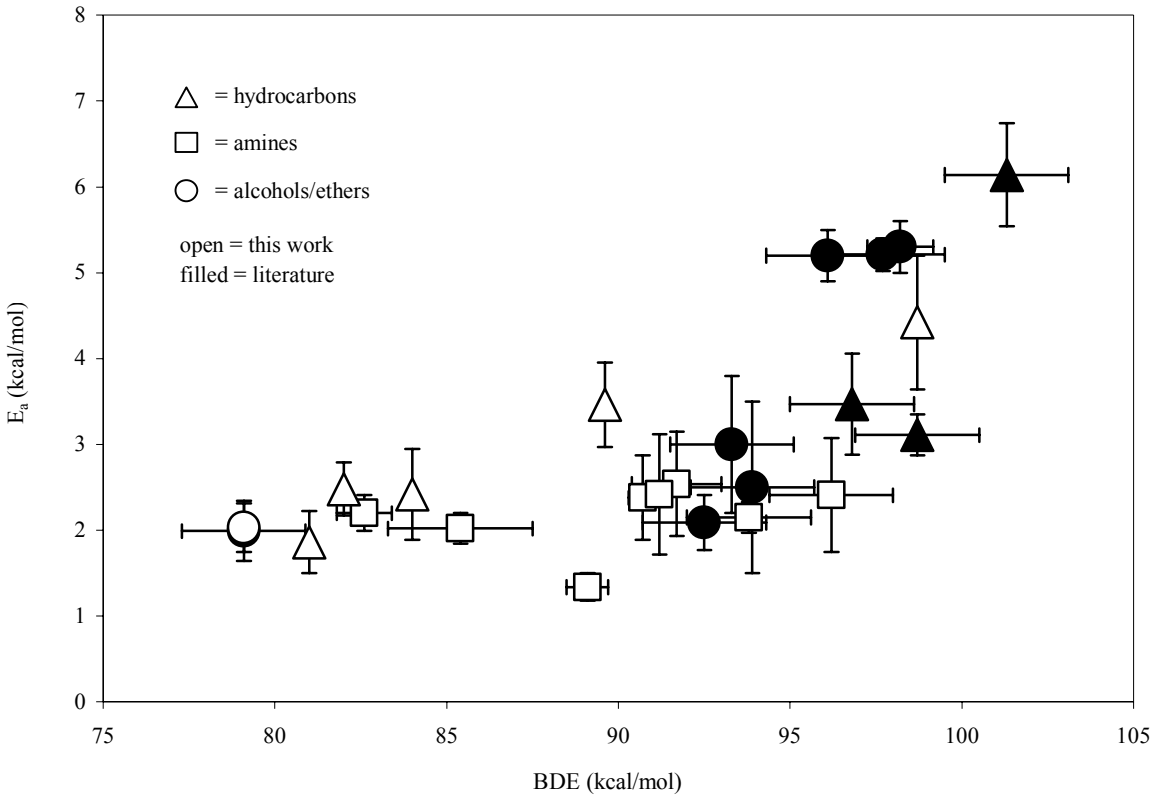

for hydrogen abstraction processes).

Figure 2.3. Activation energy for hydrogen abstraction by *t*-BuO• vs. C-H BDE

From this region of the plot, an α value of about 0.3 is obtained, suggesting an early transition state reminiscent of other high reactivity/low selectivity radicals such as Cl•.[76] (However, unlike the rate constants for hydrogen atom abstraction by Cl•,[84] the rate constants

are well below the diffusion-controlled limit). For substrates with C-H BDE's less than 92 kcal/mol, observed in the lower region, the activation energy levels off to a value of about 2 (± 0.5) kcal/mol and does not vary significantly with C-H BDE ($\alpha = 0$). Referring back to Figure 2.1, this trend separation was observed when examining the absolute rate constants as well.

2.4. SOLVENT VISCOSITY EFFECTS ON k_H.

An activation energy of ca. 2 kcal/mol is very close to the activation energy for viscous flow for relatively low viscosity solvents such as benzene, and the possibility that the level region of Figure 3 might be attributable to the onset of diffusion control was addressed. This was accomplished by examining the effect of solvent viscosity on k_H for substrates with BDE's less than 92 kcal/mol and with low E_a's. The rate constant for hydrogen atom abstraction from three tertiary amines (N,N-dimethylaniline, N,N-dibenzylaniline, and tribenzyl amine) was measured in several *n*-hydrocarbon solvents and benzene. Christopher Wohl conducted most of these experiments in connection to learning laser flash photolysis. The results are summarized in Tables 2.3 and 2.4.

Table 2.3. Effect of solvent viscosity on the rate constant for hydrogen abstraction from N,N-dimethylaniline by *t*-BuO• at 25 °C

Solvent	η (cP)	k_H ($M^{-1}s^{-1}$)
n-C_5H_{12}	0.225	1.2×10^8
n-C_6H_{14}	0.293	1.1×10^8
n-C_8H_{18}	0.518	1.1×10^8
C_6H_6	0.831	1.1×10^8
n-$C_{14}H_{30}$	1.92	9.7×10^7
n-$C_{16}H_{34}$	2.9	7.8×10^7

Table 2.4. Effect of solvent viscosity on the rate constant for hydrogen abstraction from N,N-dibenzylaniline and tribenzylamine by *t*-BuO• at 25 °C

Substrate	k_H ($M^{-1}s^{-1}$) in pentane (η = 0.2 cP)	k_H ($M^{-1}s^{-1}$) in benzene (η = 0.8 cP)	k_H ($M^{-1}s^{-1}$) in hexadecane (η = 3 cP)
N,N-dibenzylaniline	5.5×10^7	4.8×10^7	5.6×10^7
tribenzylamine	2.2×10^7	1.9×10^7	1.9×10^7

Based upon the Stokes-Einstein and von Smoluchowski equations, it is expected that the diffusion controlled rate constant (k_{diff}) will vary linearly with the inverse of solvent viscosity (at constant temperature).[79] In Figure 2.4, the effect of solvent viscosity for the reaction of *t*-BuO• with N,N-dimethylaniline (C-H BDE = 91.7 kcal/mol; E_a = 2.54 kcal/mol) is compared to the effect of solvent viscosity on a *bona fide* diffusion controlled reaction—combination/disproportionation of the *t*-butyl radical (using data of Schuh and Fischer).[85]

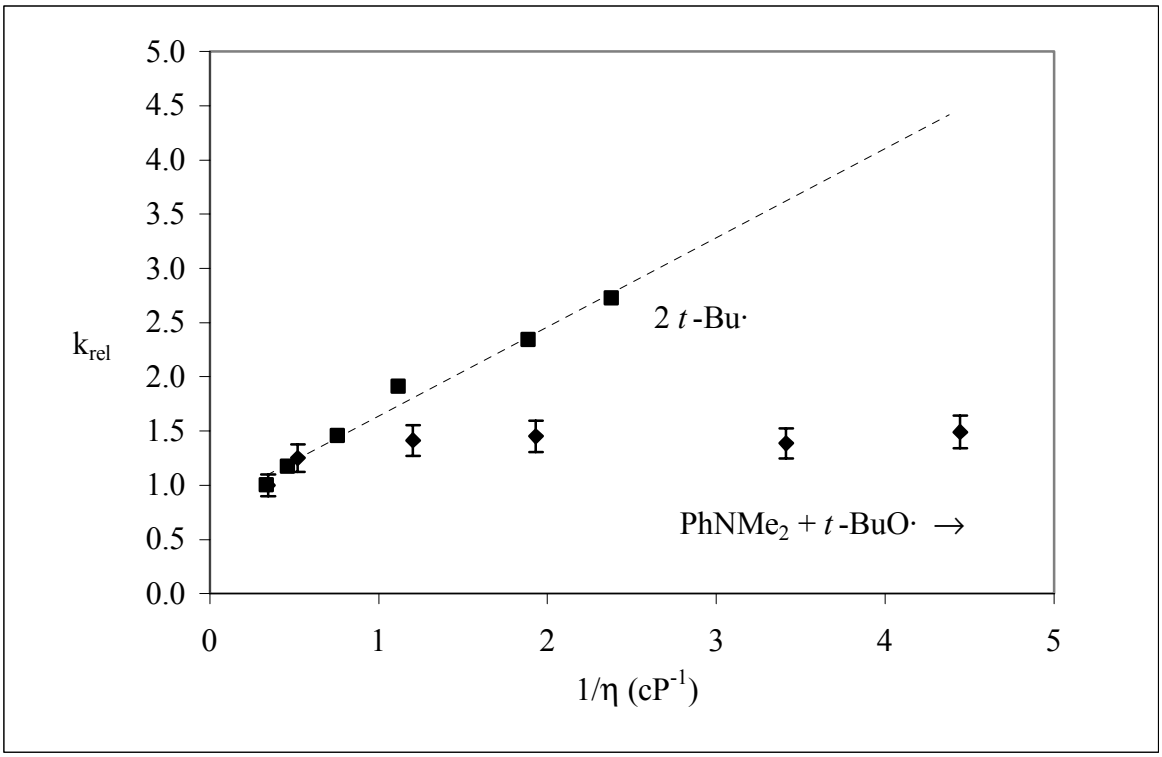

Figure 2.4. Solvent viscosity effect-hydrogen atom abstraction N,N-dimethylaniline by *t*-BuO• compared to a *bona fide* diffusion controlled

reaction (Data from Table 2.3 and reference [85])

This figure demonstrates that there is no significant effect of solvent viscosity on the rate constant for hydrogen atom abstraction from N,N-dimethylaniline by *t*-butoxyl radical. For other substrates in the "level" region of the E_a vs. C-H BDE plot such as N,N-dibenzylaniline (C-H BDE = 89.1 kcal/mol; E_a = 2.01 kcal/mol) and tribenzylamine (C-H BDE = 85.4 kcal/mol; E_a = 1.34 kcal/mol), a one order of magnitude variation in solvent viscosity had no discernable effect on k_H (Table 2.4). Consequently, it appears that the leveling off observed in the E_a vs. C-H BDE plot cannot be attributed to the onset of diffusion control.

2.5. POSSIBILITY OF ERRORS IN ARRHENIUS PARAMETERS

There are several possible explanations for the observation that the activation energies are independent of BDE (for substrates with C-H BDE < 92 kcal/mol). There are errors associated with the measurement of both E_a and the C-H BDE and a fair amount of scatter in the data. The absolute rate constants used to calculate the Arrhenius parameters and their corresponding Arrhenius plots are recorded in Tables 3-16 and Figures 2-15 in Appendix A. These errors in generating these plots may be obscuring an actual linear relationship between these two quantities.

With regard to errors in the reported activation energies, there has been some discussion in the literature regarding what is often referred to as a compensation effect in regression analysis (*i.e.*, within limits of uncertainty, the data can be fit equally well with a lower E_a/log(A) or higher E_a/log(A)).[86] However, at the present time, there appears to be no clear consensus as to how to report the error in E_a or log(A) in order to account for this compensation effect. Traditional format is to report standard errors or 95% confidence limits derived from the regression analysis. In addition, there has been discussion of the use of the linearized vs. non-linearized forms of the Arrhenius equation, and the issue of proper weighting of the data.[86-88] no defined conclusion has been made with this argument at the present moment.

In these experiments, a temperature range of ca. 10 – 80 ^{o}C was used to avoid freezing the solution or thermal decomposition of the *t*-BuO• precursor, di-*t*-butyl peroxide). For the data presented in Table 2-2, 95 % confidence limits are provided for E_a and log(A) based upon the regression statistics. Under the assumption that the error in k_H was independent of temperature, these values are derived from the fitting of the non-linear equation. However, it should be noted that within reported error limits, the results are identical using the linearized form of the Arrhenius equation. Finally, in addition to spot-checking our technique by repeating Arrhenius studies previously reported in the literature, several of the new experiments were performed and repeated several times in their entirety throughout the course of this study. All of the results from these repetitions are shown in Table 17 in Appendix A. Accordingly, there is confidence in the accuracy and reproducibility of the values of the Arrhenius parameters reported in this investigation and in the literature.

2.6. EXPLANATIONS FOR REACTIVITY

In looking deeper into the hydrogen atom abstraction reactions themselves, a few "chemical" explanations can be configured into these hypotheses.

2.6.1. Sterics

Steric interactions attributable to the bulky *t*-BuO• may force other, radical stabilizing substituents on the substrate out of conjugation with the developing radical center. For example, in the calculated (B3LYP/6-31G**) transition state for the reaction of *t*-BuO• and Ph_2CH_2, only one of the two phenyl groups is oriented properly to stabilize the developing radical center. The other phenyl ring is twisted out of conjugation, preventing stabilization. Similarly for Ph_3CH + *t*-BuO•, only one of three phenyl groups is oriented properly. With only one phenyl group available for stabilizing the transition state in each instance, it seems elementary to comprehend

why it has be observed that the activation energies for $PhCH_3$, Ph_2CH_2, and Ph_3CH are so similar. This stabilization can be observed pictorially from B3LYP (6-31G**) calculated transition states for hydrogen abstraction from a) toluene and b) triphenylmethane by *t*-BuO•, shown in Table 18 in Appendix A.

2.6.2. *Stereoelectronic Stabilization*

For the reaction *t*-BuO• + tertiary amines, stereoelectronic considerations are important.[11] Furthermore, interactions between the developing radical center and nitrogen lone pair in the transition state may be more important than interactions with other, radical stabilizing substituents (Eq. 17).

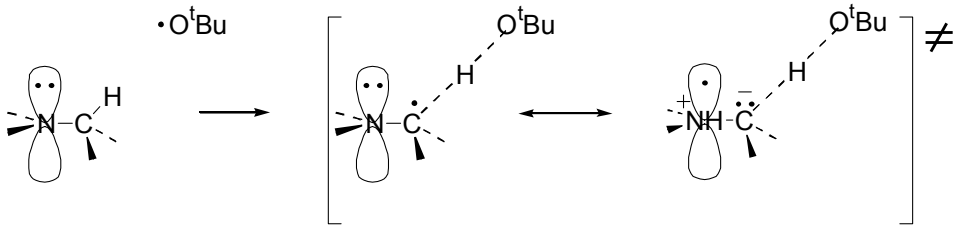

(17)

However, it should be noted that for bicyclic compounds, such as quinuclidine and DABCO, the nitrogen lone pair cannot provide this stabilization, yet the activation energies are only slightly greater than that of the other tertiary amines that do not possess this geometric constraint.

2.6.3. *Extreme Exothermic Reactions*

These hydrogen abstractions may be so exothermic that there is not a significant barrier associated with the bond making/bond breaking process. The nominal activation energies may result, once again, only from residual steric interactions between the bulky *t*-butyl group and the substrate. In connection with the reaction's exothermicity, Houk has examined the flexibility of the transition state for the reaction of hydroxyl radical and methane (HF/3-21G and MP2/6-31G**). He has found that lengthening the C-O bond in the transition state by 0.1 Å over the optimum length increases the activation energy by 1.2 kcal/mol.[89] For substrates with weak C-H bonds, although one would expect that the E_a would decrease with increasing bond strength, this trend may be interrupted because *t*-BuO• cannot get close enough to the substrate in the transition state to attain the optimal bond length.

The experimental results do not allow us to determine which (if any) of the possibilities is most likely and in future work, this will be addressed by current theories pertaining to hydrogen abstraction reactions (*e.g.*, the Zavitsas non-parametric model for calculating activation energies of hydrogen abstraction reactions,[90,91] Roberts' extended Evans-Polanyi relationship,[92] and recent approaches offered by Mayer.)[93,94] *Ab initio* calculations of transition state structures and energetics will also be performed.

The final issue, in trying to understand this species' reactivity, pertains to the magnitude of log(A), which via Eq. 16, is directly related to the entropy of activation. The statement that most hydrogen abstractions (from carbon) by *t*-BuO• are entropy-controlled does not necessarily mean that the entropy requirements in the transitions states for these reactions are unusually stringent. For the substrates listed in Table 2.1, $\Delta S^{\neq}$ ranges from - 8 to -19 eu. These values are smaller than bimolecular reactions that require a high degree of order in the transition state such as the Diels-Alder reaction. For example, for the dimerization of cyclopentadiene[10] and reaction of maleic anhydride with 9,10-dimethylanthracene,[95] $\Delta S^{\neq}$'s are -29 and -39 eu, respectively.

At this time, it is not clear whether or not log(A) varies in any sort of systematic way with structure. A plot of log(A/n) vs. C-H BDE (Figure 2.5, where n is the number of abstractable hydrogens) shows that for most substrates, log(A/n) hovers around 8.0. In looking

at the substrate groups, it appears that tertiary amines consistently have a slightly higher log(A/n) than aromatic hydrocarbons. With the debates on experimental errors with these types of results, experimental error associated with these values and the scatter seen in Figure 2.5, no meaningful conclusions can be drawn at this time.

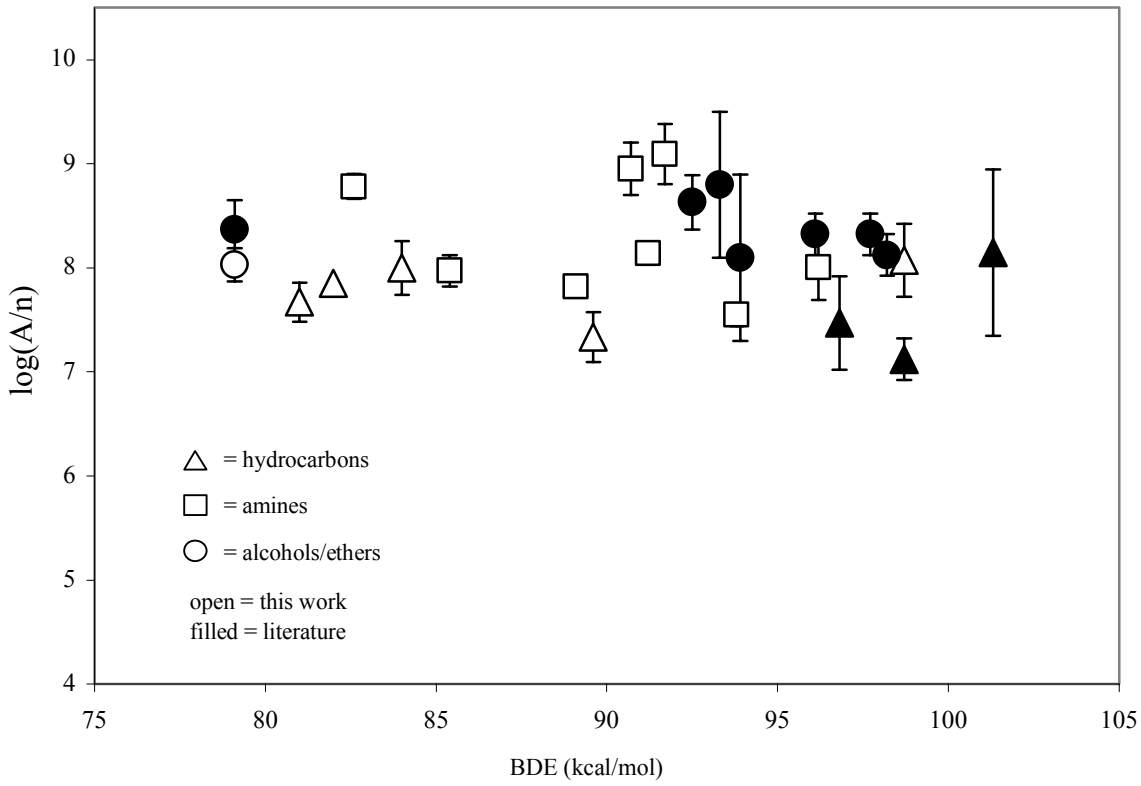

Figure 2.5. Variation of log(A/n) for hydrogen abstractions by *t*-BuO• as a function of C-H BDE (n is the number of abstractable hydrogens

2.7. CONCLUSION

This study of *t*-butoxyl radical was conducted to try to understand the alkoxyl radical's reactivity to a greater extent. In trying to gain a better understanding, the number of absolute rate constants and Arrhenius parameters for the hydrogen atom abstraction by *t*-butoxyl radical from different substrates has been greatly expanded (Table 1, Appendix A). The results discussed throughout this study have raised many new questions regarding the chemistry of this intermediate and alkoxyl radicals in general. Although new inquires have arose, some significant conclusions can be drawn from these results. First off, most hydrogen atom abstractions from carbon, at room temperature, by *t*-BuO• in solution are entropy-controlled. The free energy barrier for this reaction is governed more by $T\Delta S^{\neq}$ than by $\Delta H^{\neq}$. Across all the compounds examined, it has been shown that for substrates with C-H BDE > 92 kcal/mol, normal reactivity trends are observed; the activation energy decreases with decreasing C-H bond strength. When reacting with substrates with C-H BDE < 92 kcal/mol, the activation energy levels at a value of approximately 2 kcal/mol. Solvent viscosity studies demonstrated that this leveling is not attributable to the onset of diffusion controlled reactions.

The necessity for this study surfaced due to the use of *t*-BuO• as a chemical model for reactive oxygen-centered radicals in a variety of contexts. With all the new results and conclusions about this alkoxyl radical presented, its seems appropriate to mention a few observations about the correct use of this radical. As stated before, for reactive substrates, hydrogen atom abstractions by *t*-BuO• are dominated by entropy considerations. Due to this conclusion, any intrinsic reactivity trends associated with a substrate, or class of substrates, would almost be completely masked by the entropic control of the reactions. At this moment, it appears that much of the reactivity behavior associated with *t*-BuO• is unique, arising mainly from numerous issues pertaining to steric bulk. Therefore, *t*-BuO• may not be representative of other (smaller) alkoxyl radicals or other reactive oxygen-centered species in general. In any case, these new findings should be considered when deciding if *t*-butoxyl radical fits into being used as a chemical model.

2.8. FUTURE WORK

The goal of this study was to investigate *t*-butoxyl radical and try to understand its reactivity and selectivity properties better. It was the hope that by thoroughly understanding this alkoxyl radical, it may be used as a better chemical model for other biological systems. However, as shown by the results, *t*-butoxyl radical appears to undergo many steric considerations during its reactions. The large *t*-butyl group on the back of the oxygen-centered radical hinders this overly reactive species from reacting via normal reactivity considerations, decreasing its ability to be used as a model.

In an effort to design better chemical models, the size of the alkyl group on the alkoxyl radical needs to be addressed. Other oxygen-centered radicals need to be designed and investigated for their reactivity properties and their ability to model biological systems. Peroxyl radicals have been reviewed and compared to the reactivity with *t*-butoxyl radical. However, these radicals do not address the issue of steric bulk. All other alkyl peroxides are too reactive/explosive to generate the alkoxyl radicals through thermal or photochemical intiation. Consequently, new methods for generating alkoxyl radicals need to be pursued. Newcomb *et al.* investigated a class of *p*-nitrobenzenesulfenate esters as a precursor for generating different alkoxyl radicals using laser flash photolysis.[96] Both *t*-butoxyl radical and cumyloxyl radical have been generated through this method.

In continuing with the search for a better chemical model, it is the new direction of this project to generate smaller alkoxyl radicals, such as methoxyl or ethoxyl, using this new method with sulfenate esters in the laser flash photolysis system. By examining the abstraction rate constants and Arrhenius parameters for these new oxygen-centered radicals, more reactivity trends and conclusions can be determined about the reactivity for *t*-butoxyl radical. It is believed that by decreasing the steric bulk of the alkoxyl radical, the entropy concerns on these reactions will decrease, allowing the reactions for follow normal reactivity trends. With the compilation of all these results, these trends and conclusions will allow other investigators to make more educated decisions on the chemical models they want to utilize in studying their biological or enzymatic systems.

CHAPTER 3. HISTORICAL OVERVIEW OF RADICAL ANIONS

3.1 INTRODUCTION

Neutral free radical intermediates are not the only highly reactive, paramagnetic species that are interesting and significant to study using laser flash photolysis. In recent years, radical ions, i.e. radical anions and radical cations, have emerged as important intermediates in numerous organic and bioorganic reactions. Radical cations have been examined thoroughly in the realm of gas phase reactions through the use of mass spectrometry.[97] Although still difficult to examine, radical anions are more manageable to examine under more conventional techniques. Radical anions are generated from compounds with >C=C<, >C=N-, and >C=O functionalities. Much of the earlier studies centered around work conducted on the photoreduction of acetophenone and benzophenone, being two available ketones with reducible carbonyl functionalities. Radical anions from different substrates have been used to develop new synthetic methods, opening a new door into the world of single electron transfers. These intermediates have also been examined for their use as mechanistic probes, when certain groups, such as cyclopropyl substituents are incorporated into the compounds. The ring opening process of these cyclopropyl substituents have been examined by observing and measuring rate constants for the rearrangement of the cyclopropylcarbinyl radical under different conditions.[98-100] Electrochemical work, conducted by this research group, has been reported on different radical anions from substituted phenyl cyclopropyl ketones. Rate constants for the decay of these radical anions have been reported, some of them measuring to be $>>>10^7$ s^{-1}, and reaching close to the upper limit of this technique.

The purpose of this study is to re-examine many of these unsaturated compounds using the laser flash photolysis technique to observe the resulting radical anion and measure the observed rate constants for its decay. Hopefully the results from this study will add evidence to the interesting story unfolding for these significant radical anions.

3.2. RADICAL ANIONS

3.2.1. *Generation*

Radical anions of carbonyl compounds, commonly referred to as ketyl anions, have been previously generated by four different methods (Figure 3.1).

1) Direct chemical or electrochemical reduction of carbonyl compounds

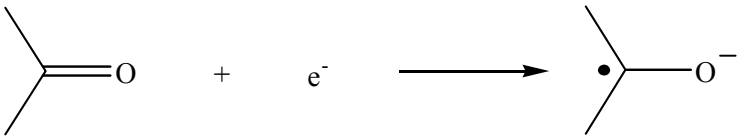

2) Deprotonation of ketyl radicals

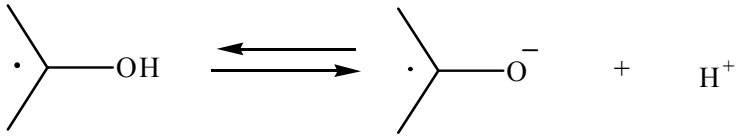

3) α-Hydrogen abstraction from alkoxides

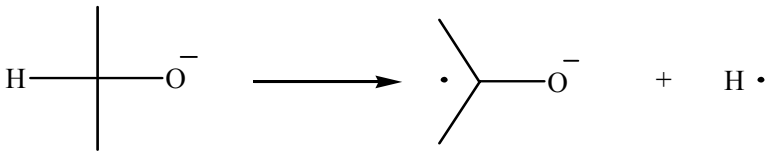

4) Photo-induced electron transfer (PIET)

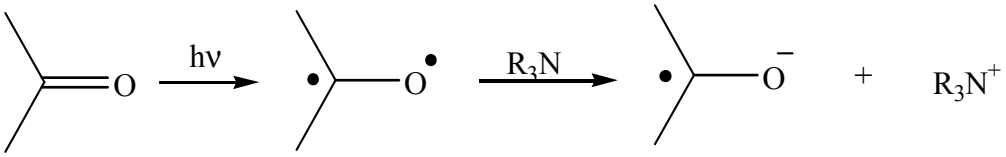

Figure 3.1: Generation of ketyl anions in solution

Each of these methods have been utilized in the literature to study these intermediate species.[101-103] The main process, direct chemical or electrochemical reduction, was originally discovered to occur using alkali metals or electrochemical techniques, with the most classic example being the reduction of benzophenone with sodium metal.[101] This reaction resulted in a deep blue colored solution, due to the generation of $\{Ph_2C=O^{\bullet-}\ M^+\}$ in solution. Reaction 2 in Figure 3.1 depicts the abstraction of a hydrogen atom from a neutral free radical to generate the ketyl anion. However, this method for generating radical anions lies within an equilibrium, producing very little of the desired intermediate.[104]

The third method has become a much less common procedure in generating radical anions. In this process, the ketyl anion is generated by abstracting an α-hydrogen from an alkoxide. The abstraction actually has been observed to occur via a free radical chain process initiated by another previously reduced compound in solution, such as an aryl halide, as shown in Scheme 18.

Scheme 18

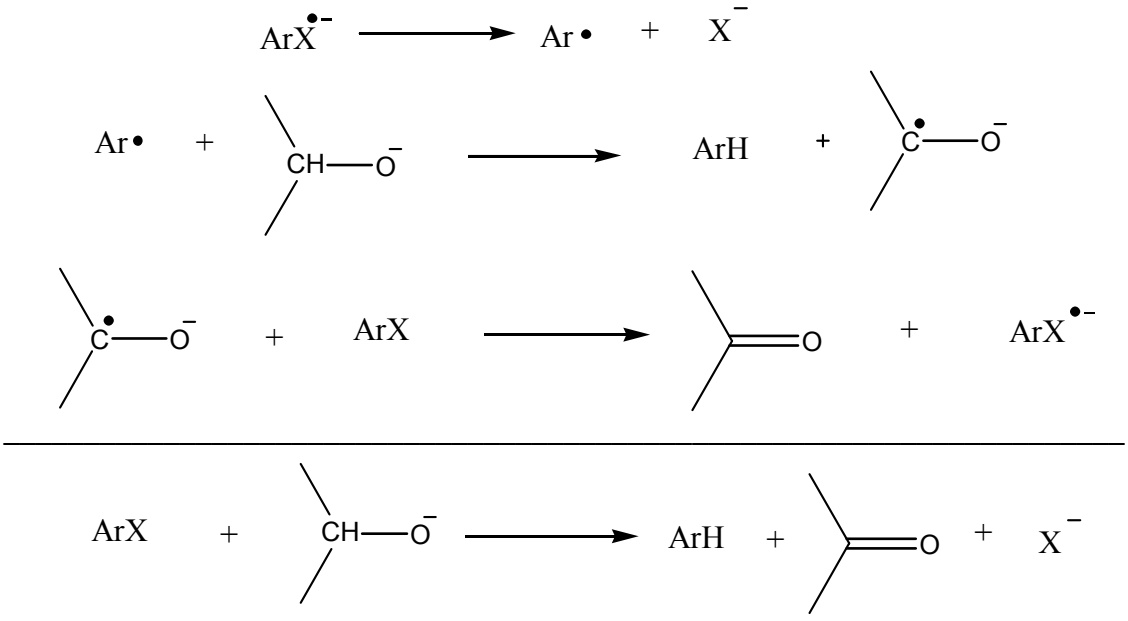

The halide is usually reduced by electrochemical means. This process was utilized to study the oxidation of primary and secondary alcoholates into aldehydes and ketones.[105] The radical

anions of these alcoholates can be oxidized with the absorption of a second electron in solution into their carbonyl compounds. Due to the number of reactions and substrates needed for this process to occur, it is not very conducive to studying the ketyl anion produced.

Reaction 4 in Figure 3.1 illustrates generating radical anions photochemically via photoinduced electron transfer (PIET). Unsaturated compounds, such as aryl ketones, can be excited to their triplet state through photochemical excitation. The 2° or 3° amine then acts as a single electron donor, allowing the triplet to accept the electron and generate the radical anion.[106] The first radical anions to be observed were generated from benzophenone and acetophenone.[107] Both of these substrates were photochemically excited to their triplet state and then reduced to their radical anions using *sec*-butylamine or triethylamine. The benzophenone radical anion, in a triethylamine solution, was found to have an absorption peak at 760 nm at 183 K. The acetophenone radical anion gave rise to an absorption maximum at 480 nm at 173 K.

Due to its application for mechanistic investigations, the ketyl anion/ammonium radical cation pair formed in this reaction and many other of these ion-pair intermediates, including contact radical ion pairs and solvent-separated radical ion pairs, have been examined. However, it is the formation of these pairs that control the products formed and make it difficult to maintain. Without complete control over the desired intermediates or products, studying the generated radical anions themselves becomes difficult.

3.2.2. *Reactions of Radical Anions*

Radical anions have been found to be able to react in many different capacities, depending on the reaction conditions in solution. Figure 7 shows examples for the main reactions that have been studied for these reactive intermediates.

In looking at the reactions for radical anions, the most basic reaction involves electron transfer from the reduced functionality to another substrate, as shown in Figure 3.2, reaction 1. The reduction process has been successfully studied through electrochemical means and used for preparative and analytical processes, often as a catalyst. For this reaction, the carbonyl

compound can often be used as an electron transfer mediator; the reduced substrate then undergoes other chemistry. This technique has been seen to be very effective in measuring different kinetic and thermodynamic data for substrates that are difficult to reduce under normal conditions.[108-110]

With electron density centralization in the functional groups, the generated radical anions have the ability to react as a base. As shown in Figure 3.2, reaction 2, the $>C=O^{\bullet-}$ can react as a Bronsted base and abstract an hydrogen from a donor, generating a neutral free radical. This reaction has been observed many times when the reactions are carried out under acidic conditions or when producing radical anions via PIET, which use $R_3N^{\bullet+}$ with available α-hydrogen. Since this reaction produces neutral free radicals, studies conducted on this process are outside the scope of this literature review.

In connection with reaction 2, the radical anion can also react as a Lewis base (e.g. nucleophile) with an electrophile in solution. This reaction is illustrated in Figure 3.2, reaction 3. The radical anion can react with an alkyl halide and under a direct nucleophilic single replacement with the substrate. However, in a study conducted by Garst and coworkers, evidence has surfaced that this alkylation reaction actually undergoes a SET reaction initially, followed by addition to the carbonyl functionality.[111,112]

These first three reactions are related to ketyl anions, but do not allow for them to be studied individually. They will not be examined further in this literature review.

Reactions 4 and 5 shown in Figure 3.2 have synthetic applications that have been utilized in different reaction such as dimerizations or pinacolizations.[113] In order to understand these reactions, the rate constant for these reactions, such as $Ph(C=O^{\bullet-})t$-Bu with a 1° radical, have been measured, equaling about 1×10^8 $M^{-1}s^{-1}$.[114] Analogous reactions, such as an electrochemically induced novel ketone/imine coupling process, have also been studied thoroughly.[115] Although these applications are extremely interesting and very useful, the main reaction of interest studied in this project is shown in reaction 6, Figure 3.2. These fragmentations can be utilized in mechanistic studies and probe experiment, which is the central direction of this project. The focus of this literature review centers around the fragmentation or rearrangement of ketyl anions from different substrates and the decay of these radical anions under certain conditions.

(1) electron transfer

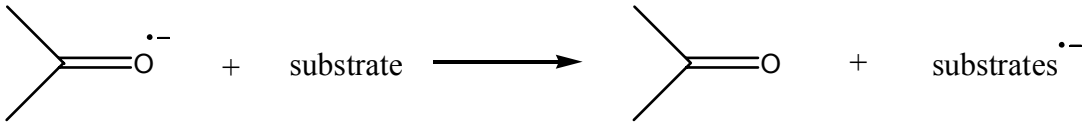

(2) proton transfer

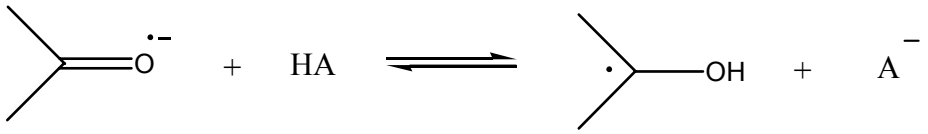

(3) reaction with electrophiles

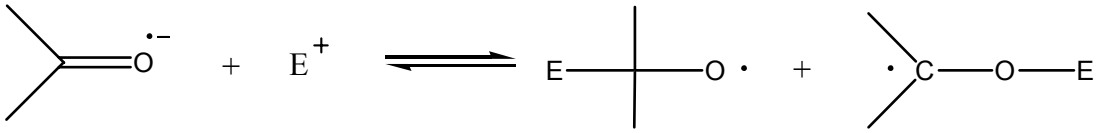

(4) reaction with radical or radical ions

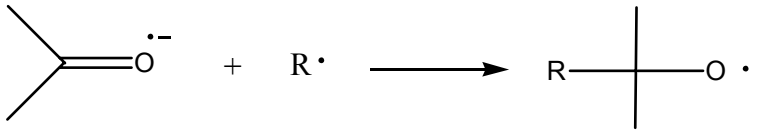

or

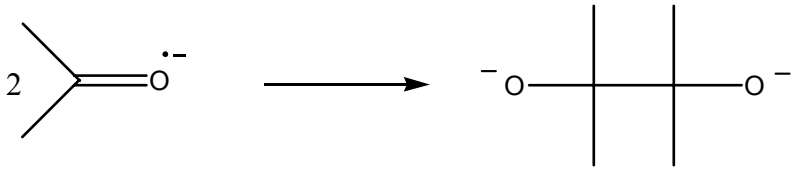

(5) addition to π-systems

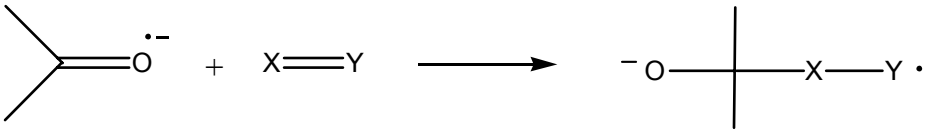

Figure 3.2. Reactions of radical anions

(6) fragmentation

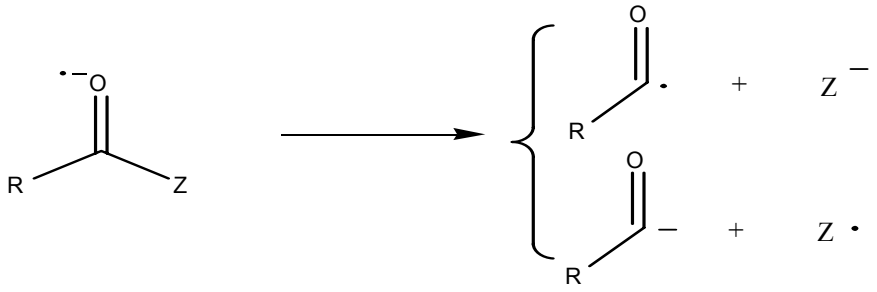

(a) α-cleavage

(b) β-cleavage

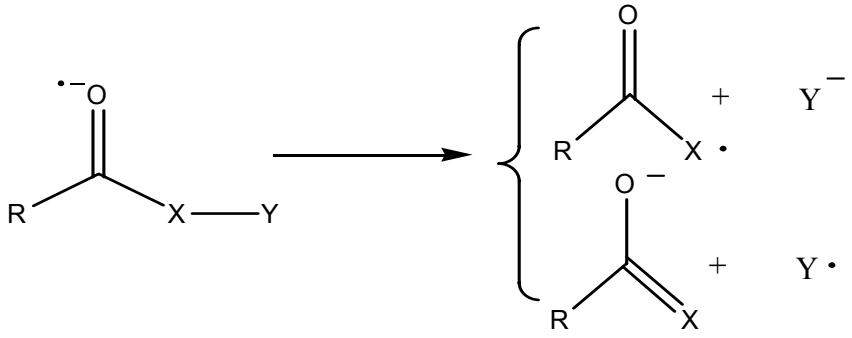

Figure 3.2.(cont.) Reactions of radical anions

3.3. LITERATURE REVIEW

3.3.1. *Radical Anion Fragmentation*

When studying the decay of certain radical anions, they have been observed to decay extremely fast under certain conditions. These radical anions may undergo bimolecular reactions, unimolecular α or β-cleavage reactions, or ring opening reactions. Some of these decay pathways have been examined by studying different aryl alkyl ketones in an attempt to

understand the properties of radical anions.[116-118] Tanner and his collaborators studied the fragmentation of ketyl anion intermediates and measured the rate constants for these radical anion's β-cleavage and dehalogenation reactions. In these competition reaction experiments (Scheme 19), the radical anions (1) were generated by reaction with 1,3-dimethyl-2-phenylbenzimidazoline (DMBI).

Scheme 19

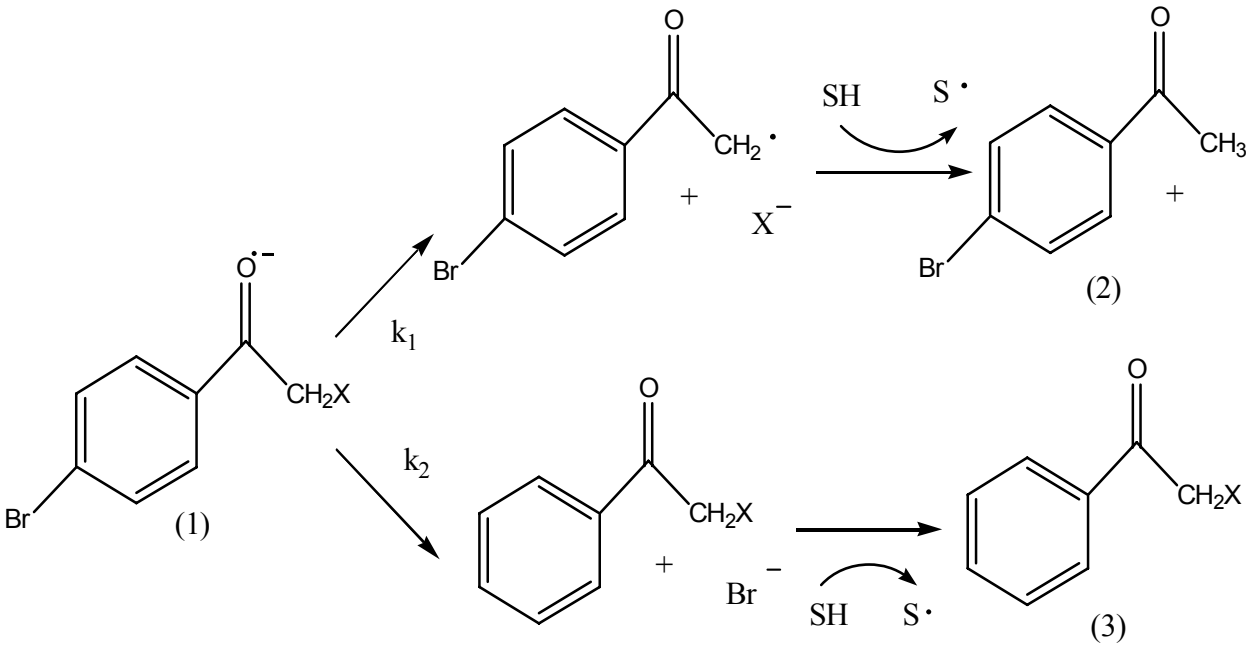

To determine the rate constants for these two reactions, the relative yields for the products 2 and 3 were measured. The results for the rate constant for β-fragmentation, k_1, are summarized in Table 3.1. In this study, it was assumed that the α-substituent did not affect the rate constant k_2. The dehalogenation rate constant, k_2, was determined to equal 3×10^7 s^{-1}.

Table 3.1. Rate constants for β-cleavage of several α-substituted acetophenone radical anions

X	k_1 (s^{-1})
Br, Cl	$>10^9$
F	5×10^9
$PhCO_2$	6.3×10^9
CH_3CO_2	9.6×10^6
PhO	9.5×10^6
PhS	9.3×10^6

The basicity of the substituents can be seen as the controlling factor for the change in β-fragmentation rate constant. As the basicity of X^- increased, the rate was observed to decrease. No significant lifetime was observed for the initial radical anion generated for any of the α-haloacetophenones examined. Due to the extremely fast nature of these intermediates, the study did not allow investigators to observe or record the spectra of the radical anions produced.

In examining substituent effects on α-phenoxyacetophenone radical anions, which also undergo β-cleavage reactions, Mathvivana *et al*. used a process which allowed the radical anions to be generated indirectly and observed using UV/vis spectroscopy.[119] This process allowed Mathvivana to record the spectra of desired radical anions in the UV/visible spectrum. With the ability to observe these intermediates, Mathvivana investigated substituent effects on the radical anion's absorption maximum and their decay rate constants. A representative sample of the results from the investigation of the reaction shown in Eq. 18 are shown in Table 3.2.

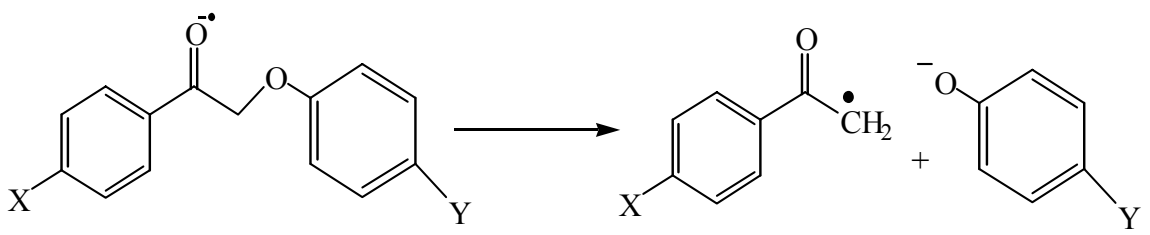

(18)

Table 3.2. Absorption maximum and decay rate constants for ketone radical anions in acetonitrile or DMF[a]

X	Y	λ_{max}, nm	k, s^{-1}
H	CH_2OPh	500[a]	7×10^6
H	$CH_2O(4\text{-}CH_3O\text{-}C_6H_4)$	490	5×10^6
H	$CH_2O(3\text{-}CH_3O\text{-}C_6H_4)$	490	1×10^6
4-CH_3	CH_2OPh	510	2.6×10^6
3-OCH_3	CH_2OPh	480	6.8×10^5
H	$C(CH_3)_3$	480	Long-Lived
3-$COCH_3$	CH_2OPh	540	Long-Lived
3-CN	CH_2OPh	530	Long-Lived
3-CF_3	CH_2OPh	510	Long-Lived

The results of this study demonstrated that the cleavage reaction shown in Eq. 18 was enhanced when substituent Y was electron withdrawing but retarded when X was electron withdrawing. The rate constant for β-cleavage of the radical anion was found to be slower when the X substituent was electron-withdrawing, as well as shifting the measured absorption towards the right of the spectrum. These radical anions measured to be much more long-lived (half-lives ≥ 10 μs) and decayed with mixed kinetics. With the generation of the radical center in the intermediate, the electron withdrawing group destabilizes the radical in the transition state. However, placing an electron withdrawing group in the Y position, the anion generated in the transition state would be enhanced, increasing the rate constant for β-cleavage.

3.3.2. *Dimethoxystilbene*

In investigations of reactive olefins, *trans*-4-4'-dimethoxystilbene (DMS) has been examined for its ability to isomerize or dimerize when excited/oxidized to its radical cation.[120,121] However, in Mathivanan's study, laser-induced photoexcitation of DMS in acetonitrile or DMF at 355 nm was performed to generate solvated electrons, in addition to the DMS radical cation and DMS radical anion (Scheme 3).

Scheme 19

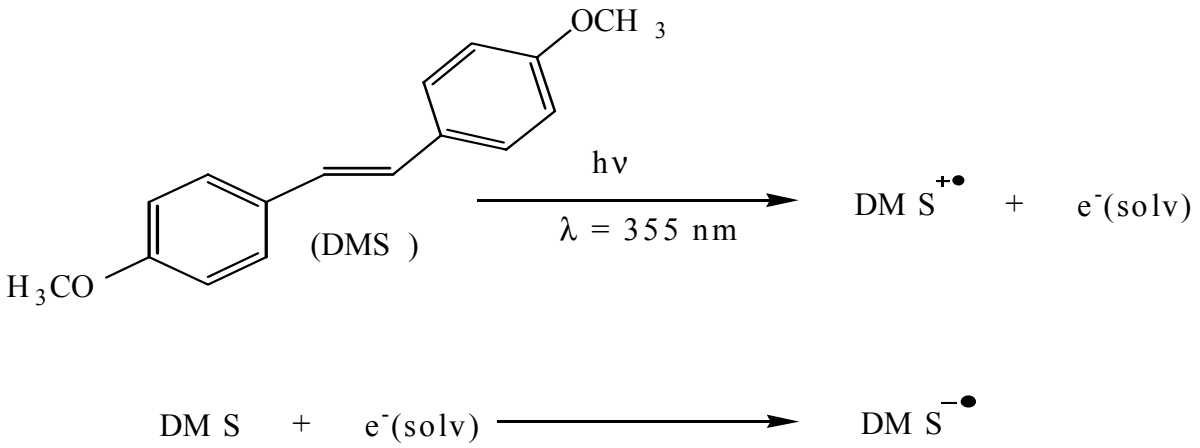

The UV/Visible spectrum generated from the excitation of DMS substrate shows an absorption at 530 nm for the $DMS^{\bullet+}$ and shows a shoulder around 490 nm for the DMS radical anion. The solvated electrons, released during this reaction can be trapped by aryl ketones to generate radical anions that are detectable by UV/visible spectroscopy. This method was developed to generate radical anions from photoreactive aryl ketones more efficiently. Once again, Mathivanan *et al.* used this procedure to study a series of α-(aryloxy)acetophenones that generate radical anions when trapping solvated electrons (Eq. 19).

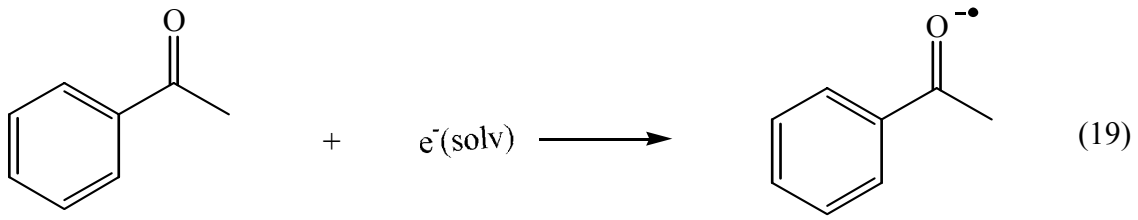

(19)

The extinction coefficient for DMS is extremely large at 355 nm. With the addition of the aryl ketones, the DMS substrate continues to be the major absorbing species in the solution. Direct excitation of the aryl ketone must be minimized because many of the studied aryl ketones absorb light at 355 nm and can be excited into their triplet states. In addition, in order to cleanly observe these generated radical anions in the UV/visible spectrum, the $DMS^{\bullet+}$ must be quenched almost immediately after excitation. To obtain this condition, tetrabutylammonium acetate/azide was used as a nucleophile to trap the $DMS^{\bullet+}$. Literature reports the quenching constant for tetrabutylammonium acetate with $DMS^{\bullet+}$ to equal 8.9×10^9 $M^{-1}s^{-1}$ at ambient temperature. Due to the persistence and absorbance of the $DMS^{\bullet-}$, the aryl ketone substrates were maintained at a concentration 10 times greater than DMS, in order to minimize the concentration of $DMS^{\bullet-}$ generated. The increased ketone concentration diminished the amount of the solvated electrons that could be absorbed by the DMS substrate, in order to generate the $DMS^{\bullet-}$.

Once this experimental protocol had been established, Mathivanan *et al.* generated the acetophenone radical anion to ensure that the indirect photoexcitation method worked before moving onto other substrates that can undergo fast unimolecular reactions. The reported spectrum for the acetophenone radical anion, using this method, showed an absorption maximum at 450 nm in 20% acetonitrile/80% water and 470 nm in pure acetonitrile, coinciding with previously reported values. He reported that transient signal at 470 nm had a decay rate constant of 7×10^5 s^{-1} in DMF for the decay of the acetophenone radical anion. The method was then confirmed by generating the radical anion of acetophenone through an electron transfer reaction between triplet acetophenone, generated by 266 nm excitation of the ketone, and triethylamine. This process generated an absorption at 450 nm for the radical anion, verifying the above procedure. Before venturing into unknown substrates, another commercially-available aryl ketone was examined. The *t*-butyl phenyl ketone radical anion was recorded to give absorption

at 480 nm in acetonitrile and measured to be a long-lived radical anion, comparable to acetophenone, under these conditions. It was also shown that if *t*-butyl phenyl ketone was excited directly at 355 nm, the resulting triplet state undergoes α-cleavage (Eq. 20) with a rate constant of 1 x 10^7 s^{-1}, giving evidence for the need to maintain DMS as the major absorbing substrate.

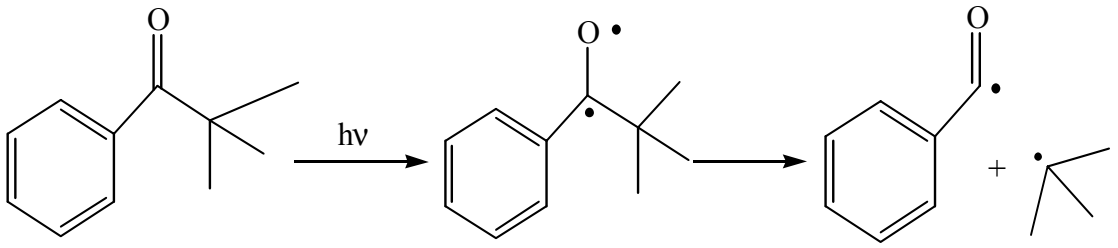

(20)

3.3.3. *Ring-opening reactions*

Many of the ketyl anions previously investigated contain conjugated cyclopropane rings and undergo ring opening reactions after the reduction of the carbonyl. These ring openings are very sensitive to stereoelectronic factors in the structure of the substrate. For this decay pathway to occur, the rupturing C-C bond in the cyclopropane ring must overlap with the π-system in C=O functional group. This stereoelectronic control was observed while investigating a new method for the stereospecific introduction of angular methyl groups during steroid synthesis.[122]

To understand the ring opening process of cyclopropane ring in a ketyl anion intermediate, previous work conducted on the cyclopropylcarbinyl radical itself offers some great insight into the reaction. The isomerization reaction, shown in Eq. 21, has become very well known in free radical chemistry.

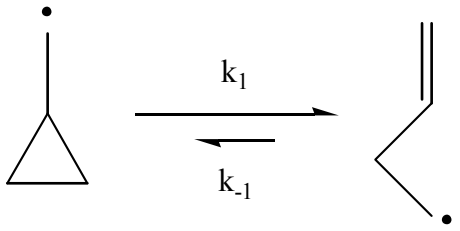

(21)

Using ESR spectroscopy, the rate of reaction for the forward reaction of this ring opening process was measured to be 1.3 x 10^8 s^{-1} at 25°C.[98] However, in this study, the equilibrium between these two intermediates was not even considered. Effio *et al*. investigated this equilibrium and found that the reaction lies towards the ring opened product with an equilibrium constant, K, equaling 1.3 x 10^4 at 25°C.[99]

The problem with studying these cyclopropylcarbinyl radical ring openings, and others like it, lies in the realm of detecting the resulting radical, since the alkyl radicals contain no chromophore to be detected. In past years, this issue has been corrected by reacting the interested radical using the "tin hydride" method and study the radical via an indirect method. However, this method has limits to the range of radicals can react with as well as a limitation due to its rate constant for radical trapping (k_H = 2.4 x 10^6 M^{-1} s^{-1} at 25°C). Many of the free radical rearrangements of interest are faster and would overwhelm the reaction kinetics. Newcomb *et al*. demonstrated the ability to measure these faster rate constants by reacting these intermediates with PhSH as a hydrogen donor to study the kinetics of these substrates (Scheme 20).

Scheme 20

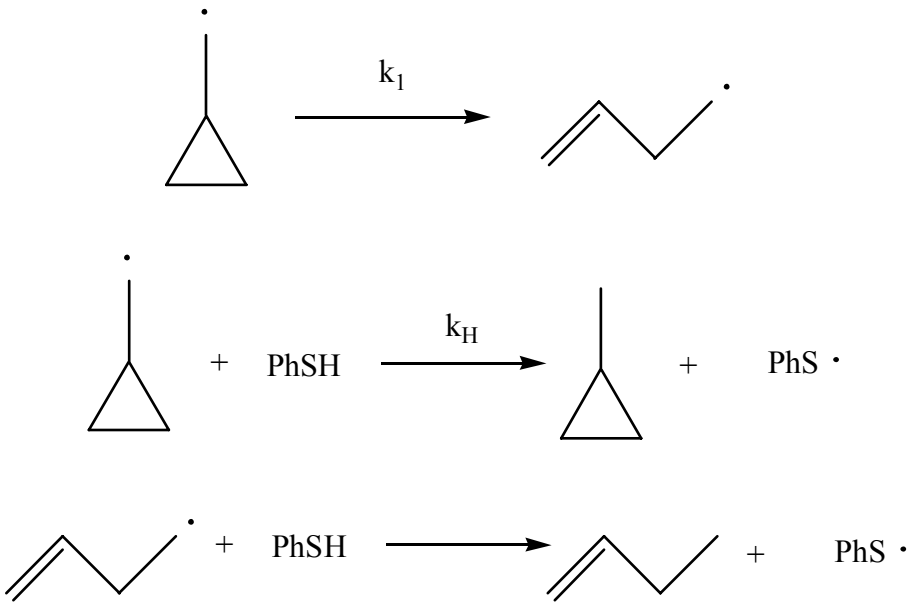

The study of this reaction was measured over a temperature range of –37 to 50°C to construct a reasonable Arrhenius function for this reaction. The rate constants measured with this method were consistent with previous results by Maillard and Effio.[99] By verifying these results, it was proven that this new method opened the door to investigate other fast free radical rearrangements and study different mechanistic probes previously unattainable.

Aryl cyclopropyl ketones have been under investigation recently for their use as mechanistic probes for electron-transfer reactions in organic reactions. Previous work done by Tanko *et al.* focused on ring opening reactions of different radical anions using electrochemical techniques. Tanko and Drumright provided evidence for the ring-opening of certain substituted phenyl cyclopropyl ketone radical anions.[114,123,124] Due to the radical nature of these intermediates, the rate constants for the decay of these radical anions are easily compared to the rate constants for ring opening of similar alkyl free radicals. This comparison can be found in Table 3.3.

Table 3.3. Effect of substituents on the rate of ring opening of cyclopropylcarbinyl radicals and related radical anions

Reaction	k_1 (s^{-1})	k_{-1}(s^{-1})	Ref.
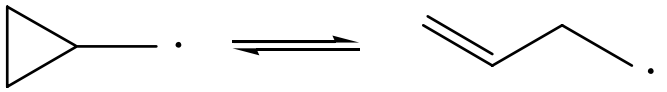	1.2×10^8	5×10^3	3
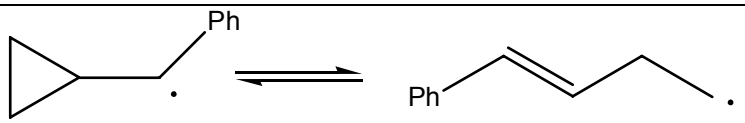	1×10^6	1.2×10^7	125
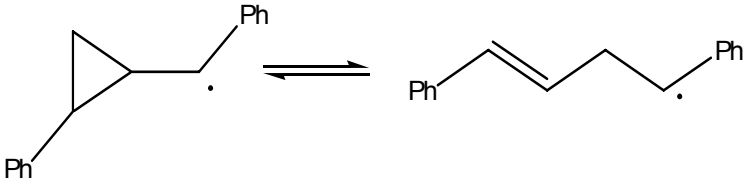	3.6×10^8	----	126
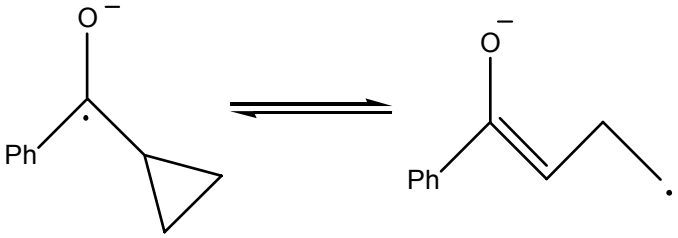	≤ 2	8×10^7	123
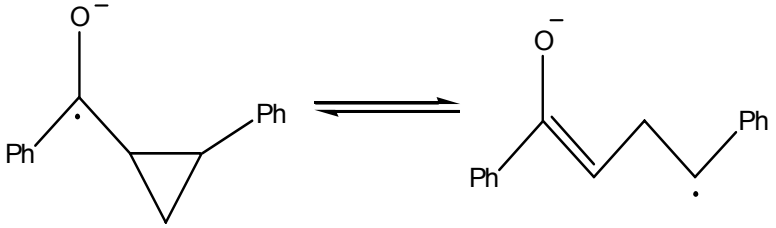	1×10^7	----	127
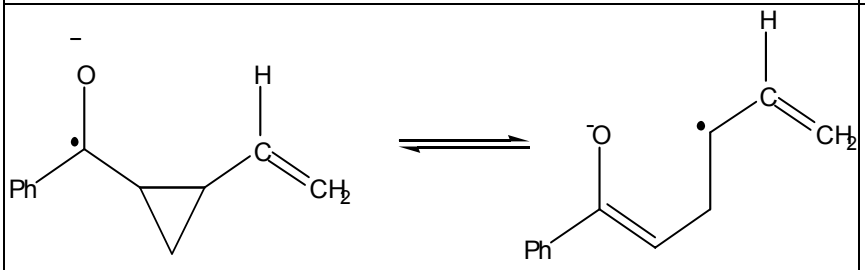	$\geq 5 \times 10^5$	----	127

Looking at the cyclopropylcarbinyl radicals, the release of the ring strain drives the reaction to its ring opened form, although all of the reactions are found in equilibrium between the two forms. In addition, the measured rate constants showed sensitivity to the stability of the resulting radical. In the phenyl substituted substrates, the equilibrium was forced towards the benzyl radical form, with a rate constant for the backward reaction measuring a full order of magnitude greater than the forward.[126]

Tanko *et. al.*'s study illustrated that radical anions undergo the ring opening rearrangements as fast or faster than the alkyl radicals. However, the equilibrium constants were found to be in much greater favor towards the ring closed forms for some of the ketyl anions. Phenyl cyclopropyl ketone's radical anion was found to favor its ring-closed form, having a rate constant $\leq 2\ s^{-1}$ for the ring opening decay pathway. This ring opening equilibrium can be shifted by adding radical stabilizing substituents on the cyclopropane ring. The ketyl anions were investigated in a subsequent study and measured to have greater decay rate constants for the ring opening pathways.[123] Once again, it is the generation of a benzyl radical or π-system stabilized radical that stabilizes the intermediate. Many of these conjugated aryl ketones studied by this group will be re-examined in this LFP study.

3.3.4. *Hypersensitive Probe for Single Electron Transfer*

As stated before, the motivation to examine these ketyl radicals lies within their exploitation as a mechanistic probe for single electron transfers in organic reactions. Some radical anions do not undergo the expected ring opening process due to factors such as strain energy and resonance energy.[114,123,124] However, investigations conducted in this research group have shown that the radical anion generated from 1,1-dimethyl-5,7-di-*tert*-butylspiro[2.5]octa-4,7-dien-6-one through electrochemical reduction undergoes facile ring opening, just like the well characterized cyclopropylcarbinyl free radical.[127] This radical anion

rearrangement relieves ring strain and increases resonance energy in the molecule. The study of these substrates have demonstrated that this system is a highly effective "probe" to distinguish between SET and conventional polar pathways in reactions with nucleophiles with carbonyl compounds.[128] These pathways can be illustrated in Scheme 21.

Scheme 21

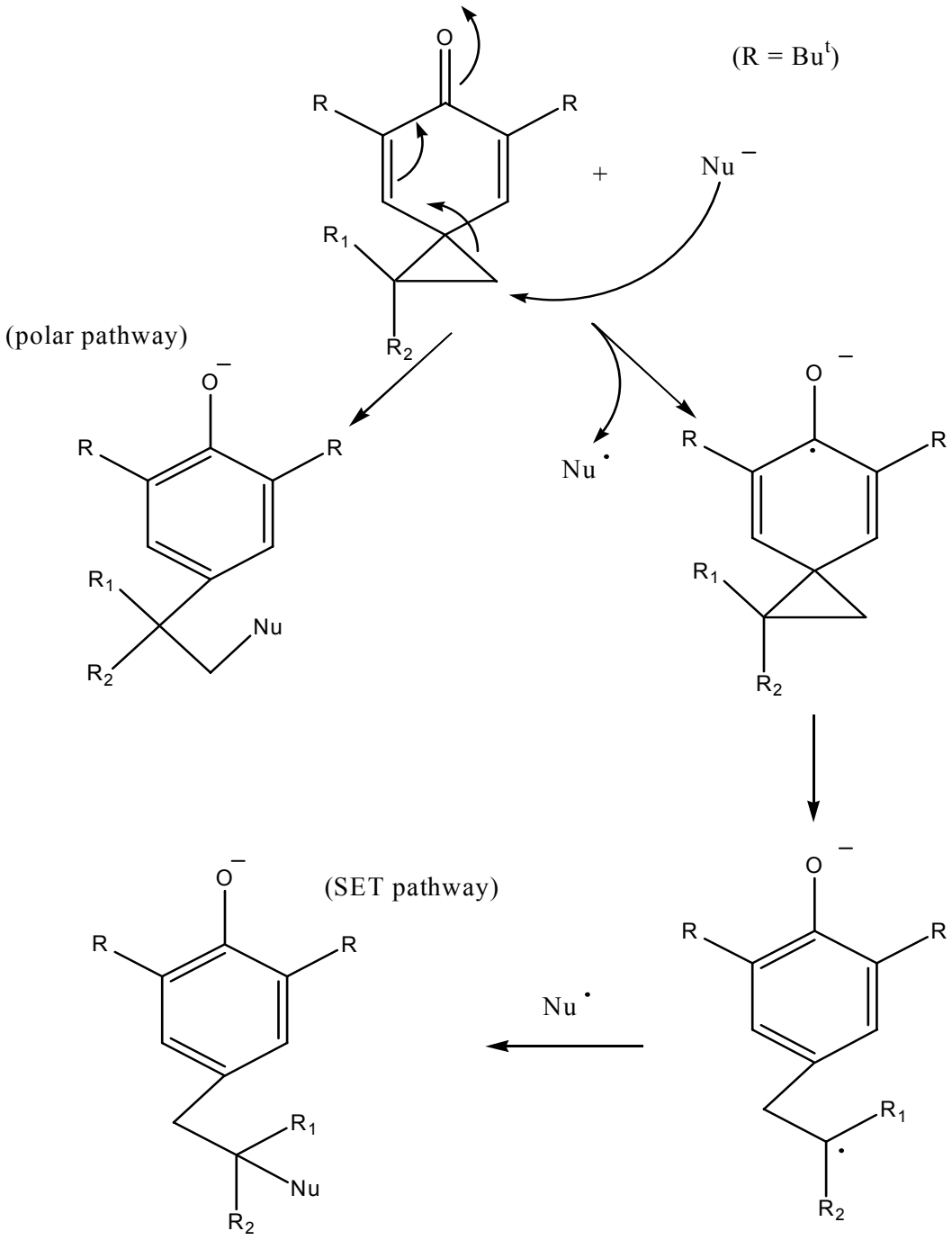

The products of these reactions were examined when the R-groups on the cyclopropane ring were: R_1 and R_2 = H, R_1 = H and R_2 = CH_3, and R_1 = CH_3 and R_2 = CH_3. All of the radical anions generated from these substrates showed ring opening products through the SET transfer reaction. Selectivity towards the more substituted, stable 3° radical intermediate was observed between the three compounds, identical to studies conducted on 2,2-dimethylcyclopropycarbinyl and 1-methylcyclopropylcarbinyl neutral free radical.[129] The rate constants for the ring opening of these neutral free radicals were measured to be $>10^8$ s^{-1}. It was assumed that the ring opening of these radical anions are comparable to these rate constants. This electrochemical study showed that the rate limiting step is the electron transfer, giving rise to the extremely fast ring opening reaction. Nevertheless, it was determined that the electron transfer and ring opening reaction was not concerted and these radical anions have a finite lifetime. The rate constants for electron transfer were measured with different mediators using electrochemical techniques. These substrates will be re-examined to obtain the rate constants for the ring opening rearrangements of these radical anions.

3.3.5. *Aromatic α,β-Epoxy Ketones*

The mechanistic study of radical anions has been expanded to include the photoreduction of α,β-epoxy ketones. The α,β-epoxy ketone triplet has been examined in previous work and was shown to undergo a number of decay pathways, including α or β-cleavage reactions. However, radical anions can be generated from these substrates, using alkylamine electron donors such as triethylamine or 1,3-dimethyl-2-phenylbenzimidazoline.[130-132] In numerous studies conducted by Hasegawa, product analysis after the quenching of different radical anions from the α,β-epoxy ketones illustrated only one true decay pathway for these ketyl anions, shown in Scheme 22.

Scheme 22

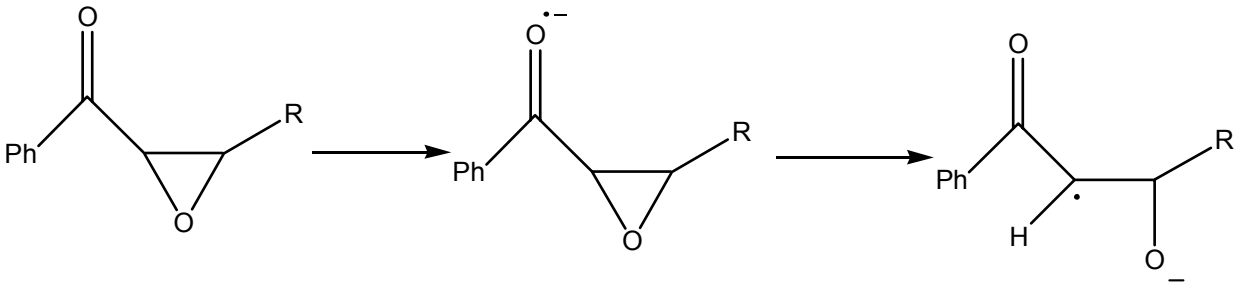

(R = H or Ph)

A diketone or β-hydroxy ketone appeared to be the main product for all of the different α,β-epoxy ketones examined. Cleavage of the epoxide ring from the opposite side did not generate the observed products. It is believed that after the radical anion/amine radical cation pair was generated, ring opening occurred and then a formal 1,2-hydrogen migration followed, shown in Scheme 23. The migration was found to take place with all the radical anions examined, although radical anions without the phenyl substituent in the R-position were found to be less stable. A few of these epoxides will also be examined in this radical anion study to measure the rate constants for ring opening of these radical anions.

Scheme 23

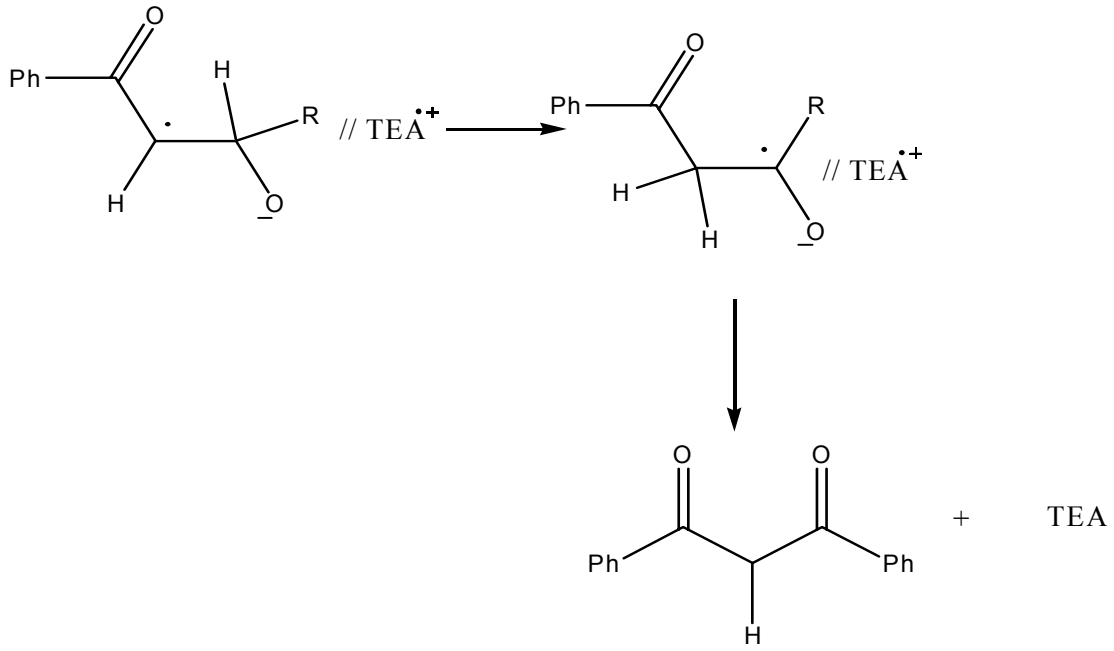

3.4. SUMMARY

Drawing attention to a cousin of the neutral free radical, investigations in recent years have uncovered the significance of radical anion intermediates in different organic and bio-organic reactions. These paramagnetic species are mostly generated from compounds with unsaturated functionalities. Many techniques have been used to facilitate their production and these reactive species have been seen to undergo a range of reactions, from acid/base reactions to addition and cleavage reactions.

A large number of the earlier studies on radical anions revolved around their ability to undergo β-cleavage reactions after generation. However, it has been difficult to obtain spectra of these intermediates. In recent studies, dimethoxystilbene has been used as an electron donor to generate the radical anions through an indirect excitation process with the laser flash photolysis technique. With this new technique, these β-cleavage reactions were investigated and the UV/visible spectra of the intermediates could be recorded and provide kinetic data.

Within studies of these reactive intermediates, different cyclopropyl carbonyl compounds have been investigated for their ability to undergo ring-opening process to allow the radical anion to decay. These decay pathways have been compared to the ring opening of neutral free radicals. These radical anion ring-opening processes have been investigated using electrochemical techniques and some rate constants for decay have been published. Radical anions generated from certain smaller aryl ketones were observed to be very persistent with this technique, showing no evidence for unimolecular decay pathways. However, compounds with extended conjugation and additional phenyl substituents showed a drastic increase in the decay rate constants, proving they undergo ring-opening processes. In addition, there have been significant investigations into the use of compounds as hypersensitive probes for single electron transfers. An investigation of these compounds and their reactive intermediates using laser flash photolysis will allow a more complete understanding of this interesting, and frequently overlooked species.

CHAPTER 4. RADICAL ANIONS GENERATED FROM ARYL KETONES

4.1. INTRODUCTION

The substrates examined in this study have been previously examined in this research group using electrochemical techniques, such as cyclic voltammetry.[114,123] Although these experiments measured rate constants for the decay of the radical anions, it did not allow for the determination of the intermediates. Using indirect excitation through laser flash photolysis of the electron donor, dimethoxystilbene, we now have the ability to examine these radical anions and record their presence in the UV/visible region, as well as verify previously measured decay rate constants.

Laser flash photolysis has become a very useful technique in studying different reaction intermediates that used to be invisible to investigators. In addition to being able to record the UV/visible spectra of these species, kinetic data, such as rate constants with greater magnitude (i.e. $>>>10^6$ s^{-1}), can be recorded with much more accuracy than previously used techniques. With using such a fast techique, rate constants for the radical anions with known persistent lifetimes may be difficult to investigate. Many invisible reactions maybe occurring during the lifetime of the radical anion that causes its decay much faster under these experimental conditions. However, the radical anions that undergo unimolecular decays after the single electron transfers, many with phenyl and cyclopropyl substituents, are the focus of this chapter. These substrates, especially the compounds with cyclopropyl groups, have seen extensive usage as rearrangement probes for detecting electron transfer reaction mechanisms in chemical and biological reactions. The goal of this project is perfect the procedure to generate radical anions using the indirect photoexitation method with laser flash photolysis and examine faster decays of these radical anions, in an effort to gain an improved understanding of single electron transfer reactions.

4.2. ELECTRON DONOR SOURCE

4.2.1. *Generation of DMS Radical Cation*

The generation of the $DMS^{\bullet+}$ was verified by recording its absorbance at 530 nm and observing the shoulder at 490 nm for the appearance of the DMS radical anion (Fig. 4.1).

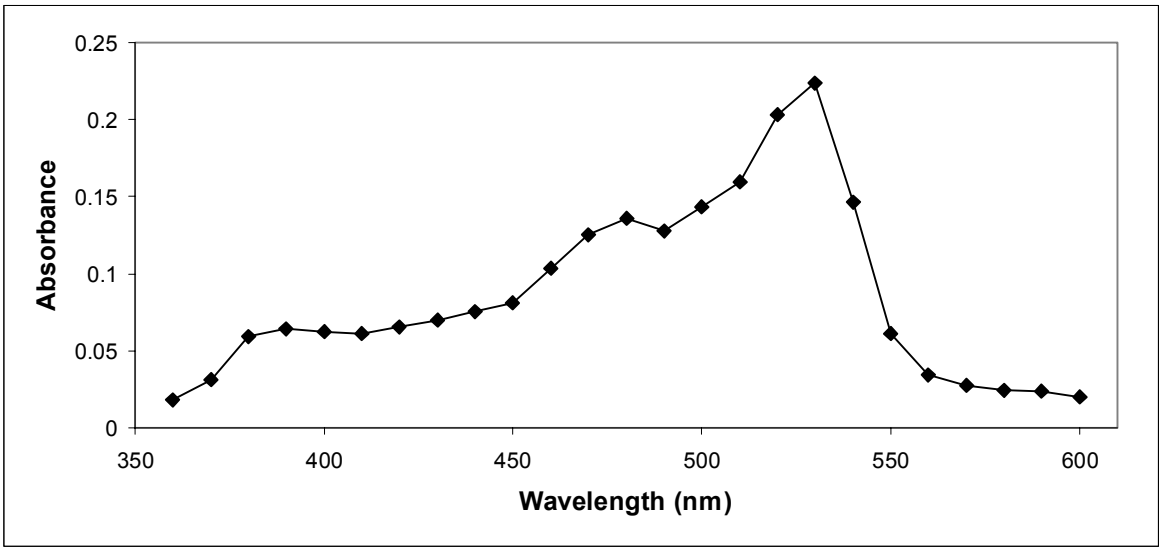

Figure 4.1. UV/Visible Spectrum of $DMS^{\bullet+}$ and $DMS^{\bullet-}$ by Irradiating 0.00067 M DMS in Acetonitrile at 355 nm

This absorption for the $DMS^{\bullet+}$ at 530 nm was observed by recording the transient signal (Fig. 4.2) at this wavelength in the absence of any nucleophile in solution. The rate of build up for the radical cation can be measured from this transient signal.

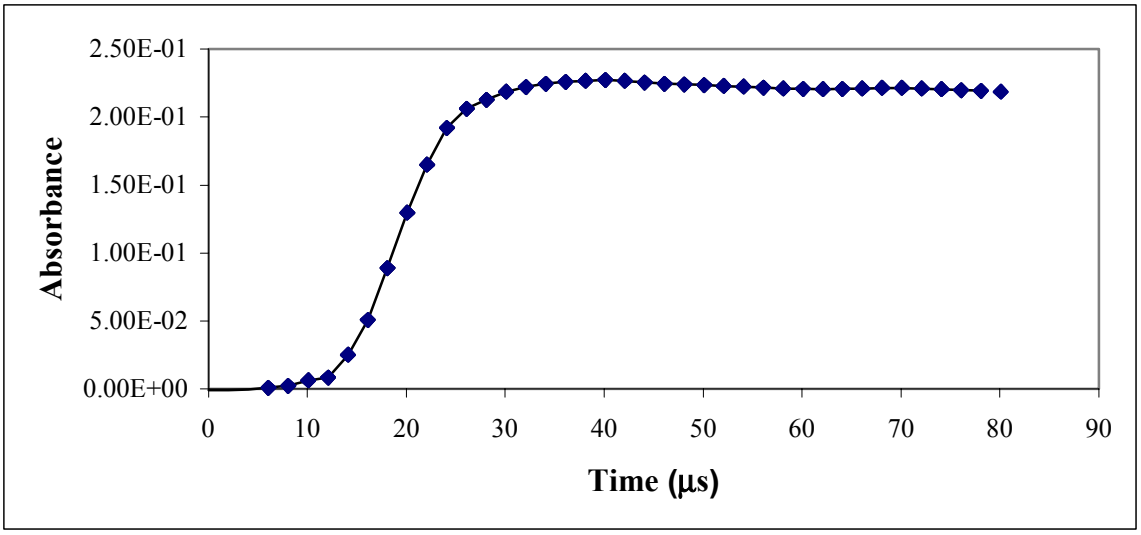

Figure 4.2. Transient Signal for the $DMS^{\bullet+}$ from the Irradiation of 0.00067 M DMS at 355 nm in Acetonitrile

4.2.2. *Quenching of DMS Radical Cations*

The quenching of the DMS radical cation was achieved by the addition of 0.1 M tetrabutylammonium azide into a 4.4 x 10^{-4} M DMS solution in acetonitrile. The disappearance of the radical cation was observed by recording the transient signal at 530 nm (Fig. 4.3) and producing a spectra (Figure 4.4) that showed the immediate disappearance of the 530 nm absorption, leaving the 490 nm absorbance due to the DMS radical anion. An unknown peak was observed at 380 nm in both spectra as well, which was not reported in Mathivanan's original work.

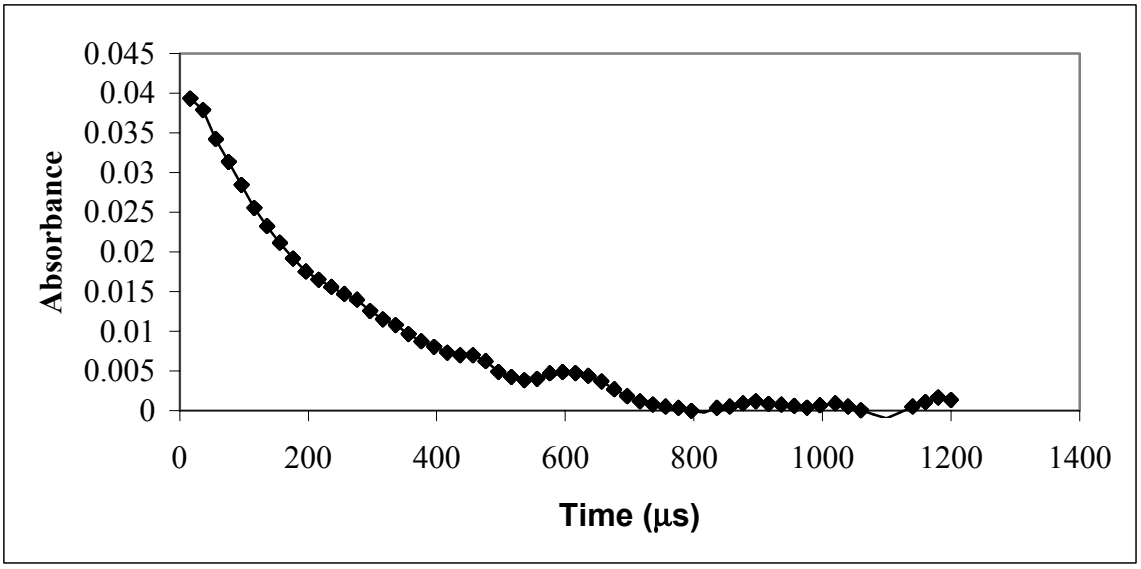

Figure 4.3. Transient Signal for the Quenching of the $DMS^{\bullet+}$ at 530 nm by 0.01 M Tetrabutylammonium Azide in 4.4 x 10^{-4} M DMS in Acetonitrile

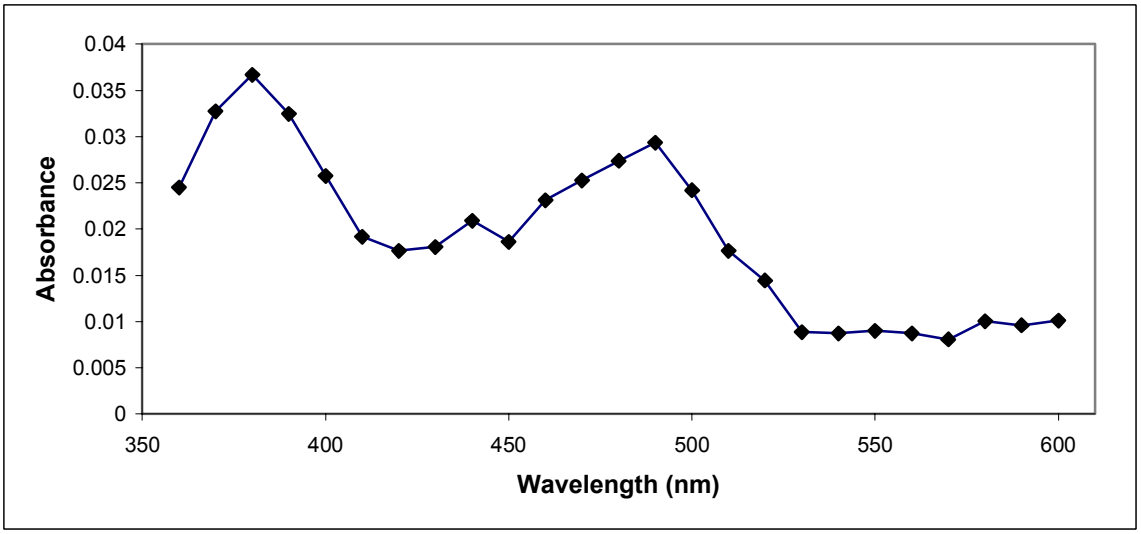

Figure 4.4. Spectrum of $DMS^{\bullet-}$ Alone, After Quenching of $DMS^{\bullet+}$ by 0.01 M Tetrabutylammonium Azide in 4.4 x 10^{-4} M DMS in Acetonitrile

Mathivanan stated that the yield of $DMS^{\bullet+}$ was a function of laser intensity. Due to this, experiments were conducted to determine the lowest, most efficient laser power for these experiments. While maintaining constant DMS and tetrabutylammonium azide concentrations, subsequent experiments were conducted across a range of laser intensities. It was determined that a laser power of ca. 40 mJ should be maintained, although laser power dependence was only observed in the signal intensity, not in the observed rate constants.

In order to obtain the quenching rate constant for the nucleophile with the $DMS^{\bullet+}$, a concentration profile on tetrabutylammonium azide was conducted. At five different nucleophile concentrations, the observed rate constant for the decay of the $DMS^{\bullet+}$ transient signal was measured. By plotting the observed rate constant (k_{obs}) vs. concentration (Fig. 4.5), the quenching rate constant by tetrabutylammonium azide of the DMS radical cation was found to equal 1.84(18) x 10^{10} $M^{-1}s^{-1}$. With such a large measured rate constant, the nucleophilic attack on the radical cation can be labeled as a known diffusion-controlled reaction. The half-life for the $DMS^{\bullet+}$ with a 0.1M nucleophile concentration is 3.7 ns, destroying the cation within the necessary timeframe to avoid interfering with observation of the generated radical anions.

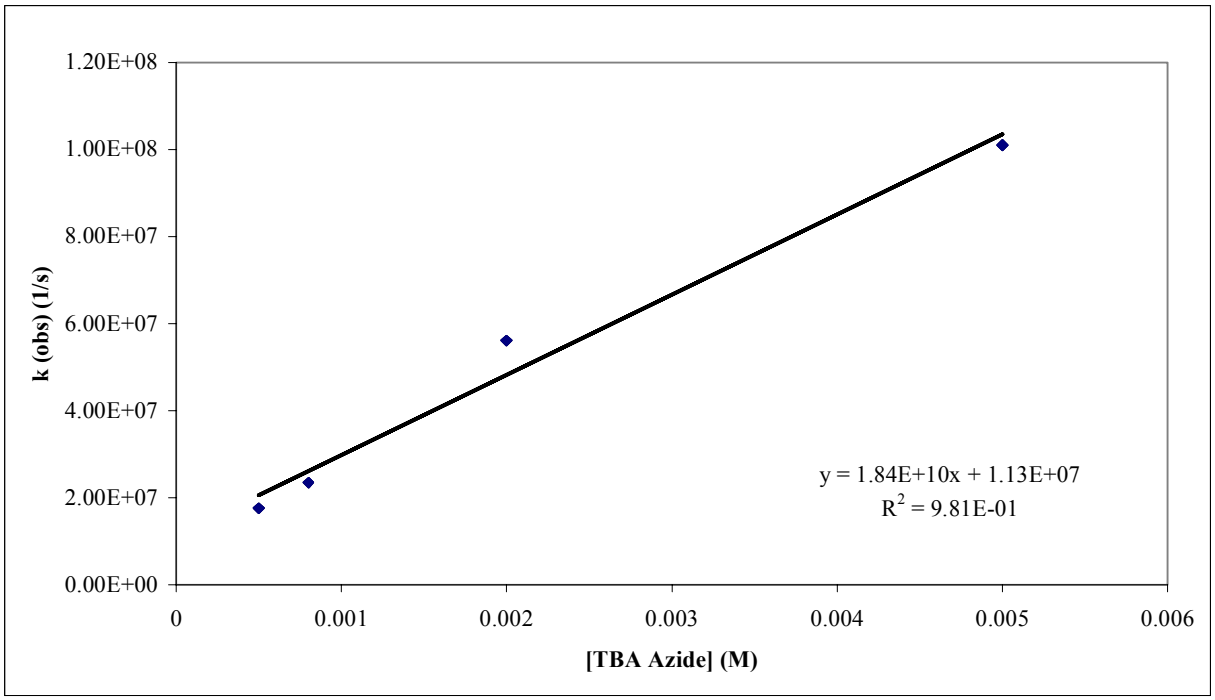

Figure 4.5. Concentration Profile for the Quenching of the $DMS^{\bullet+}$ with 0.0005 M-0.005 M Tetrabutylammonium Azide in 3.0 x 10^{-4} M DMS in Acetonitrile.

A temperature study from 70 – 10 °C was conducted to determine the activation parameters for the radical cation trapping. Using the observed rate constants measured over the above concentration range and temperature range, an Arrhenius plot, shown in Figure 4.6, was constructed. The activation energy for this reaction was measured to be 1.99 ± 0.10 kcal/mole

with a log A value equaling 8.85 ± 0.07, which are results expected for a diffusion-controlled reaction.

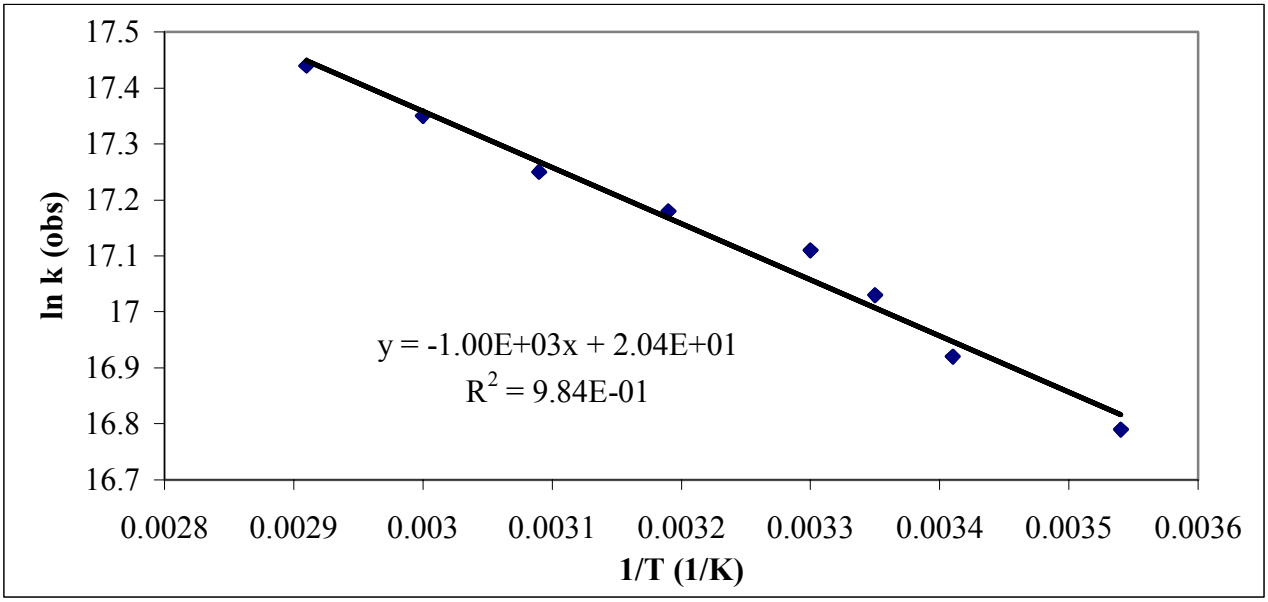

Figure 4.6. Arrhenius Plot for the Quenching of the $DMS^{\bullet+}$ with 0.0005 M-0.005 M tetrabutylammonium Azide in Acetonitrile with 8.7 x 10^{-4} M DMS.

4.3. SIMPLE ARYL KETONES

The initial aryl ketones examined were mostly commercially available ketones with known radical anions that were persistent on the time scale of these experiments. The radical anion decay rate constants for these substrates were extremely slow, due to the absence of unimolecular decay pathways. Even the few substrates that have cyclopropane rings that could possibly open for a unimolecular radical anion decay have been measured to decay at extremely slow rates (i.e. $\leq 2\ s^{-1}$ for the ring opening decay of phenyl cyclopropyl ketone).[123]

Steady-state UV/visible spectra were recorded in a quartz cuvette for all the ketones studied. The extinction coefficients for the ground state ketones at 354 nm are recorded in Table 4.1. The ketones were excited by themselves in acetonitrile at their experimental concentrations,

in order to determine if any absorbance was observed due to the generation of their triplet states. At a concentration of 6.0 x 10^{-3} M, the aryl ketones were poorly excited, represented by the laser-generated spectrum in Figure 4.7 of *t*-butyl phenyl ketone in acetonitrile.

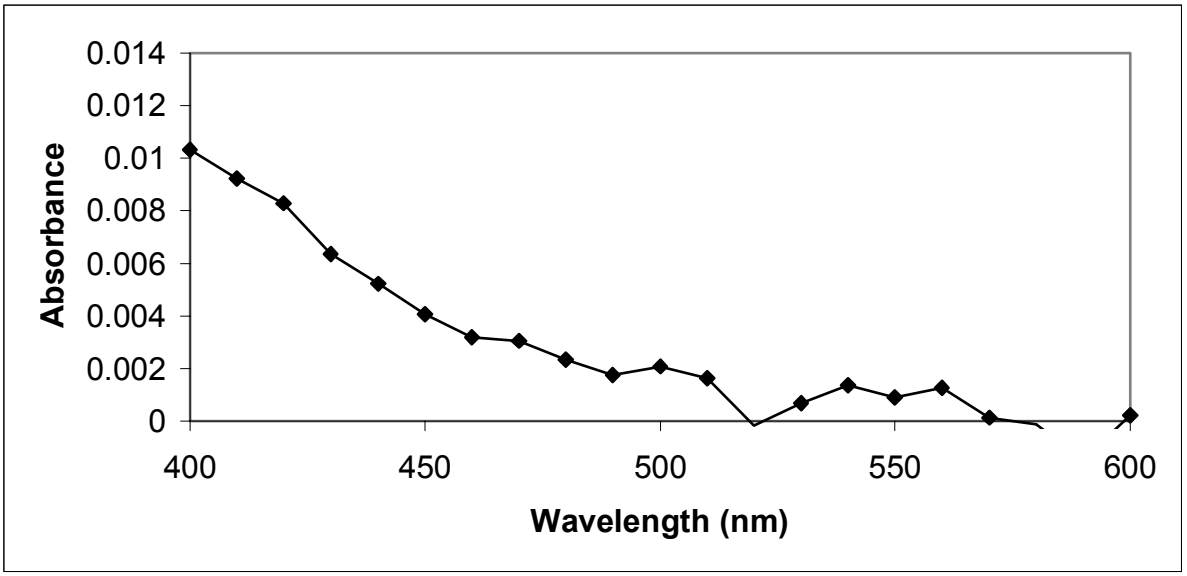

Figure 4.7. Spectrum of 0.006 M *t*-Butyl Phenyl Ketone Alone in Acetonitrile Recorded 200 ns After Laser Excitation

As shown previously, the $DMS^{\bullet-}$ is generated efficiently from side reactions with the solvated electrons. However, the absorption of this undesired radical anion interferes with observing the desired radical anions from the aryl ketone substrates. The ketone concentration implemented in these experiments maintains the necessary excess over the DMS substrate to greatly decrease the amount of $DMS^{\bullet-}$ generated, but still allows the DMS substrate to remain as the main absorbing species. All of the laser-generated spectra were taken at a time base between 200ns and 1μs after laser excitation. The transient absorption spectra for the commercially available ketones, with and without DMS/Azide, were verified through literature.

Further evidence towards the generation of the radical anions was collected via experiments with 1,4-diazabicyclo[2.2.2]octane (DABCO). Tertiary amines have been used as single electron donors for the photoreduction of different triplet ketones in various solvents.[130,133,134] Once the aromatic ketone has been photoexcited to its triplet state, the triplet accepts an electron from one of the nitrogen lone pair, generating the resulting radical anion and the DABCO radical cation (Eq. 22). The spectra for the resulting radical anion species

were recorded and compared to the previous results. The laser-generated spectrum for *t*-butyl phenyl ketone and DABCO is shown in Figure 4.8.

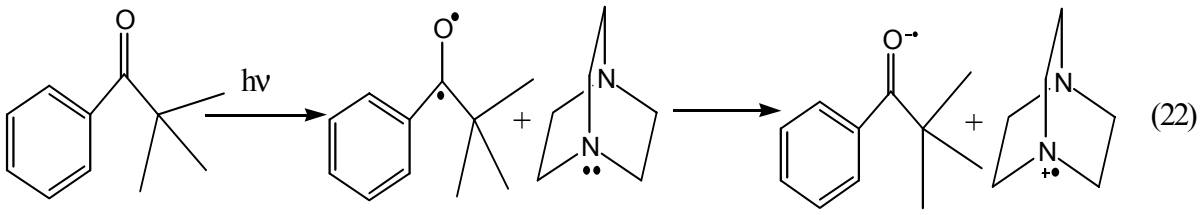

(22)

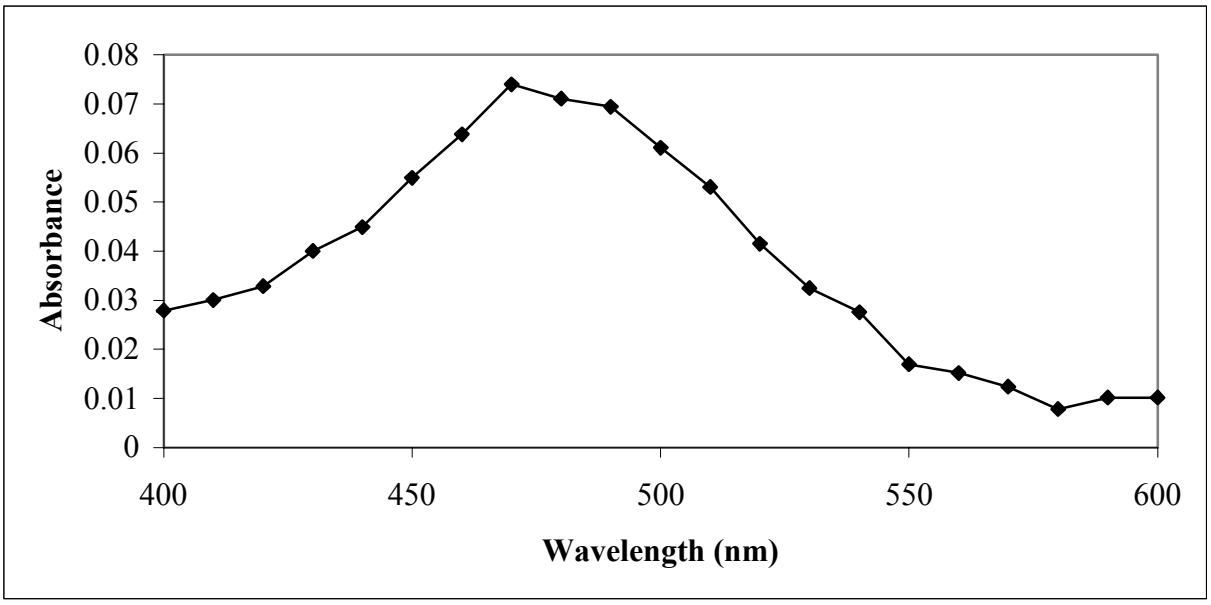

Figure 4.8. Spectrum of *t*-Butyl Phenyl Ketone Radical Anion Generated From Laser-Excitation at 355 nm of 0.0177 M Ketone and 0.103 M DABCO in Acetonitrile

Once verification for the generation of the radical anion was achieved, the observed rate constants and activation parameters for their decay were measured. Due to limited sample availability, the temperature dependent k_{obs} could only be measured for the commercially available aryl ketones. Table 4.1 shows the λ_{max} for the radical anions, the measured rate constants for the decay of these species, and the measured activation parameters. The spectra and corresponding transient signals for radical anions for ketones 2-6 are shown in Figures 1, 3, 5-7 in Appendix B.

Table 4.1. **Results for Indirect Photoexcitation of Simple Persistent Aryl Ketones with DMS**

Compound	ε ($M^{-1}cm^{-1}$) Ketone at 354 nm	λ_{max} (nm) Radical Anion	k_d (10^5 s^{-1})	E_a (kcal/mol)	log A
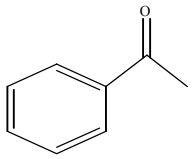 **(1)**	13.5	460-490	6.87	5.88(51)	9.94(36)
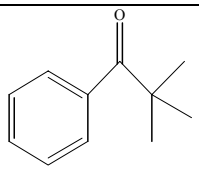 **(2)**	181	490	8.33	5.24(35)	9.52(24)
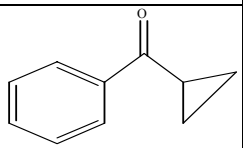 **(3)**	125	480	10.8	5.92(91)	9.86(65)
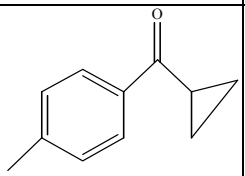 **(4)**	72.4	490	9.93		
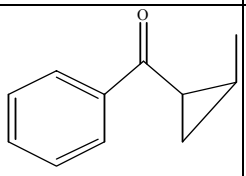 **(5)**	41.8	470	8.86		
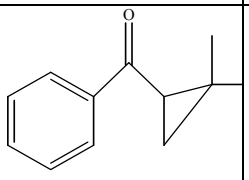 **(6)**	83.3	470-490	11.5		

The spectrum and transient signal measured at 470 nm for the acetophenone radical anion is shown in Figure 4.9. In addition, the Arrhenius plot can be found in Figure 4.10. All other Arrhenius plots for the commercially available ketones in Table 4.1 can be found in Figures 2 and 4 in Appendix B.

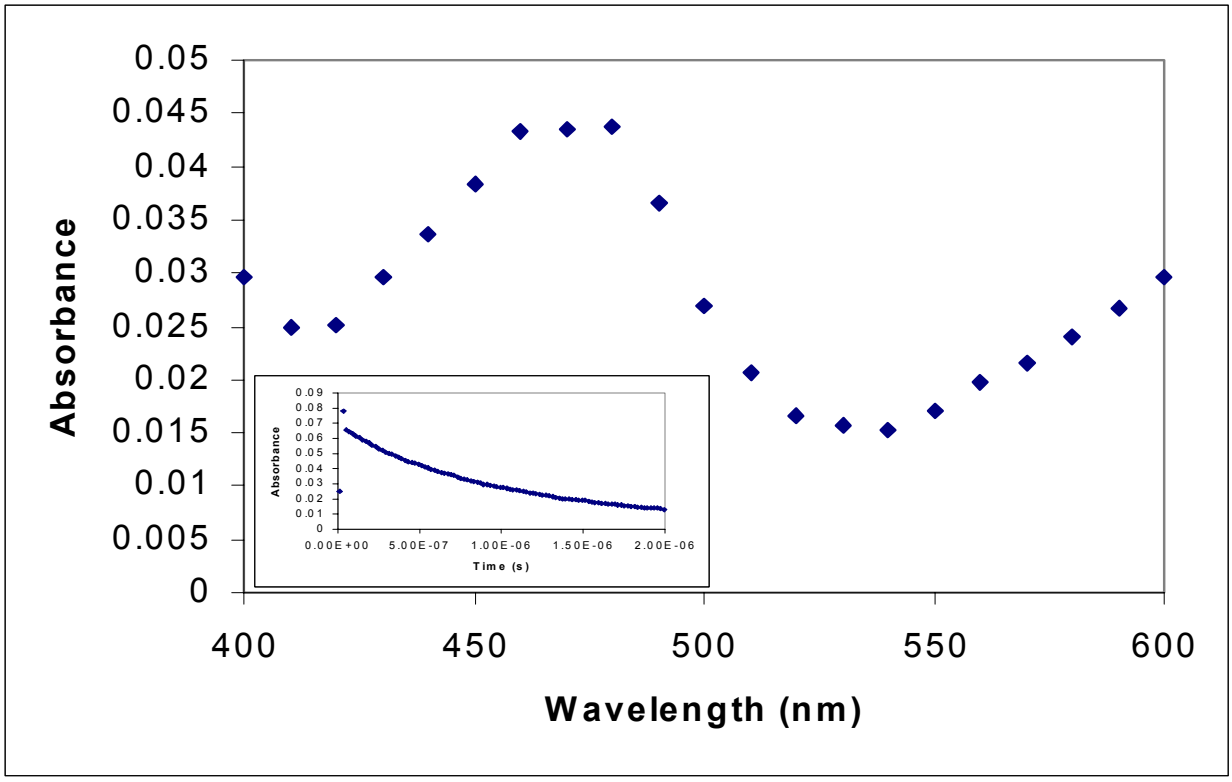

Figure 4.9. Spectrum and Transient Signal for the Decay of the Acetophenone Radical Anion at 470 nm Generated by the Excitation of 0.006 M Acetophenone with 0.0003 M DMS and 0.01 M Tetrabutylammonium Azide in Acetonitrile

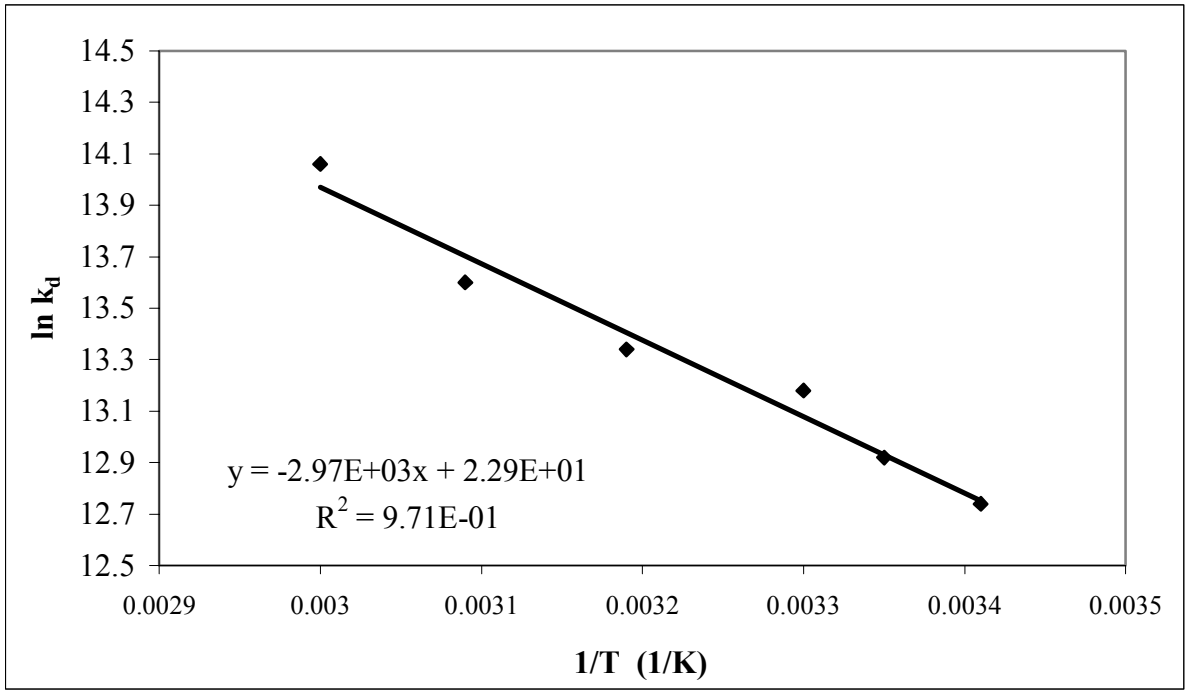

Figure 4.10. Arrhenius Plot for the Decay of the Acetophenone Radical Anion Generated by the Excitation of 0.006 M Acetophenone with 0.0003 M DMS and 0.01 M Tetrabutylammonium Azide in Acetonitrile

The first-order decay rate constants for the ketones in Table 4.1 are all approximately 1.0 x 10^6 s^{-1}. However, since product studies were not conducted on these reactions to determine if the decays were occurring through unimolecular or bimolecular pathways, these measurements will be considered apparent decay rate constants.

The cyclopropyl ring and/or substituents (methyl groups) did not change the absorbance in the UV/visible spectra for the radical anion. In addition, the rate constant for the decay of these radical anions, measured via electrochemical means, are known to be small. The measured observed rate constants for these radical anions were extremely slow (≤ 15 $M^{-1}s^{-1}$)[114] with corresponding large activation energies (≥ 7 kcal/mol).[135,136] Even the radical anion of cyclopropyl phenyl ketone had an extremely small rate constant, confirming that the cyclopropyl group in this compound does not ring open. Although the observed rate constants measured by laser flash photolysis do not correspond to the rate constants measured in the electrochemical experiments, it can be believed that no unimolecular decays or ring-opening processes are occurring in solution These radical anions are known to be very persistent under other

conditions. Since the apparent rate constant was measured to be identical for all of these structurally different intermediates, they must be undergoing other types of reactions to destroy the radical anion in solution. The measured activation energies for ketones **1-3** provide additional evidence for this conclusion. They all have activation energies of approximately 5.5 kcal/mol and log A values equaling 9.5. Once again, in examining these results, the cyclopropyl ring appears to allow no additional decay pathways for the radical anion, when compared to acetophenone and *t*-butyl phenyl ketone. Even adding the methyl groups to the cyclopropyl ring (ketone **6**) allowed for no increase in the rate constant, though ring opening would lead to a stable tertiary radical.

With the generation of the radical anion spectra for these simple aryl ketones, it has been proven that this method for the indirect photoexcitation of aryl ketones does work. Transient signals for the decay of radical anions can be recorded and measured. Under these experimental conditions, these radical anions undergo rapid decay, many with half-lives equaling 0.5 μs. All of these simple ketones do not appear to undergo any unimolecular decays, since all of them decay with rate constants of approximately 10^6 s^{-1}. In order to study unimolecular rearrangements of radical anions generated from other aryl ketones, these different radical anions will have to "beat out" these reaction decay processes, decaying with a rate constant greater than 10^6 s^{-1}.

4.4. RING OPENING OF RADICAL ANIONS GENERATED FROM ARYL KETONES

The compounds used in this part of the study have been shown electrochemically[114,123] to undergo unimolecular rearrangement with a rate constant >> 10^6 s^{-1}. For these radical anions, in which ring opening is assumed to be the decay pathway for these reactions, the decay of radical anions were too fast to measure under electrochemical conditions. Due to this problem, it has become more conducive to examine these aryl ketones using the laser flash system with the indirect excitation process. Table 4.2 reports the results for these ketones with radical stabilizing

substituents on the cyclopropane ring, plus compounds with an epoxy ring exchanged for the cyclopropane ring. The laser flash photolysis spectra for their radical anions are shown in Figures 8, 10, and 12 in Appendix B.

Table 4.2. Results for Indirect Photoexcitation of Aryl Ketones with DMS that Undergo Ring Opening Decay Processes

Compound	ε ($M^{-1}cm^{-1}$) Ketone at 354 nm	λ_{max}(nm) Radical Anion	k_o (10^6 s^{-1})	E_a (kcal/mole)	log A
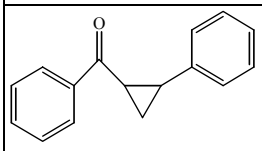 **(7)**	247.8	550	9.56	2.83(33)	8.31(24)
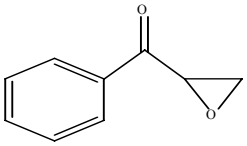 **(8)**	17.0	480	0.68	6.06(29)	10.0(25)
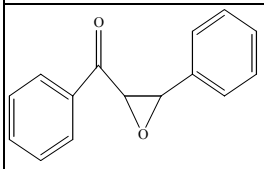 **(9)**	104	530	13.8	2.36(29)	8.86(20)

With the additional conjugation added into the substrates, the absorbance for the radical anions was shifted further into the visible region. The measured decay rate constant for ketone **7** increased by a factor of 10, surpassing 1.0 x 10^7 s^{-1} when compared to rate constants measured for compounds, which are assumed not to ring-open. The activation parameters for these radical anion decays decreased by half to 2.5 kcal/mol and measured a log A value of 8.5. The plots for these activation parameters are shown in Figure 9 in Appendix B. These results show that an additional decay pathway for this radical anion was created due to the addition of the phenyl group hanging off the cyclopropyl ring, facilitating the ring opening pathway. This substituent allows for the generation of a benzyl radical through a decay pathway of the radical anion (Eq.

23). In comparison to phenyl cyclopropyl ketone, ketone **3**, the same decay pathway would generate an energetically unstable primary radical (Eq. 24). Once again, although a stable tertiary radical could be generated in ketone **6**, the measured rate constant shows a minimal change compared to the results for the highly conjugated substrate. These results support the argument previously mentioned about the absence of unimolecular decay for these smaller radical anions. Experiments run under electrochemical conditions showed no increase in the decay rate constant for the radical anions with methyl groups on the cyclopropane ring.[114] Observed rate constants for ketones **3** and **5** equaled 4.5 $M^{-1}s^{-1}$ and 13.1 $M^{-1}s^{-1}$, respectively. Once the phenyl ring is added to the substrate, the rate constant for decay increases greatly, due to the ring opening decay pathway.

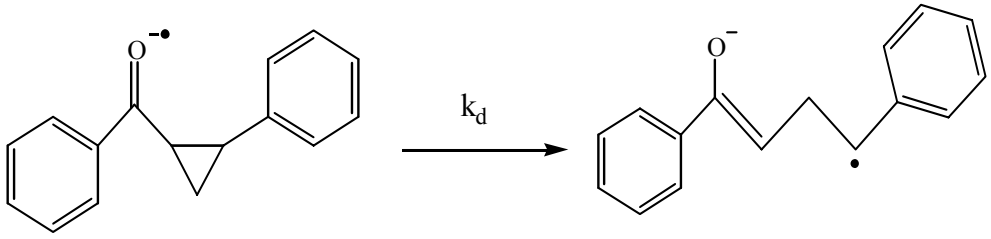

(23)

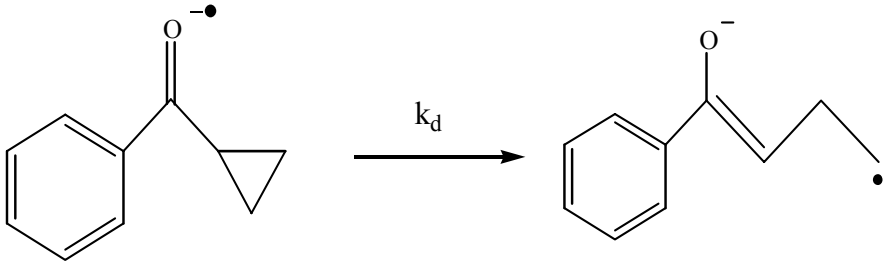

(24)

After examining these substrates, it was fitting to examine Hasegawa's epoxide substrates and measure the rate constant for decay of these radical anions. Both 2,3-epoxy-1-phenyl propan-1-one **(8)** and *trans*-2,3-epoxy-1,3-diphenyl propan-1-one **(9)** were investigated within these experiments. The maximum absorbance for the radical anion from ketone **8** was recorded to be identical to cyclopropyl phenyl ketone; in addition, the observed rate constant was similar to all the smaller unconjugated aryl ketones in Table 4.1. The Arrhenius parameters, shown in Figure 11 in Appendix B, were measured, having an activation energy of 6.06 kJ/mol and a log

A value of 10.0. In examining the results for both substrates, the same rationalization can be used as stated before in Hasegawa's research.[131,132,137] In both substrates, the epoxide ring can open and generate a carbon radical center and oxygen centered anion. However, ketone **9**, with its extra phenyl substituent, allows for the generation of a benzyl radical through a formal 1,2 hydrogen rearrangement shown in Eq. 25. This formal 1,2-hydrogen rearrangement does occur for ketone **8**, although at a much slower rate, due to no change in radical stability for the intermediate. The stabilization for this radical center can be seen in the Arrhenius parameters measured for the radical anion, equaled to values measured for ketone **7**. The Arrhenius parameter plot for *trans*-2,3-epoxy-1,3-diphenyl propan-1-one can be found in Figure 13 in Appendix B. By investigating both ketone **8** and **9,** the argument that generating this stable benzyl radical facilitates the enhancement of the decay rate constants measured and a decreasing of the Arrhenius parameters is strengthened.

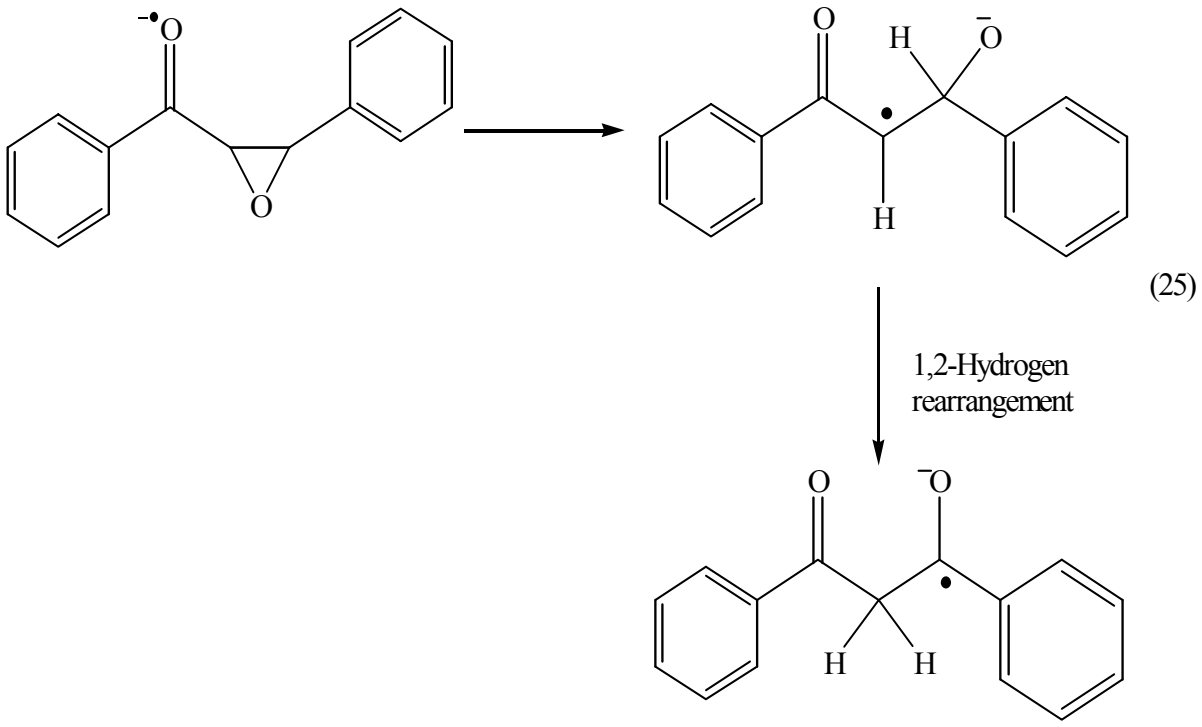

(25)

4.5. INVESTIGATION OF SIGNIFICANT ARYL KETONES

In striving to understand the possible decay mechanisms for these radical anions, some structurally unique ketones were examined. These substrates provided some challenges to obtain their transient signals and spectra, either due to their extended conjugation and size or the decay rate of their radical anion. Ketone **10**, *trans*-1,2-dibenzoyl cyclopropane, a commercially available aryl ketone proved to be one of those challenges. The spectrum of *trans*-1,2-dibenzoyl cyclopropane radical anion is shown in Figure 14 in Appendix B. Unlike the other aryl ketones, once excited, this substrate rapidly generated a product, yellow in color, which interfered with the instrument's ability to measure a clean LFP spectrum or the activation parameters for the decay of this radical anion. The yellow product can be observed immediately after laser firing, as shown by the bleaching area in the recorded UV/visible spectra from 420-450nm. The transient signal's decay for this intermediate was too fast to be measured with any accuracy with the current instrumentation. Ketone **11**, 10-spirocyclopropyl-9-anthracenone, proved to generate the most stable radical anion, remaining persistent for over 5 μs. The spectrum for ketone **11** is shown in Figure 15 in Appendix B. This result is consistent with new electrochemical results for this ketone, measuring a decay rate constant approximately 160 s^{-1} for the radical anion ring opening.[138] Results for these complex ketones and the other structurally different ketones are found in Table 4.3.

Table 4.3. Results for the Indirect Excitation for Significant Aryl Ketones

Compound	ε ($M^{-1}cm^{-1}$) Ketone at 354 nm	λ_{max}(nm) Radical Anion	k_o (10^7 s^{-1})	E_a (kcal/mole)	log A
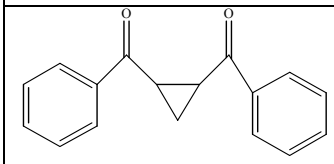 **(10)**	Large	560	> 1.0		
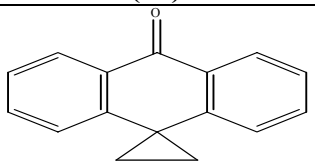 **(11)**	No Recordable Abs.	540	Persistent on Time Scale		
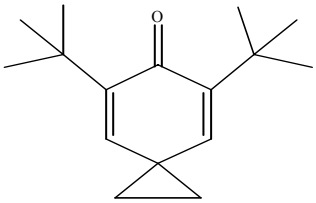 **(12)**	433.2	400*	40.6	1.12(17)	9.44(13)
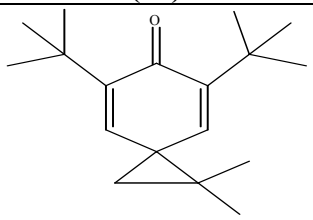 **(13)**	103.5	410*	28.6	1.09(20)	9.36(14)

*Assigned to the cyclopropane-ring opened (diatomic) radical anion

The rate constants and Arrhenius parameters for 5,7-Di-*tert*-butylspiro[2.5]octa-4,7-dien-6-one and 1,1-dimethyl-5,7-di-*tert*-butylspiro[2.5]octa-4,7-dien-6-one (ketones **12** and **13**, respectively) in Table 4.3 were measured uniquely. These substrates have been previously characterized as hypersensitive probes for single electron transfer reactions.[127] Their radical anions have known decay rate constants ≥ 10^7 s^{-1}. However, for this study, the observed rate constants for these two compounds were not measured from the transient signal of the decaying radical anions. Instead, the growth of the phenoxy anion in solution was used to measure the observed rate constants. The phenoxide anions gave a strong signal that could be followed at approximately 400 nm. The spectra for these two compounds are shown in Figure 16 and 18 in the Appendix B. A representative transient signal is shown in Figure 4.11.

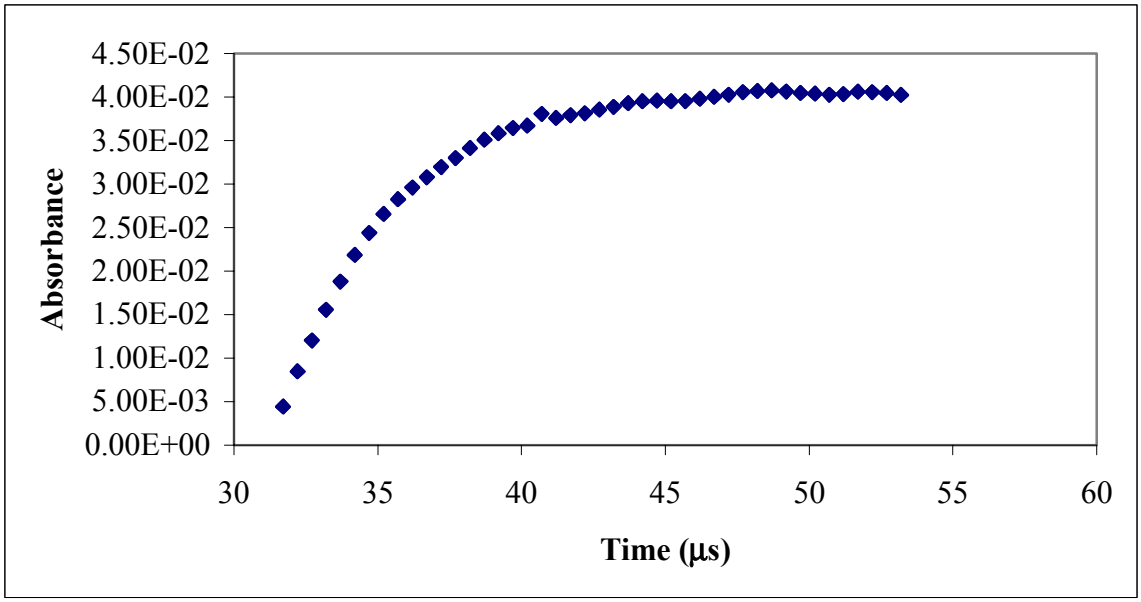

Figure 4.11. Transient Signal for the Growth of the Phenoxy Anion of 1,1-dimethyl-5,7-di-*tert*-butylspiro[2.5]octa-4,7-dien-6-one at 410 nm Generated by Laser Excitation at 355 nm of 0.005 M 1,1-dimethyl-5,7-di-*tert*-butylspiro[2.5]octa-4,7-dien-6-one and 0.0003 M DMS with 0.01 M TetrabutylAmmonium Azide in Acetonitrile

The UV/visible absorbance for the anion was verified by running an experiment with tri-2,4,6-*tert*-butyl-phenol and potassium *t*-butoxide in the steady-state UV/visible spectrophotometer. The phenoxide anion absorbed around 410 nm, matching the spectra generated from the laser experiments with ketone **12** and **13**. The decay pathway for these intermediates generate a more conjugated species with the ring opening of the cyclopropyl group, shown in Eq. 26.

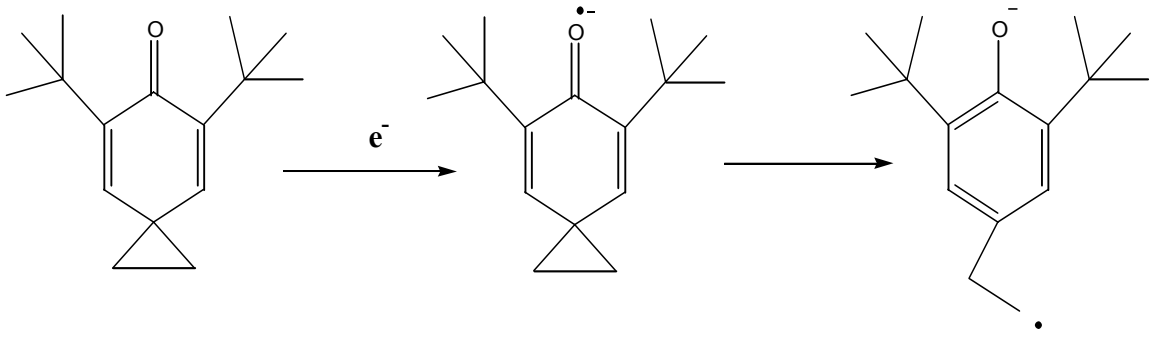

(26)

The measured rate constant for this radical anion is faster than any of the other ketones, greater than 2 x 10^8 s^{-1}. This result corresponds with the smallest activation energy observed for these substrates, equaling 1.10 kcal/mol for both ketones. Their Arrhenius plots are recorded in Figure 17 and 19 in Appendix B. The decay pathways for these radical anions appear to be more beneficial than the decay pathways opened for the larger aryl ketones in Table 24. The generation of an aromatic ring appears to be the driving force for the decay pathway, since the stability between the generated primary or tertiary radical does not change the resulting activation parameters for the reaction. The two probe compounds are structurally different due to the addition of the two methyl groups on the cyclopropyl substituent. Both compounds undergo the ring opening process to generate the conjugated ring extremely fast. It may have been assumed that since the extra methyl groups would cause the generation of a tertiary radical that the rate constant for decay of ketone **13** would be faster. However, since this phenomenon was not recorded, it may prove that the radical center appears late in the transition state and does not have any control on the rate determining step.

In verifying that the radical anion intermediate undergoes the ring opening process, it was investigated which step in the pathway is the rate-determining step, either the one electron transfer or the ring opening decay. A laser power dependency experiment was conducted on ketone **13** substrate with the exact experimental conditions used previously. The experiment was conducted with a laser power range approximately from 35 kJ to 1 kJ. The flow-cell apparatus was used once again for continuous refreshing of the solution. Ten different laser powers were used in the experiments. The laser powers and the average observed rate constants for each experiment are recorded in Figure 4.12.

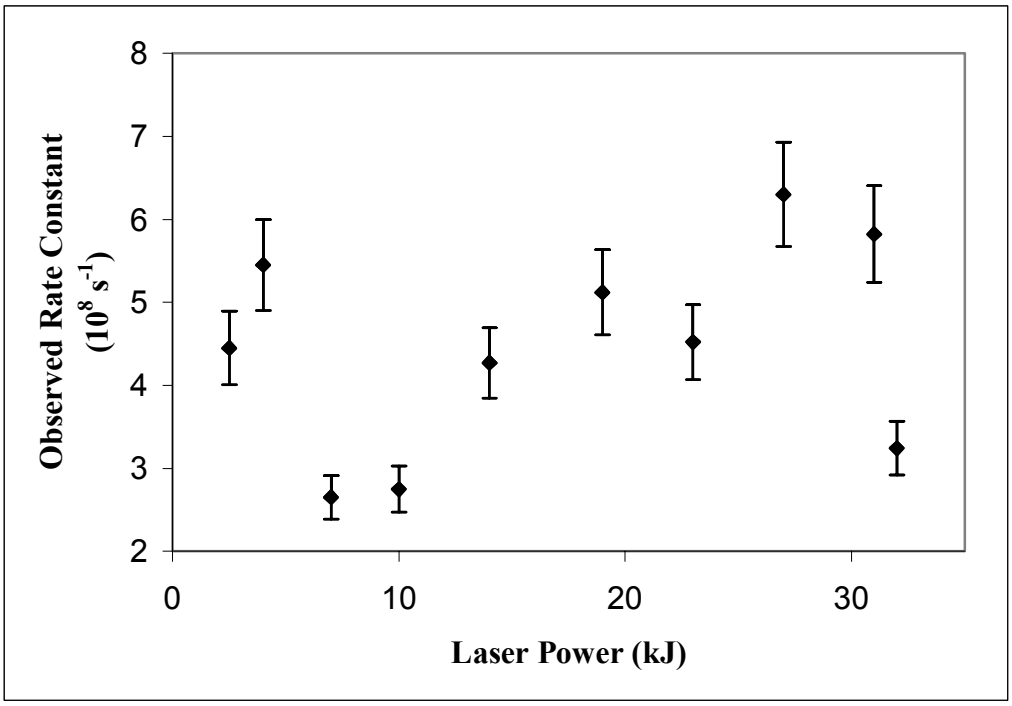

Figure 4.12. Laser Power Dependency Experiment: Laser Power vs. Average Measured Rate Constants from Transient Signals for Decay of the 1,1-dimethyl-5,7-di-*tert*-butylspiro[2.5]octa-4,7-dien-6-one Radical Anion at 410 nm Generated by the Excitation of 0.005 M 1,1-dimethyl-5,7-di-*tert*-butylspiro[2.5]octa-4,7-dien-6-one with 0.0003 M DMS and 0.01 M Tetrabutylammonium Azide in Acetonitrile.

None of the transient signals recorded showed a noticeable difference, within experimental error, over the laser power range and no trend could be established. The only noticeable change was observed in the signal intensity, shown by the amount of absorbance recorded at the 400 nm wavelength. Lowering the laser power decreased the amount of solvated electrons introduced into the solution, which decreased the amount of radical anions that could be recorded in the signal. These experiments gave evidence that the rate-determining step for this pathway must be the ring-opening process of the radical anion, not the acceptance of the one electron from solution to substrate. With the ring-opening process being the rate-determining step, it is once again interesting to note the activation energies for the decay of both ketones **12** and **13** are almost identical, though they are producing two different radical centers. Therefore, perhaps it is correct in believing that the radical center is generated late in the transition state of the ring-opening reaction.

4.6. CONCLUSION

A new indirect method for producing radical anions in solution has proven instrumental in recording and studying radical anions beyond traditional electrochemical techniques. The photoexcitation of DMS to generate solvated electrons, which are then accepted by aryl ketone substrates in solution, has provided an easy method for the generation of radical anions. Using this method through laser flash photolysis, the radical anion's can be recorded and measured at their absorbance maximums in the UV/visible region. From these transient signals, the apparent rate constants for decay of the radical anions can be measured.

In comparing the rate constants from electrochemical experiments to the ones measured in this LFP study, a remarkable difference in the limits of these techniques were observed. The laser flash photolysis technique was found unreliable to measure the slow radical anion decays ($< 10^6$ s^{-1}) , for the radical anions that were known to be extremely persistent. For all of these compounds, the apparent rate constant was measured to be approximately 1.0×10^6 s^{-1}. However, for radical anions that can undergo ring-opening processes for unimolecular decay, the laser flash photolysis method proves to be quite accurate in verifying the rate constants measured using the electrochemical technique. The rate constants measured through electrochemical experiments are compared to the results from this laser flash photolysis investigation in Table 4.4. Clearly, the rate constants not only correspond to the previously measured rate constants, but also validated the mechanistic results found in Hasegawa's investigation.

Table 4.4. Comparison of Aryl Ketone Decay Rate Constants for Electrochemical Experiments and Laser Flash Photolysis Experiments

Aryl Ketone	Electrochemical k_o	LFP k_o (s^{-1})
$_6$123	211 s^{-1}	Too Slow
$_7$124	1×10^7 s^{-1}	9.56×10^6
$_{12}$127	$>10^8$ s^{-1}	4.06×10^8

In examining the decay pathways for these radical anions, the stability of the resulting radical (i.e. primary vs. tertiary) proved to have no influence on the decay of any of these radical anions. The measured decay rate constants were only affected when the resulting radical center, after initial decay, could become a benzyl radical. This influence was observed in the cyclopropyl aryl ketones, as well as the epoxides. These results have lead to a clear understanding between the structure of the examined aryl ketones and the reactivity of the generated radical anions in solution.

4.7. FUTURE WORK

The purpose of this study was to examine radical anions through another technique besides cyclic voltammetry. Electrochemical experiments are extremely tedious and time consuming as well as still being a technique that many investigators do not completely understand. In addition, due the complexity of the experiments, it is difficult to correlate the results from these studies with other studies due to the experimental conditions. With using the indirect photoexcitation method with laser flash photolysis, single election transfer reactions, such as the generation of radical anions, can be investigated more easily. The rate constants and Arrhenius parameters for the decay of the radical anions measured in this study are the foundation for other investigations. From these results, the influence of the resulting radical (i.e. benzyl radical) during the decay of the radical anion was observed. The next direction for this project is to examine the decay rate constants for other radical anions that may undergo unimolecular decays to different radical centers. In addition, substituent effects on the decay of these radical anions can be examined as well. These results would allow for a more extended understanding of the reactivity for these virtually invisible intermediates.

This indirect method for generating intermediates through electron transfer reactions may actual open a door to connect these two laser flash photolysis projects. Reactions, such as the oxidation of MPTP, may undergo a hydrogen atom abstraction pathway or a single electron transfer pathway. This procedure could be utilize to obtain more evidence for these arguments. Derivatives of MPTP, such as 4-phenyl-1-cyclopropyl-1,2,3,6-tetrahydropyridine, could be

investigated for their ability to undergo a single electron transfer reaction. Other biological processes undergo electron transfer reactions as well and this method will allow another technique to be used to investigate those reactions and gain insight into their mechanistic pathways.

CHAPTER 5. EXPERIMENTAL

5.1 *t*-BUTOXYL RADICAL STUDY

5.1.1 *Instrumentation*

Steady-state UV/visible spectra were recorded on a Hewlett Packard diode array UV/Visible Spectrophotometer (HP8452A). Samples were excited by using the third harmonic of a Continuum Surelite I-10 Nd:YAG laser (4-6 ns pulse, 355 nm). The transient signal absorptions were monitored by a Hewlett-Packard Infinium digital oscilloscope HP54820A with nanosecond response times. Data analysis was performed on an Applied Photophysics SpectraKinetic Workstation software package (v. 4.59). Variable temperature experiments were performed with a jacketed cell holder connected to a VWR Scientific Products (PolyScience) variable temperature circulating bath (model 1150-A). The cell holder was equipped with a thermocouple to measure the temperature directly adjacent to the cuvette. Samples were thermally equilibrated prior to photolysis by placing the cuvettes in the spectrometer for at least ten minutes. (This protocol was checked by placing a thermometer directly into representative samples and verifying that the internal temperature was identical to that measured by the thermocouple over the temperature range of these studies, 80-10 °C).

5.1.2. MATERIALS

Benzene (Aldrich) was used as received as the co-solvent for the absolute rate constant measurements and variable temperature experiments. Additional solvents for viscosity study, C_5 through C_{16} (Aldrich), were used as received.

5.1.2.1. *Activation of Di-tert-butyl peroxide*

Di-*tert*-butyl peroxide was obtained from Aldrich. The liquid was purified by column chromatography with activated alumina to remove any superoxides. The activated peroxide was kept in a covered Erlenmeyer flask in the freezer.

5.1.2.2. *Sublimation of Diphenylmethanol*

Diphenylmethanol (Benzhydrol) was obtained from Aldrich in 99% purity. To remove benzophenone impurity, fresh samples were sublimed at 40°C, under a vacuum of 20 mm Hg, and encased in aluminum foil. Sublimation of diphenylmethanol was conducted directly before each experimental use.

5.1.2.3. *Purification of Amines and Hydrocarbons*

All liquid amines and hydrocarbons were available from Aldrich. Triethylamine, triallylamine, N,N-dimethylaniline, N,N-diphenylaniline, toluene, cyclohexane were distilled

under vacuum (1 mm Hg, 44°C) to remove any yellow color. Tribenzylamine, quinuclidine, DABCO, diphenylmethane, and triphenylmethane (Aldrich) were used as received.

5.1.3. EXPERIMENTAL RUNS

5.1.3.1. *Photolysis Experiments*

All samples were conducted in a 2:1 solution by volume of di-*tert*-butyl peroxide:benzene. In each experiment, diphenylmethanol (0.1M constant) was utilized as the reaction probe. All of the samples examined in this work were deoxygenated by argon purging. Argon was gently bubbled into the samples for ten minutes to ensure complete deoxygenation. All observed rate constants were measured at 535 nm. Low laser power (ca. 10 mJ) was used for all experiments to keep the concentration of generated radicals approximately constant. Substrate concentrations were varied over a factor of ten throughout five separate experiments. The samples were excited five different times with a laser pulse, generating five separate transient signals. The observed rate constants for each excitation was measured and the average rate constant recorded. The Arrhenius parameter studies were conducted from 80-10 °C in 10 degree increments, including 25 °C, and conducted at the same concentrations as previously mentioned.

5.1.3.2. *Viscosity studies*

Viscosity measurements were conducted using a Oswald viscometer at 25 °C. The amount of di-*tert*-butyl peroxide in solution was decreased to 7.5% by volume in order to allow for the solvent to be changed. Concentration profiles were constructed for experiments with n-

alkane solvents, C_5 through C_{16}. The rate constants for hydrogen atom abstraction was measured again and compared to the original rate constants measured in benzene.

5.2. ARYL KETONE RADICAL ANION STUDY

5.2.1. INSTRUMENTATION

Steady-state UV/visible spectra were recorded on a Hewlett Packard diode array UV/Visible Spectrophotometer (HP8452A). The sample solutions were run through a constant flow cell to keep fresh sample in the cell while recording the spectrum. The flow cell apparatus was purged for five minutes by flowing nitrogen through Tygon tubing and the sample cuvette. The sample was then poured into the 250 ml separatory funnel reservoir and degassed with argon for fifteen minutes. Once degassed, the sample flowed into the quartz cuvette at a rate of 2 ml/minute. Samples were excited by using the third harmonic of a Continuum Surelite I-10 Nd:YAG laser (4-6 ns pulse, 355 nm). The transient signal absorptions were monitored by a Hewlett-Packard Infinium digital oscilloscope HP54820A with nanosecond response times. Data analysis was performed on an Applied Photophysics SpectraKinetic Workstation software package (v. 4.59). Variable temperature experiments were performed with a jacketed cell holder connected to a VWR Scientific Products (PolyScience) variable temperature circulating bath (model 1150-A). The cell holder was equipped with a thermocouple to measure the temperature

directly adjacent to the cuvette. Samples were thermally equilibrated prior to photolysis by placing the cuvettes in the spectrometer for at least ten minutes.

5.2.2. MATERIALS

5.2.2.1. *Purification of Acetonitrile*

Acetonitrile was used as the solvent for all the sample preparation. The solvent was stirred over calcium hydride, 1 g/100 ml, and under argon for at least 3 days. The solvent was then refluxed in a distillation apparatus over phosphorus pentaoxide, 2 g/100 ml, under nitrogen.

5.2.2.2. *Purification of Substrates*

trans-4-4'-Dimethoxystilbene (DMS) (Aldrich) was recrystallized in methanol. Tetrabutylammonium azide (TBAA) was obtained from TCI and used as received. Solutions of TBAA and acetonitrile were prepared in a nitrogen dry box and kept in a dessicator. Acetophenone **(1)**, *t*-butyl phenyl ketone **(2)**, cyclopropyl phenyl ketone **(3)** were obtained from Aldrich and vacuum distilled (1 mmHg, 38°C) immediately before use. *trans*-1,2-Dibenzoyl cyclopropane(**10**) was also obtained from Aldrich and used as received. *p*-Tolyl cyclopropyl ketone **(4)**, *trans*-1-benzoyl-2-methyl cyclopropane **(5)**, 1-benzoyl-2,2-dimethyl cyclopropane **(6)**,[139] *trans*-1-benzoyl-2-phenylcyclopropane **(7)**,[140] 2,3-epoxy-1-phenyl propan-1-one **(8)**[141] and 2,3-epoxy-1,3-diphenyl propan-1-one **(9)**,[142] and 10-spirocyclopropyl-9-anthracenone[143] **(11)** were prepared previously in this group, according to published procedures. 5,7-Di-*tert*-butylspiro[2.5]octa-4,7-dien-6-one **(12)** and 1,1-dimethyl-5,7-di-*tert*-butylspiro[2.5]octa-4,7-dien-6-one **(13)** were synthesized using published procedures from this group.[144-147]

5.2.3. PHOTOLYSIS EXPERIMENTS

The concentration of DMS for all samples was approximately 3.0×10^{-4} M. For the purpose of quenching $DMS^{\bullet+}$, tetrabutylammonium azide was easier to use as it is less hygroscopic than tetrabutylammonium acetate. The concentration of the nucleophile was 0.01 M for all experiments. Steady-state UV/visible spectra were recorded to verify that all substrate concentrations were absorbing minimal light at the excitation wavelength. All of the ketones studied in this investigation were kept at a concentration of approximately 6.0×10^{-3} M. Minimal laser power (ca. 30-40 mJ) was used in all experiments to eliminate any laser power dependency to the observed rate constants. To measure decay rate constants, sample concentrations were varied over a factor of ten in five separate experiments. Each sample cuvette was degassed by bubbling argon into the solution for 10 minutes. To measure the observed rate constant, the samples were excited by the laser five individual times and the rate constant was measured from the generated transient signal. Those five observed rate constants were then averaged for the recorded value.

Variable temperature experiments, to obtain Arrhenius parameters, were conducted from 70 - 20°C, including 25°C. Fresh samples were degassed with argon for ten minutes and then allowed to equilibrate at the respective temperatures for 8 minutes. (Once again, this protocol was checked by placing a thermometer directly into representative samples and verifying that the internal temperature was identical to that measured by the thermocouple over the temperature range of these studies, 70-20°C). Observed rate constants were then measured at each temperature for one specific concentration to generate the Arrhenius parameter plot in order to obtain the activation energy and log A values for the observed decay.

LITERATURE CITED

1) Hudson, A.; Waterman, D.; Alberti, A. *J. Chem. Soc. Perkin Trans. 2* **1995**, 2091-2093.
2) Catala, J.-M.; Jousset, S.; Lamps, J.-P. *Macromolecules* **2001**, *34*, 8654-8656.
3) Ahrens, B.; Davidson, M. G.; Forsyth, V. T.; Mahon, M. F.; Johnson, A. L.; Mason, S. A.; Price, R. D.; Raithby, P. R. *J. Am. Chem. Soc.* **2001**, *123*, 9164-9165.
4) Sobek, J.; Martschke, R.; Fischer, H. *J. Am. Chem. Soc.* **2001**, *123*, 2849-2857.
5) Karki, S. B.; Dinnocenzo, J. P.; Jones, J. P.; Korzekwa, K. R. *J. Amer. Chem. Soc.* **1995**, *117*, 3657-63.
6) Manchester, J. I.; Dinnocenzo, J.; Higgins, L.; Jones, J. P. *J. Amer. Chem. Soc.* **1997**, *119*, 5069-5070.
7) Choi, S.-Y.; Eaton, P. E.; Hollenberg, P. F.; Liu, K. E.; Lippard, S. J.; Newcomb, M.; Putt, D. A.; Upadhyaya, S. P.; Xiong, Y. *J. Amer. Chem. Soc.* **1996**, *118*, 6547-6555.
8) Rabion, A.; Chen, S.; Wang, J.; Buchanan, R. M.; Seris, J.-L.; Fish, R. H. *J. Amer. Chem. Soc.* **1995**, *117*, 12356-12357.
9) Walling, C.; Thaler, W. *J. Amer. Chem. Soc.* **1961**, *83*, 3877.
10) Walling, C.; Wagner, P. *J. Amer. Chem. Soc: Comm.* **1963**, *85*, 2333-2334.
11) Griller, D.; Howard, J. A.; Marriott, P. R.; Scaiano, J. C. *J. Amer. Chem. Soc.* **1981**, *103*, 619-623.
12) Wong, P. C.; Griller, D.; Scaiano, J. C. *J. Amer. Chem. Soc.* **1982**, *104*, 5106-5108.
13) Carlsson, D. J.; Ingold, K. U. *J. Amer. Chem. Soc.* **1967**, *89*, 4885-4891.
14) Carlsson, D. J.; Ingold, K. U. *J. Amer. Chem. Soc.* **1967**, *89*, 4891-4894.
15) Walling, C.; Clark, R. T. *J. Amer. Chem. Soc.* **1974**, *96*, 4530-4534.
16) Walling, C.; McGuinness, J. A. *J. Amer. Chem. Soc.* **1969**, *91*, 2053-2058.
17) Paul, H.; R.D. Small, J.; Scaiano, J. C. *J. Amer. Chem. Soc.* **1978**, *100*, 4520-4527.
18) Raley, J. H.; Rust, F. F.; Vaughn, W. E. *J. Amer. Chem. Soc.* **1948**, *70*, 1336, 2767.
19) Williams, A. L.; Oberright, E. A.; Brooks, J. W. *J. Amer. Chem. Soc.* **1956**, *78*, 1190.
20) Lossing, F.; Tickner, A. W. *J. Chem. Phys.* **1952**, *20*, 907.
21) Tsentalovich, Y. P.; Kulik, L. V.; Gritsan, N. P.; Yurkovskaya, A. V. *J. Phys. Chem. A* **1998**, *102*, 7975-7980.
22) Walling, C.; Wagner, P. J. *J. Amer. Chem. Soc.* **1964**, *86*, 3368-3375.
23) Weber, M.; Fischer, H. *J. Amer. Chem. Soc.* **1999**, *121*, 7381-7388.
24) Choo, K. Y.; Benson, S. W. *Inter. J. Chem. Kinetics* **1981**, *13*, 833-844.
25) Kim, S. S.; Kim, S. Y.; Ryou, S. S.; Lee, C. S.; Yoo, K. H. *J. Org. Chem.* **1993**, *58*, 192-196.
26) Encinas, M. V.; Diaz, S.; Lissi, E. *Inter. J. Chem. Kinetics* **1981**, *XIII*, 119-123.
27) Kim, S. S.; Koo, H. M.; Choi, S. Y. *Tetrahedron Letters* **1985**, *26*, 891-894.
28) Sakurai, H.; Hosomi, A. *J. Amer. Chem. Soc.* **1967**, 458-460.
29) Encinas, M. V.; Lissi, E. A. *Inter. J. Chem. Kinetics* **1978**, *X*, 653-656.
30) Wong, S. K. *J. Amer. Chem. Soc.* **1979**, *101*, 1235-1239.
31) Kerr, J. A.; Stocker, D. W. *Strengths of Chemical Bonds*; CRC Press LLC, 2000.
32) Sway, M. I. *J. Chem. Soc., Faraday Trans* **1991**, *87*, 2157-2159.
33) Sway, M. I.; Waddington, D. J. *J. Chem. Soc., Perkin Trans. 2* **1984**, *3*, 63-69.
34) Wade, L. G. *Organic Chemistry*; 3 ed.; Prentice Hall, Inc: New Jersey, 1995.
35) Hefter, H. J.; Hecht, T. A.; Hammond, G. S. *J. Amer. Chem. Soc.* **1971**, *94*, 2793-2797.
36) Cuthbertson, M. J.; Rizzardo, E.; Soloman, D. H. *Aust. J. Chem.* **1983**, *36*, 1957-1973.

37) Lissi, E. A.; Collados, J.; Olea, A. *Inter. J. Chem. Kinetics* **1985**, *17*, 265-269.
38) Unruh, J. D.; Gleicher, G. J. *J. Amer. Chem. Soc.* **1971**, *93*, 2008-2014.
39) McMillen, D. F.; Golden, D. M. *Ann. Rev. Phys. Chem.* **1982**, *33*, 493-532.
40) Mahiou, B.; Gleicher, G. J. *J. Org. Chem.* **1987**, *52*, 1555-1559.
41) Griller, D.; Ingold, K. U. *J. Amer. Chem. Soc.* **1974**, *96*, 630-632.
42) Akell, N. Y. A.; Selby, K.; Waddington, D. J. *J. Chem. Soc., Faraday Trans.* **1981**, 1036-1042.
43) Lindsay-Smith, J. R.; Nagatomi, E.; Stead, A.; Waddinton, D. J.; Beviere, S. D. *J. Chem. Soc. Perkin Trans. 2* **2000**, 1193-1198.
44) Das, P. K.; Encinas, M. V.; Steenken, S.; Scaiano, J. C. *J. Amer. Chem. Soc.* **1981**, *103*, 4162-4166.
45) Encinas, M. V.; Scaiano, J. C. *J. Amer. Chem. Soc.* **1981**, *103*, 6393-6397.
46) Yip, R. W.; Loufty, A. C.; Chow, Y. L.; Magdzinski, L. K. *Can. J. Chem.* **1972**, *50*, 3426.
47) Henvest, H. B.; Reid, J. A. W.; Stirling, C. J. *J. Chem. Soc.* **1961**, 5239.
48) Nazran, A. S.; Griller, D. *J. Amer. Chem. Soc.* **1983**, *105*, 1970-1971.
49) Elford, P. E.; Roberts, B. P. *J. Chem. Soc., Perkin Trans. 2* **1998**, *8*, 1413-1422.
50) Dombrowski, G. W.; Dinnocenzo, J. P.; Farid, S.; Goodman, J. L.; Gould, I. R. *J. Org. Chem.* **1999**, *64*, 427-431.
51) Wayner, D. D. M.; Clark, K. B.; Rauk, A.; Yu, D.; Armstrong, D. A. *J. Amer. Chem. Soc.* **1997**, *119*, 8925-8932.
52) Malatesta, V.; Scaiano, J. C. *J. Org. Chem.* **1982**, *47*, 1455-1459.
53) Murov, S. L. *Handbook of Photochemistry* New York, 1973.
54) Abbot, G. D.; Phillips, D. *Molec. Photochem.* **1977**, *8*, 289.
55) Karki, S. B.; Dinnocenzo, J. P. *Xenobiotica* **1995**, *25*, 711-724.
56) Dinnocenzo, J. P.; Karki, S. B.; P.Jones, J. *J. Amer. Chem. Soc.* **1993**, *115*, 7111-7116.
57) Evans, C.; Scaiano, J. C.; Ingold, K. U. *J. Am. Chem. Soc.* **1992**, *114*, 4589-4593.
58) Jovanovic, S. V.; Steenken, S.; Boone, C. W.; Simic, M. G. *J. Amer. Chem. Soc.* **1999**, *121*, 9677-9681.
59) Valgimigli, L.; Ingold, K. U.; Lusztyk, J. *J. Amer. Chem. Soc.* **1996**, *118*, 3545-3549.
60) Barclay, L. R. C.; Vinqvist, M. R.; Mukai, K.; Goto, H.; Hashimoto, Y.; Tokunaga, A.; Uno, H. *Org. Lett.* **2000**, *2*, 2841-2843.
61) Lu, X.; Silverman, R. B. *J. Amer. Chem. Soc.* **1998**, *120*, 10583-10587.
62) Kuhn, D. M.; Murphy, D. L.; Youdim, M. B. H. *Physiological clinical aspects of monamine oxidase. Structure and function of amine oxidases*; CRC: Boca Raton, 1985; Vol. 22.
63) Wang, Y.-X.; Mabic, S.; Jr., N. C. *Bioorganic & Medicinal Chem.* **1997**, *6*, 143-149.
64) Franot, C.; Mabic, S.; Neal Castagnoli, J. *Bioorganic and Med. Chem.* **1997**, *5*, 1519-1529.
65) Franot, C.; Mabic, S.; Neal Castagnoli, J. *Bioorganic and Med. Chem.* **1998**, *6*, 283-291.
66) Trevor, A.; Neal Castagnoli, J.; Singer, T. P. *Pharmacology and Toxicology of MPTP: A Neurotoxic By-Product of Illicit Drug Chemistry*; Kinfe, R., Walker, C. A., Barnett, G., Fannin, L. D., Ed.; CRC Press: Florida, 1989, pp 163-174.
67) Langston, J. W.; Ballard, P.; Tetrud, J. W.; Irwin, I. *Science* **1983**, *219*, 979-980.
68) Heikkila, R. E.; Manzino, L.; Cabbat, F. S.; Duvoisin, R. C. *Nature* **1984**, *311*, 467-469.
69) Heikkila, R. E.; Hess, A.; Duvoisin, R. C. *Science* **1984**, *224*, 1451-1453.
70) Langston, J. W.; Irwin, I.; Langston, E. B. *Science* **1984**, *225*, 1481-1482.
71) Markey, S. P.; Johannessen, J. N.; Chiueh, C. C.; Burns, R. S.; Herkenham, M. A. *Nature* **1984**, *311*, 464-466.

72) Ottoboni, S.; P.Caldera; Trevor, A.; N. Castagnoli, J. *J. Bio. Chem.* **1989**, *264*, 13684-13688.
73) Suleman, N. K.; Tanko, J. M. *Unpublished results: Virginia Polytechnic Institute and University* **2000**.
74) Lalevee, J.; Allonas, X.; Foussaier, J. P. *J. Am. Chem. Soc.* **2002**, *124*, 9613-9621.
75) Tsang, W. *Heats of Formation of Organic Free Radicals by Kinetic Methods*; Simoes, J. A. M., Greenberg, A. and Liebman, J., Ed.; Chapman & Hall: New York, 1996, pp 22-58.
76) Russell, G. A. *Reactivity, Selectivity and Polar Effects in Hydrogen Atom Transfer Reactions*; Wiley: New York, 1973.
77) Becke, A. D. *J. Chem. Phys.* **1993**, *98*, 5648-5651.
78) Lee, C.; Yang, W.; Parr, R. G. *Phys. Rev. B.* **1988**, *37*, 785-789.
79) Tanko, J. M.; Suleman, N. K. *Solvent Effects in the Reactions of Neutral Free Radicals*; Simoes, J. A. M., Greenberg, A. and Liebman, J., Ed.; Chapman & Hall: New York, 1996, pp 224-293.
80) Benson, S. W. *The Foundations of Chemical Kinetics*; McGraw-Hill: New York, 1960.
81) Tanko, J. M.; Friedline, R. A.; Suleman, N. K.; Castagnoli, N. *J. Am. Chem. Soc.* **2001**, *123*, 5808-5809.
82) Moss, R. A.; Lawrynowicz, W.; Turro, N. J.; Gould, I. R.; Cha, Y. *J. Am. Chem. Soc.* **1986**, *108*, 7028-7032.
83) Houk, K. N.; Rondan, N. G. *J. Amer. Chem. Soc.* **1984**, *106*, 4293-4294.
84) Bunce, N. J.; Ingold, K. U.; Landers, J. P.; Lusztyk, J.; Scaiano, J. C. *J. Am. Chem. Soc.* **1985**, *107*, 5464-5472.
85) Schuh, H.; Fischer, H. *Int. J. Chem. Kin.* **1976**, *VIII*, 341-356.
86) Heberger, K.; Kemeny, S.; Vidoczy, T. *Int. J. Chem. Kinet.* **1987**, *19*, 171-181.
87) Calverley, E. M. *AIChE Journal* **1993**, *39*, 725-726.
88) Klicka, R.; Kubacek, L. *Chemometrics and Intelligent Laboratory Systems* **1997**, *39*, 69-75.
89) Dorigo, A. E.; Houk, K. N. *J. Org. Chem.* **1988**, *53*, 1650-1664.
90) Zavitsas, A. A.; Melikian, A. A. *J. Amer. Chem. Soc.* **1975**, *97*, 2759-2763.
91) Zavitsas, A. A.; Chatgilialoglu, C. *J. Am. Chem. Soc.* **1995**, *117*, 10645-10654.
92) Roberts, B. P.; Stell, A. J. *J. Chem. Soc. Perkin Trans. 2* **1994**, 2155-2162.
93) Mayer, J. M. *Acc. Chem. Res.* **1998**, *31*, 441-450.
94) Bryant, J. R.; M., M. J. *J. Am. Chem. Soc.* **2003**, *85*, 607-612.
95) Andrews, L. J.; Keefer, R. M. *J. Am. Chem. Soc.* **1955**, *77*, 6284-6289.
96) Newcomb, M.; Daublain, P.; Horner, J. H. *J. Org. Chem.* **2002**, *67*, 8669-8671.
97) McLafferty, F. W. *Interpretation of Mass Spectra*; 3rd ed.; University Science Books: Mill Valley, CA, 1980.
98) Maillard, B.; Forrest, D.; Ingold, K. U. *J. Am. Chem. Soc.* **1976**, *98*, 7024-7026.
99) Effio, A.; Griller, D.; Ingold, K. U.; Beckwith, A. L. J.; Serelis, A. K. *J. Am. Chem. Soc.* **1980**, *102*, 1734-1736.
100) Newcomb, M.; Glenn, A. G. *J. Am. Chem. Soc.* **1988**, *111*, 275-277.
101) Beckman, E.; Paul, T. *Ann. Chem.* **1891**, *266*, 1.
102) Amatore, C.; Badoz-Lambling, J.; Bonnel-Huyghes, C.; Pinson, J.; Saveant, J.-M.; Thiebault, A. J. *J. Am. Chem. Soc.* **1982**, 1979.
103) Cohen, S. G.; Parola, A.; Parsons, G. H. *Chem. Rev.* **1973**, *73*, 141.
104) Forno, A. E. J.; Peover, M. E.; Wilson, R. *Trans. Faraday Soc.* **1970**, *66*, 22.
105) Amatore, C.; Badoz-Lambling, J.; Bonnel-Huyghes, C.; Pinson, J.; Saveant, J. M.; Thiebault, A. *J. Am. Chem. Soc.* **1982**, *104*, 1979-1986.

106) Cohen, S. G.; Parola, A.; Parsons, G. H. *Chem. Rev.* **1973**, *73*, 141-153.
107) Hoshino, M.; Arai, S.; Imamura, M. *J. Phys. Chem.* **1976**, *80*, 2724-2727.
108) Andrieux, C. P.; Hapiot, P.; Saveant, J.-M. *Chem. Rev.* **1990**, *90*, 723.
109) Daasbjerg, K.; Pedersen, S. U.; Lund, H. *Acta Chem. Scand.* **1991**, *45*, 455.
110) Lund, T.; Lund, H. *Acta Chem. Scand., Ser. B.* **1986**, *40*, 470.
111) Garst, J. F.; Smith, C. D. *J. Am. Chem. Soc.* **1976**, *98*, 1520.
112) Garst, J. F.; Smith, C. D. *J. Am. Chem. Soc* **1976**, *98*, 1526.
113) Armstrong, N. R.; Vanderborgh, N. E.; Quinn, R. K. *J. Electrochem. Soc.* **1975**, *122*, 615.
114) Tanko, J. M.; Drumright, R. E. *J. Am. Chem. Soc.* **1990**, *112*, 5362-5363.
115) Shono, T.; Kise, N.; Fujimoto, T.; Yamanami, A.; Nomura, R. *J. Org. Chem.* **1994**, *59*, 1730.
116) Lewis, F. D.; Magyar, J. G. *J. Org. Chem.* **1972**, *37*, 2102-2107.
117) Netto-Ferreira, J. C.; Avellar, I. G. J.; Scaiano, J. C. *J. Org. Chem.* **1990**, *55*, 89-92.
118) Tanner, D. D.; Chen, J. J.; Chen, L.; Luelo, C. *J. Am. Chem. Soc.* **1991**, *113*, 8074-8081.
119) Mathivanan, N.; Johnston, L. J.; Wayner, D. D. M. *J. Phys. Chem.* **1995**, *99*, 8190-8195.
120) Steckhan, E. *J. Amer. Chem. Soc.* **1978**, *100*, 3526-3533.
121) Zeglinski, D. M.; Waldeck, D. H. *J. Phys. Chem.* **1988**, *92*, 692-701.
122) Dauben, W. G.; Deviny, E. J. *J. Org. Chem.* **1966**, *31*, 3794-3797.
123) Tanko, J. M.; Drumright, R. E. *J. Am. Chem. Soc.* **1992**, *114*, 1844-1854.
124) Tanko, J., M; Drumright, R. E.; Suleman, N. K.; Brammer, L. E. *J. Am. Chem. Soc.* **1994**, *116*, 1785-1791.
125) Bowry, V. W.; Hughes, L.; Ingold, K. U. *J. Chem. Soc. Chem. Commun.* **1990**, 923.
126) Hollis, R.; Hughes, L.; Bowry, V. W.; Ingold, K. U. *J. Org. Chem.* **1992**, *57*, 4284.
127) Tanko, J. M.; Brammer, L. E.; Herves, M.; Campos, K. *J. Chem. Soc. Perkin Trans. 2* **1994**, 1407-1409.
128) Phillips, J. P.; Gilmore, J.; Schwartz, P.; Brammer, L. E.; Berger, D. J.; Tanko, J. *J. Am. Chem. Soc.* **1998**, *120*, 195-202.
129) Beckwith, A. L. J.; Bowry, V. W. *J. Org. Chem.* **1989**, *54*, 2681.
130) Hasegawa, E.; Ishiyama, K.; Horaguchi, T.; Shimizu, T. *J. Org. Chem.* **1991**, *56*, 1631-1635.
131) Hasegawa, E.; Ishiyama, K.; Fujita, T.; Kato, T.; Abe, T. *J. Org. Chem.* **1997**, *62*, 2396-2400.
132) Hasegawa, E.; Yoneoka, A.; Suzuki, K.; Kato, T.; Kitasume, T.; Yanagi, K. *Tetrahedron* **1999**, *55*, 12957-12968.
133) Devadoss, C.; Fessenden, R. W. *J. Phys. Chem.* **1990**, *94*, 4540-4549.
134) Buntinx, G.; Valat, P.; Wintgens, W.; Poizat, O. *J. Phys. Chem.* **1991**, *95*, 9347-9352.
135) Parker, V. D. ; Gold, V. and Bethell, D., Ed.; Academic Press: New York, 1983, pp 131-223.
136) Parker, V. D. *Electroanal. Chem.* **1986**, *14*, 1.
137) Hasegawa, E.; Ishiyama, K.; Kato, T.; Horagucki, T.; Shimizu, T. *J. Org. Chem.* **1992**, *57*, 5352-5359.
138) Tanko, J. M. ; Li, Ed.; VPI: Unpublished Results, 2003.
139) Costa, L.; Young, G.; Whitesides, G. *J. Organomet. Chem.* **1977**, *134*, 151.
140) Corey, E.; Chaykovsky, M. *J. Am. Chem. Soc.* **1965**, *87*, 1353.
141) House, H. O.; Reif, D. R.; Wasson, R. L. *J. Am. Chem. Soc.* **1957**, *79*, 2490-2493.
142) Kawakmi, T.; Shibata, I.; Baba, A. *J. Org. Chem* **1996**, *61*, 82-87.

143) Mustafa; Hilmy *J. Chem. Soc.* **1952**, 1434.
144) Portnykh, N. V.; Volodkin, A. A.; Ershov, V. V. *Bull. Acad. Sci. USSR, Div. Chem. Sci.* **1966**, 2181.
145) Schwartz, L. H.; Flor, R. V. *J. Org. Chem* **1969**, *34*, 1499.
146) Volodkin, A. A.; Belostotskaya, I. S.; Ershov, V. V. *Bull. Acad. Sci. USSR Div. Chem. Sci.* **1967**, 1328.
147) Schwartz, L. H.; Flor, R. V.; Gullo, V. P. *J. Org. Chem.* **1974**, *39*, 219.

APPENDIX A. RESULTS FOR HYDROGEN ABSTRACTION BY *t*-BUTOXYL RADICAL

Table 1. Complete list of rate constants and Arrhenius parameters for hydrogen abstraction by *t*-BuO• from a variety of substrates. (95% confidence limits in the last reported digits are in parentheses).

Substrate	Temperature range (°C)	log(k_H) at 25 °C[a]	E_a. (kcal/mol)	log A (A in units of M^{-1} s^{-1})	C-H BDE (kcal/mol)
Amines[b]					
tribenzylamine (3)	5 → 80	7.62	1.34(16)	8.60(10)	89.1(6)[c]
N,N-dibenzylaniline (2)	10 → 80	7.27	2.02(18)	8.75(15)	85(2)[c]
DABCO (2)	10 → 70	7.06	2.15(18)	8.63(11)	94(2)[d]
triallylamine (2)	10 → 80	7.95	2.20(21)	9.56(12)	82.6(8)[c]
triethylamine (3)	10 → 70	7.99	2.38(49)	9.73(25)	90.7(4)[c,e]
quinuclidine (2)	10 → 70	7.02	2.41(66)	8.78(31)	96(2)[d]
N-methylpyrrole (1)	10 → 80	6.86	2.42(70)	8.62(32)	91(2)[f]
N,N-dimethylaniline (2)	10 → 80	8.01	2.54(61)	9.87(29)	92(1)[c]
Hydrocarbons					
triphenylmethane (1)	10 → 70	6.31	1.86(36)	7.67(19)	81(1)[g]
diphenylmethane (2)	10 → 70	6.53	2.42(53)	8.30(26)	84(1)[g]
allylbenzene (1)	10 → 80	6.51	2.48(31)	8.15(18)	82(2)[f]
cyclohexane (4)	10 → 70	5.91 5.92[i]	4.42(78) 3.11(24)[i]	9.15(35) 8.2(20)[i]	98.7(5)[h] 98.7(5)[h]
toluene (3)	10 → 80	5.28	3.46(49)	7.81(24)	90(1)[h]
cyclopentane	-20 → 25	5.93[i]	3.47(59)[i]	8.47(45)[i]	97(2)[f]
t-butylbenzene	-26 → 10	4.60[i]	6.14(60)[i]	9.1(8)[i]	101(2)[f]

Alcohols					
diphenylmethanol (1)	10 → 70	6.84	2.03(28)	8.33(16)	79(2)[f]
	-35 → 70	6.91[j]	1.99(35)[j]	8.37(28)[j]	79(2)[f]
methanol	-20 → 30	4.72[k]	5.30(30)[k]	8.6(2)[k]	98(1)[h]
Ethers					
1,3-dioxolane	-35 → 70	6.90[j]	3.00(80)[j]	9.1(7)[j]	93(2)[f]
2-methyl-1,3-dioxolane	-35 → 70	7.10[j]	2.09(32)[j]	8.63(26)[j]	93(2)[f]
THF	-35 → 70	6.87[j]	2.5(10)[j]	8.7(8)[j]	94(2)[f]
t-butyl methyl ether	-20 → 30	4.99[k]	5.2(3)[k]	8.8(2)[k]	96(2)[f]
anisole	-42 → 20	4.98[i]	5.21(19)[i]	8.8(2)[i]	98(2)[f]
	-20 → 30	4.48[k]	5.9(3)[k]	8.8(.2)[k]	

[a]Calculated from Arrhenius parameters. [b]Value in parentheses indicates number of times study was performed. [c]Reference 50. [d]Reference 74. [e]Reference 51. [f]Calculated (B3LYP/6-31G*/CC-PVTZ(-F)) as described herein. [g]Reference 39. [h]Reference 75. [i]Reference 23. [j]Reference 52.

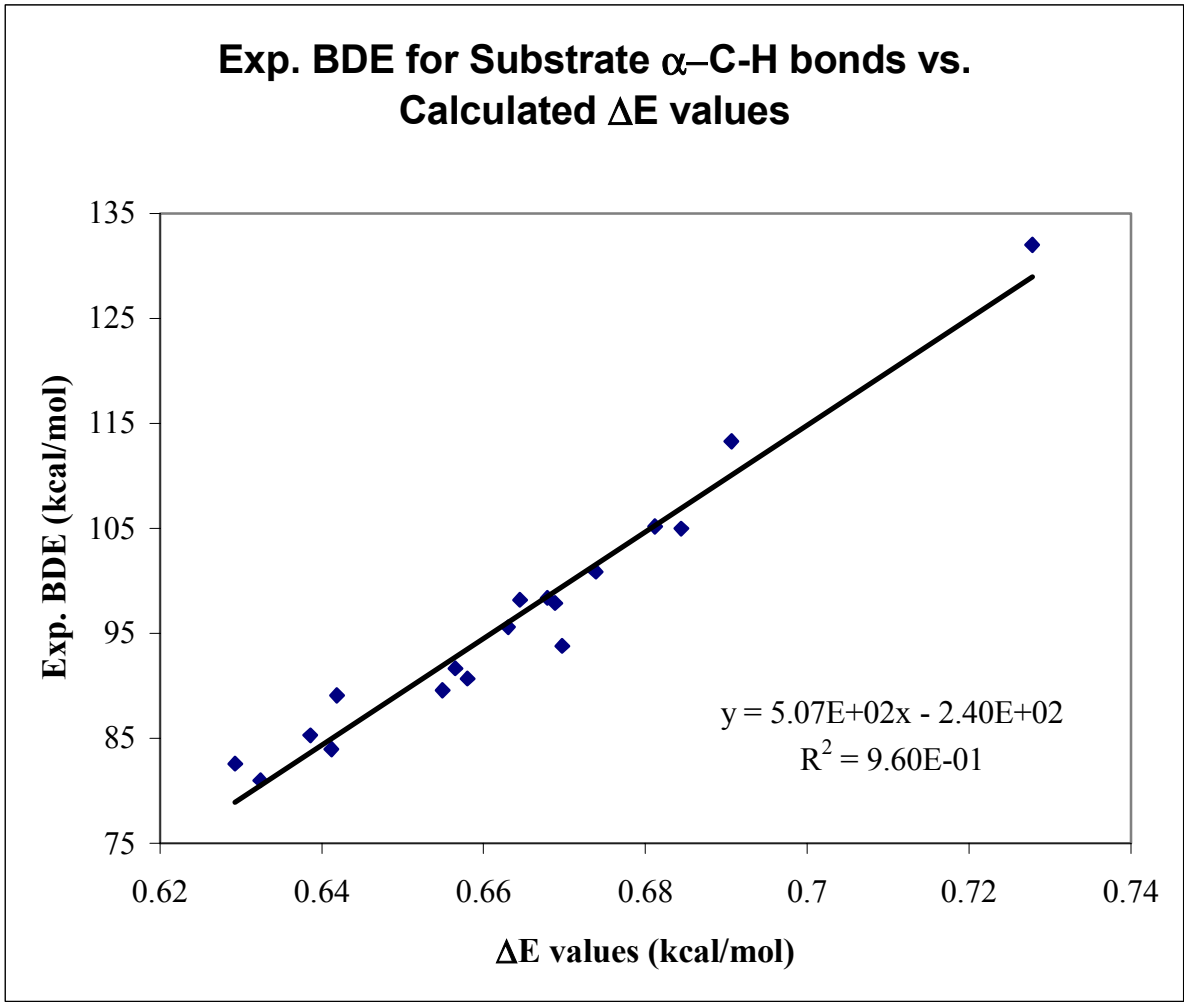

Figure 1. **Experimental C-H bond dissociation energies vs. calculated ΔE values.**

Table 2. Results of B3LYP/CC-PVTZ(-F)//B3LYP/6-31 G* calculations to estimate unknown C-H bond dissociation energies (BDE)

Substrate	Energy (R-H, hartrees)	Energy (R•, hartrees)	ΔE (hartrees)	BDE (expt'l, kcal/mol)	BDE (calc'd, kcal/mol)
triphenylmethane	-733.883164	-733.2507612	0.63240278	81	80.80184499
triallylamine	-251.952206	-251.322908	0.629298	82.6	79.2120409
diphenylmethane	-502.7707795	-502.12956	0.64121951	84	85.31644855
dibenzylaniline	-597.4520287	-596.8134345	0.63859415	85.3	83.97213356
tribenzylamine	-405.6563301	-405.0144589	0.64187122	89.1	85.65015828
toluene	-271.654211	-270.999292	0.654919	89.6	92.33127395
triethylamine	-292.5123756	-291.8543772	0.65799833	90.7	93.90804645
dimethylaniline	-366.331492	-365.6749752	0.65651671	91.7	93.14938086
DABCO	-345.4379595	-344.768258	0.66970154	93.8	99.90067268
isobutene (3^o)	-158.5169919	-157.8539404	0.66305154	95.6	96.49554243
quinuclidene	-329.4122068	-328.7433703	0.66883649	97.9	99.45772347
methanol	-115.769616	-115.105113	0.664503	98.2	97.23876115
propane (2^o)	-119.189364	-118.521473	0.667891	98.4	98.97358655
ethane	-79.86248302	-79.18863231	0.6738507	100.9	102.0252534
cyclopropane	-117.938332	-117.253902	0.68443	105	107.4423815
methane	-40.537581	-39.856414	0.681167	105.2	105.7715624
benzene	-232.324426	-231.633797	0.690629	113.3	110.6165795
acetylene	-77.360585	-76.632761	0.727824	132	129.6622792
diphenylmethanol	-578.0104231	-577.380929	0.6294941		79.05012764
allylbenzene	-349.070483	-348.437148	0.633335		80.9988456
N-methylpyrrole	-249.55654	-248.902176	0.654364		91.66811904
2-methyl-1,3-dioxane	-307.778136	-307.122129	0.656007		92.50171152
1,3-dioxane	-268.441669	-267.784052	0.657617		93.31856112
THF	-232.531929	-231.873179	0.65875		93.8934
methyl t-butyl ether	-273.074088	-272.411072	0.663016		96.05779776
cyclopentane	-196.623847	-195.959433	0.664414		96.76708704
anisole	-346.886771	-346.2205654	0.66620562		97.6760813
cyclohexane	-235.9591827	-235.2909874	0.66819531		98.68557172
t-butylbenzene	-389.628316	-388.955062	0.673254		101.2521494

Table 3. Absolute rate constants for the reaction of *t*-BuO• with tribenzylamine

T (°C)	k_H ($M^{-1}s^{-1}$)
80	5.85E+07
70	5.51E+07
60	5.26E+07
50	4.87E+07
40	4.54E+07
30	4.42E+07
25	4.20E+07
20	4.04E+07
10	3.76E+07
5	3.26E+07

Figure 2. Arrhenius plot for the reaction of *t*-BuO• with tribenzylamine

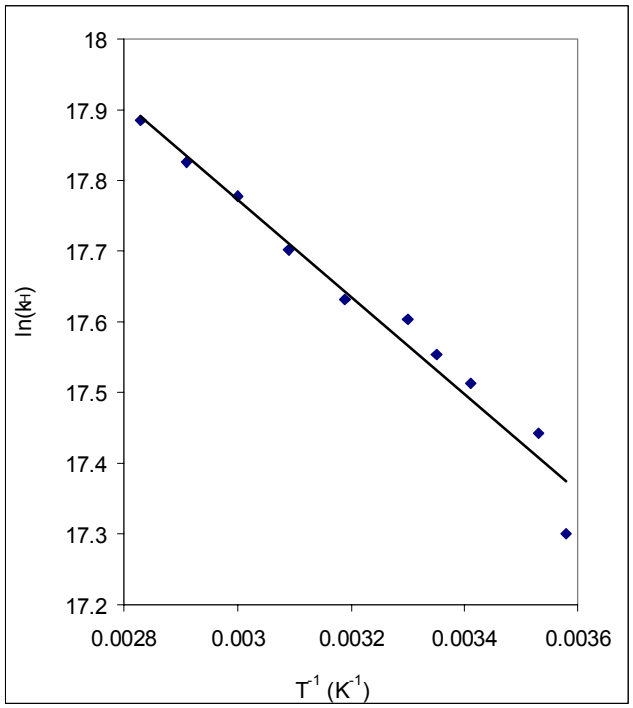

Table 4. Absolute rate constants for the reaction of *t*-BuO• with N,N-dibenzylaniline

T (°C)	k_H ($M^{-1}s^{-1}$)
80	3.20E+07
70	2.92E+07
60	2.62E+07
50	2.34E+07
40	2.23E+07
30	1.94E+07
25	1.83E+07
20	1.72E+07
10	1.65E+07

Figure 3. Arrhenius plot for the reaction of *t*-BuO• with N,N-dibenzylaniline

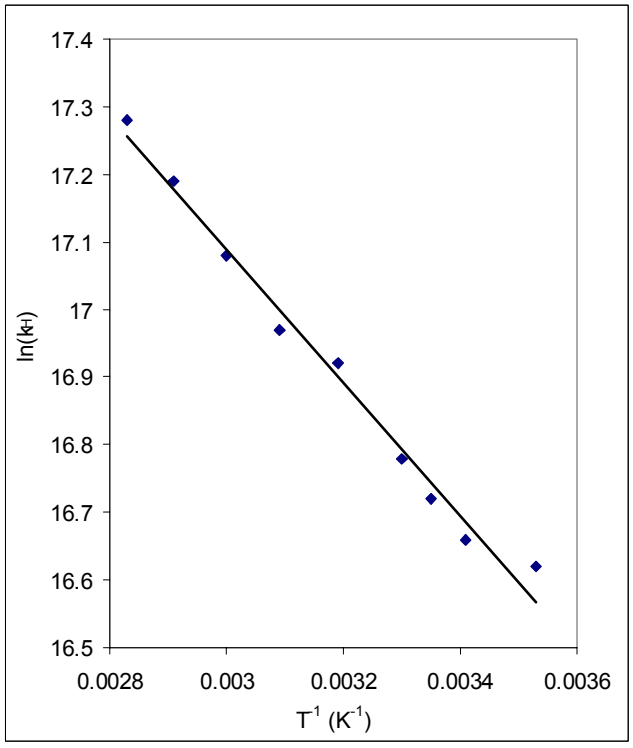

Table 5. Absolute rate constants for the reaction of *t*-BuO• with DABCO

T (°C)	k_H ($M^{-1}s^{-1}$)
70	1.85E+07
60	1.66E+07
50	1.49E+07
40	1.38E+07
30	1.23E+07
25	1.14E+07
20	1.02E+07
10	9.63E+06

Figure 4. Arrhenius plot for the reaction of *t*-BuO• with DABCO

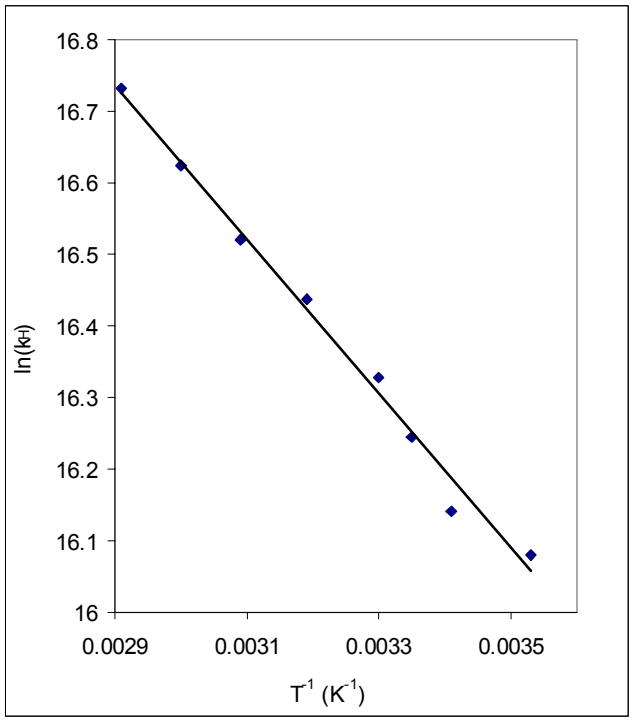

Table 6. Absolute rate constants for the reaction of *t*-BuO• with triallylamine

T (°C)	k_H ($M^{-1}s^{-1}$)
80	1.58E+08
70	1.46E+08
60	1.32E+08
50	1.21E+08
40	1.03E+08
30	8.97E+07
25	8.80E+07
20	8.37E+07
10	7.84E+07

Figure 5. Arrhenius plot for the reaction of *t*-BuO• with triallylamine

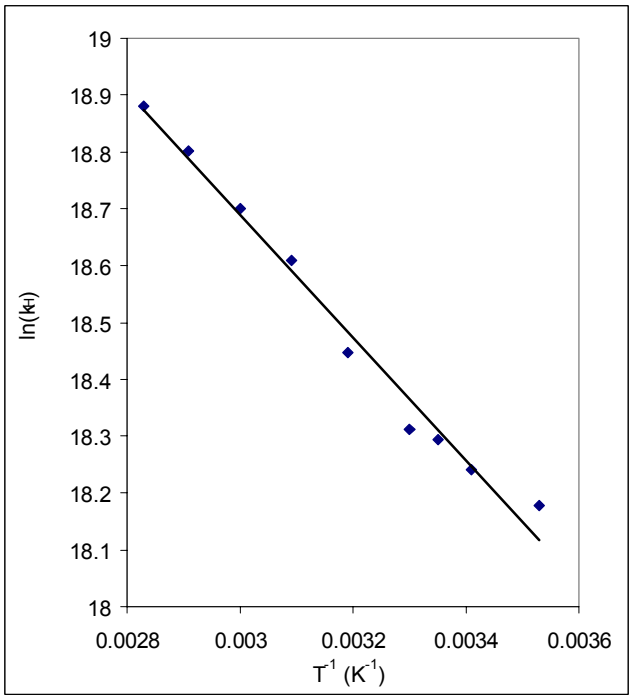

Table 7. Absolute rate constants for the reaction of *t*-BuO• with triethylamine

T (^{o}C)	k_H ($M^{-1}s^{-1}$)
70	1.65E+08
60	1.55E+08
50	1.30E+08
40	1.10E+08
30	1.09E+08
25	1.01E+08
20	9.77E+07
10	7.23E+07

Figure 6. Arrhenius plot for the reaction of *t*-BuO• with triethylamine

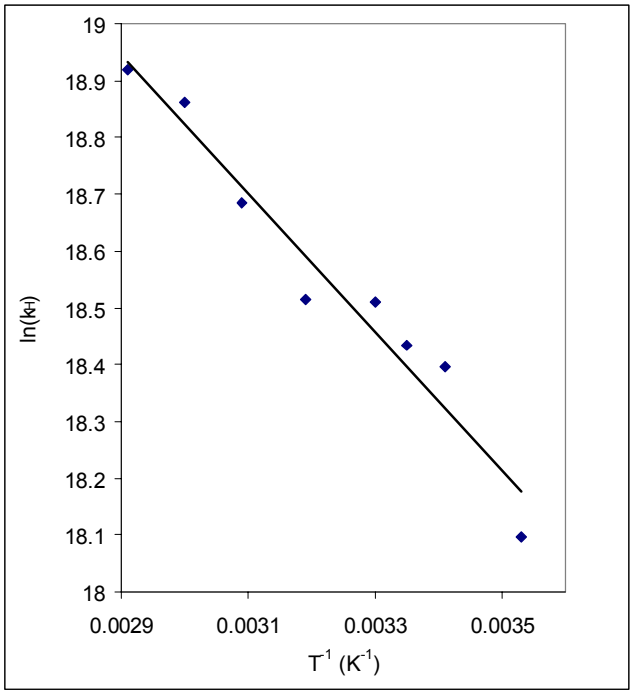

Table 8. Absolute rate constants for the reaction of *t*-BuO• with quinuclidine

T (^{o}C)	k_H ($M^{-1}s^{-1}$)
70	1.62E+07
60	1.60E+07
50	1.54E+07
40	1.23E+07
30	1.09E+07
25	1.07E+07
20	8.71E+06
10	7.52E+06

Figure 7. Arrhenius plot for the reaction of *t*-BuO• with quinuclidine

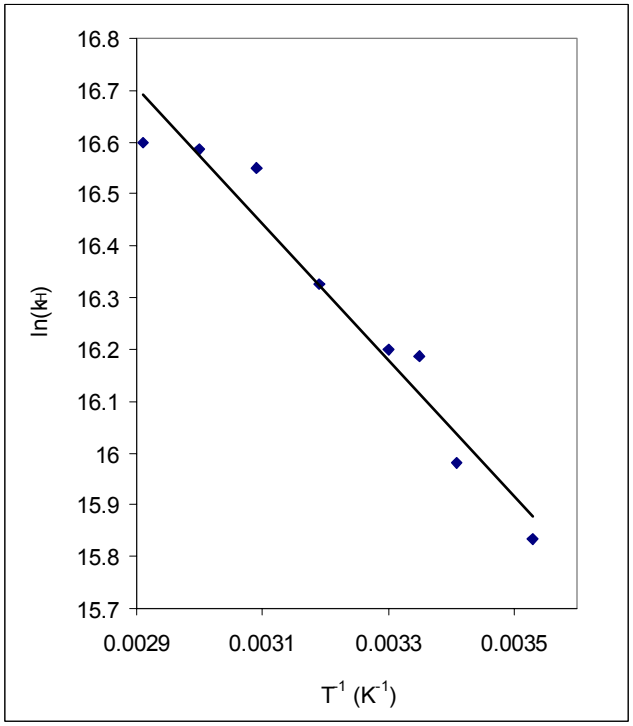

Table 9. Absolute rate constants for the reaction of *t*-BuO• with N-methylpyrrole

T (^{o}C)	k_H ($M^{-1}s^{-1}$)
80	1.45E+07
70	1.21E+07
60	9.58E+06
50	8.52E+06
40	8.14E+06
30	8.02E+06
25	7.34E+06
20	6.78E+06
10	6.36E+06

Figure 8. Arrhenius plot for the reaction of *t*-BuO• with N-methylpyrrole

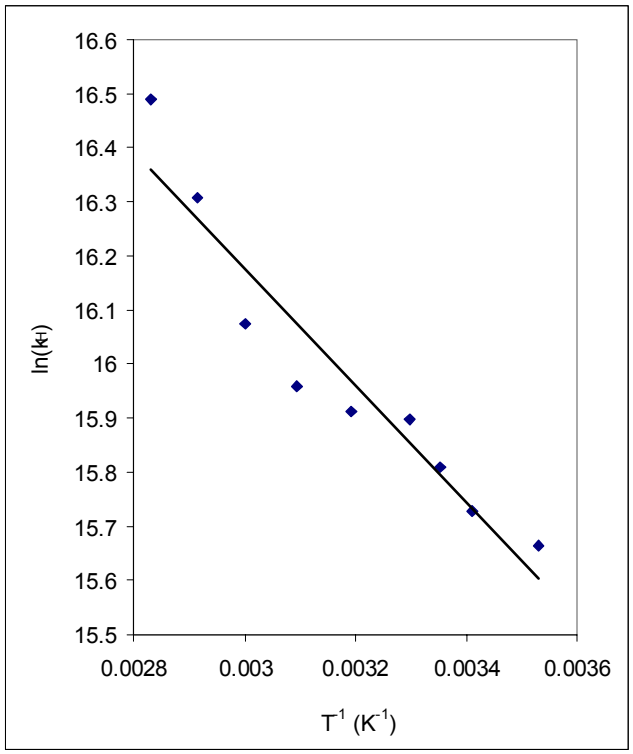

Table 10. Absolute rate constants for the reaction of *t*-BuO• with N,N-dimethylaniline

T (^{o}C)	k_H ($M^{-1}s^{-1}$)
80	3.20E+07
70	2.92E+07
60	2.62E+07
50	2.34E+07
40	2.23E+07
30	1.94E+07
25	1.83E+07
20	1.72E+07
10	1.65E+07

Figure 9. Arrhenius plot for the reaction of *t*-BuO• with N,N-dimethylaniline

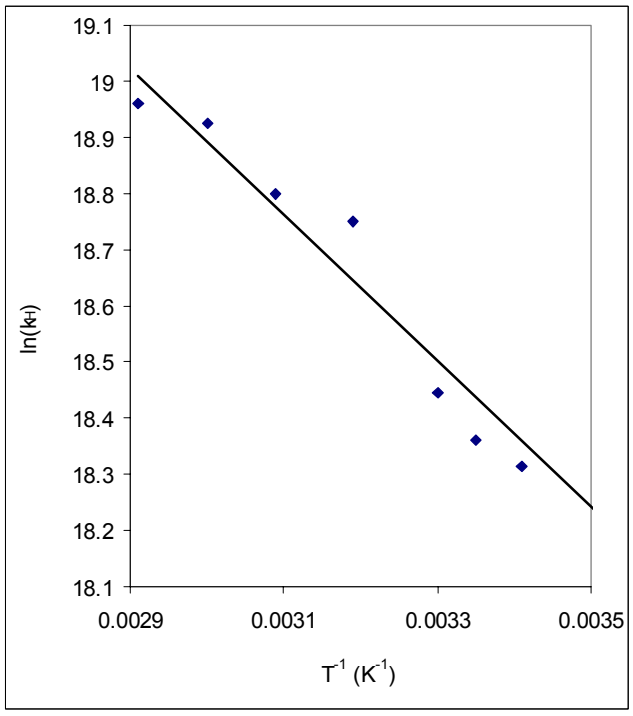

Table 11. Absolute rate constants for the reaction of *t*-BuO• with triphenylmethane

T (^{o}C)	k_H ($M^{-1}s^{-1}$)
70	2.93E+06
60	2.84E+06
50	2.65E+06
40	2.47E+06
30	2.00E+06
25	1.96E+06
20	1.91E+06
10	1.69E+06

Figure 10. Arrhenius plot for the reaction of *t*-BuO• with triphenylmethane

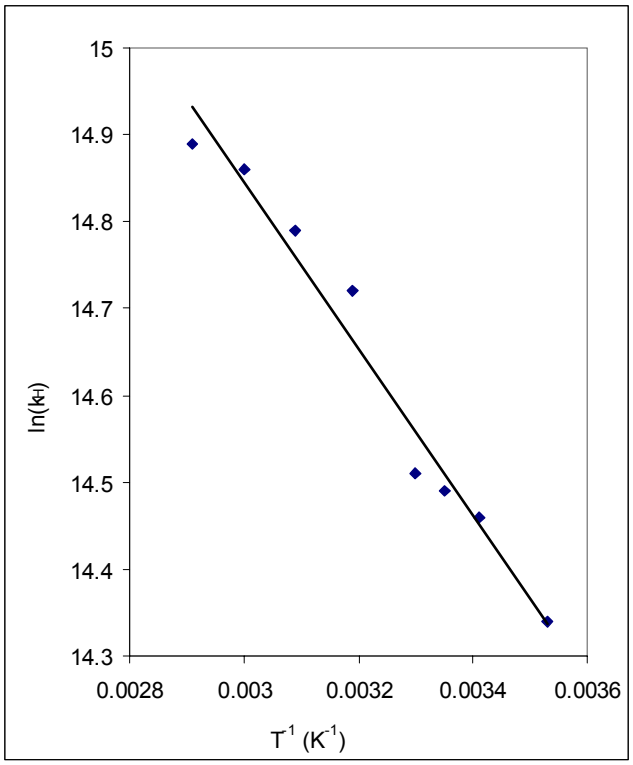

Table 12. Absolute rate constants for the reaction of *t*-BuO• with diphenylmethane

T (^{o}C)	k_H ($M^{-1}s^{-1}$)
70	5.71E+06
60	4.96E+06
50	4.59E+06
40	4.25E+06
30	3.87E+06
25	3.56E+06
20	2.88E+06
10	2.39E+06

Figure 11. Arrhenius plot for the reaction of *t*-BuO• with diphenylmethane

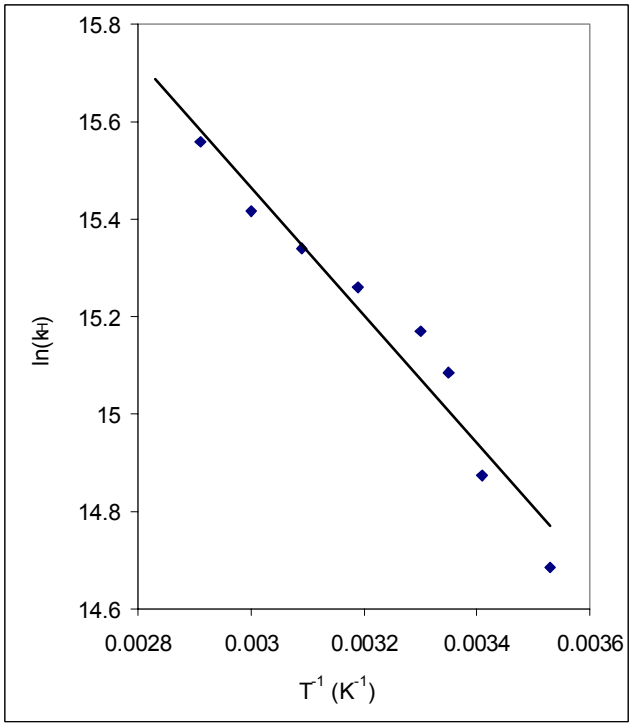

Table 13. Absolute rate constants for the reaction of *t*-BuO• with allylbenzene

T (^{o}C)	k_H ($M^{-1}s^{-1}$)
80	3.91E+06
70	3.34E+06
60	3.04E+06
50	2.50E+06
40	2.70E+06
30	2.22E+06
25	1.94E+06
20	1.97E+06
10	1.36E+06

Figure 12. Arrhenius plot for the reaction of *t*-BuO• with allylbenzene

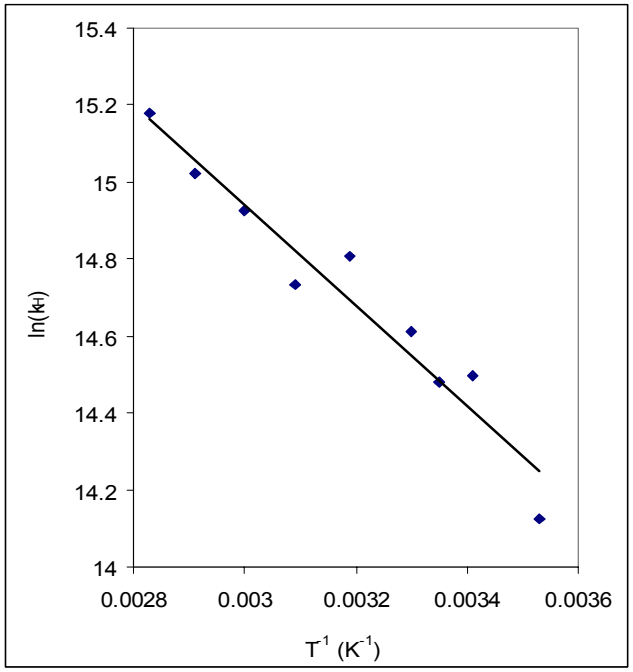

Table 14. Absolute rate constants for the reaction of *t*-BuO• with cyclohexane

T (^{o}C)	k_H ($M^{-1}s^{-1}$)
70	2.21E+06
60	1.86E+06
50	1.36E+06
40	1.01E+06
30	9.89E+05
25	8.53E+05
20	8.19E+05
10	5.31E+05

Figure 13. Arrhenius plot for the reaction of *t*-BuO• with cyclohexane

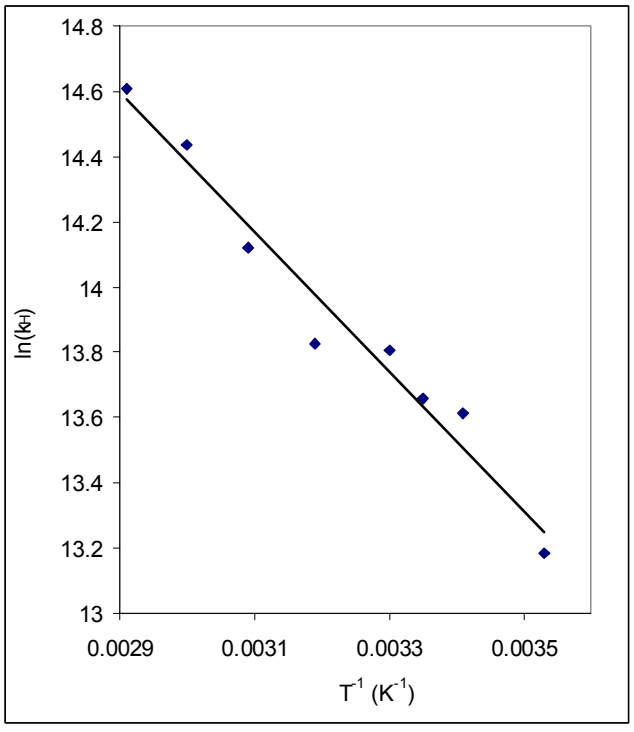

Table 15. Absolute rate constants for the reaction of *t*-BuO• with toluene

T (^{o}C)	k_H ($M^{-1}s^{-1}$)
80	4.89E+05
70	3.93E+05
60	3.55E+05
50	3.06E+05
40	2.29E+05
30	1.98E+05
25	1.90E+05
20	1.74E+05
10	1.71E+05

Figure 14. Arrhenius plot for the reaction of *t*-BuO• with toluene

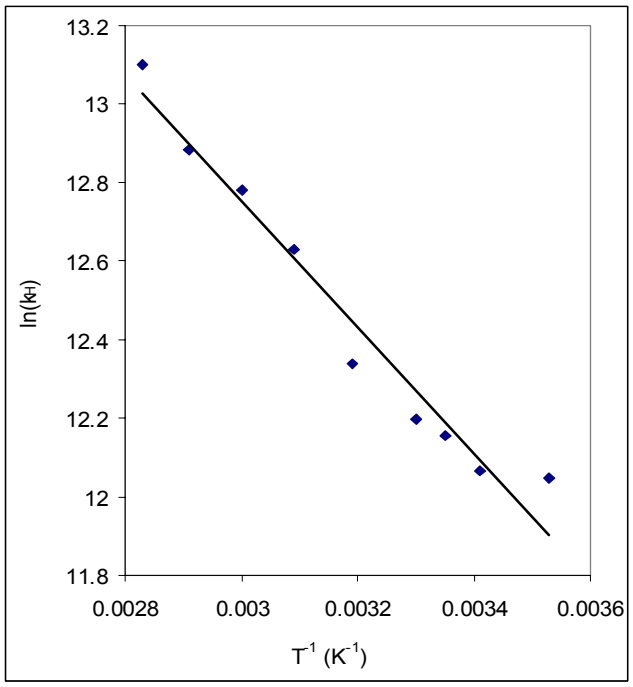

Table 16. Absolute rate constants for the reaction of *t*-BuO• with diphenylmethanol

T (^{o}C)	k_H ($M^{-1}s^{-1}$)
70	1.05E+07
60	1.02E+07
50	9.25E+06
40	7.96E+06
30	7.50E+06
25	6.78E+06
20	6.65E+06
10	5.55E+06

Figure 15. Arrhenius plot for the reaction of *t*-BuO• with diphenylmethanol

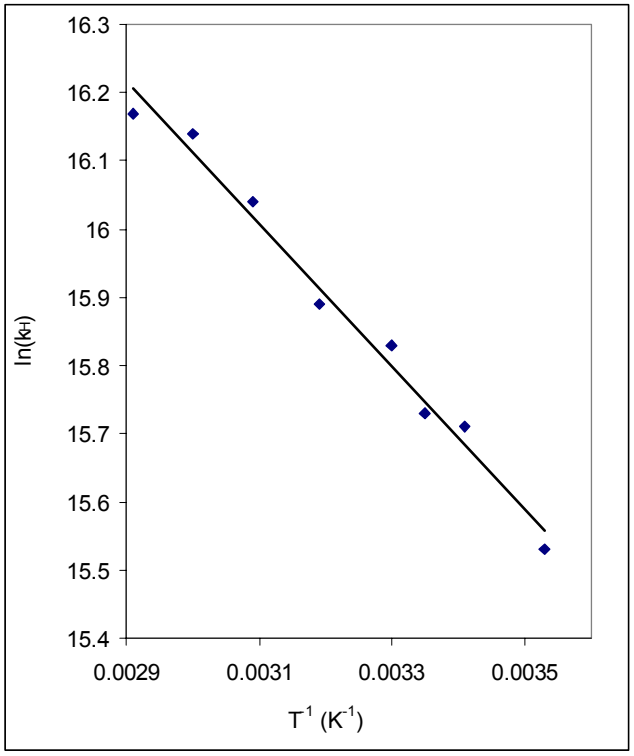

Table 17. Arrhenius parameters for hydrogen abstraction by *t*-BuO• from various substrates obtained by linear and non-linear fitting (separate trials listed; Arrhenius parameters obtained from average rate constants summarized in Table 2.2).

	Linear		*non-linear*	
Substrate	**E_a. (kcal/mol)**	**log A (A in units of M^{-1} s^{-1})**	**E_a. (kcal/mol)**	**log A (A in units of M^{-1} s^{-1})**
Amines				
tribenzylamine	1.23(15)	8.43(21)	1.25(16)	8.45(10)
	1.22(15)	8.53(20)	1.22(15)	8.53(10)
	1.30(15)	8.63(21)	1.50(32)	8.76(18)
N,N-dibenzylaniline	1.95(21)	8.70(29)	2.01(19)	8.74(11)
	1.96(23)	8.64(16)	1.94(25)	8.63(21)
DABCO	1.98(12)	8.55(17)	1.98(14)	8.55(09)
	2.35(47)	8.73(33)	2.37(42)	8.74(22)
triallylamine	2.29(30)	9.61(42)	2.32(29)	9.62(16)
	2.01(27)	9.45(38)	2.10(25)	9.51(14)
triethylamine	2.46(83)	10.0(12)	2.75(77)	10.2(3)
	1.92(26)	9.52(27)	1.89(27)	9.50(16)
quinuclidine	2.4(11)	8.8(16)	2.1(12)	8.52(47)
	2.71(72)	9.0(10)	2.25(.70)	8.68(32)
N-methylpyrrole	2.14(60)	8.43(83)	2.42(70)	8.62(32)
N,N-dimethylaniline	2.42(65)	9.78(92)	2.39(63)	9.75(30)
	2.75(60)	10.0(8)	2.69(60)	9.98(29)
Hydrocarbons				
triphenylmethane	1.91(33)	7.70(47)	1.86(36)	7.67(19)
diphenylmethane	2.88(74)	8.7(10)	2.61(64)	8.53(31)
	2.05(41)	7.91(58)	1.96(37)	7.85(19)
allylbenzene	2.47(28)	8.16(39)	2.48(31)	8.15(18)
	2.8(14)	8.29(96)	2.5(10)	8.10(43)
cyclohexane	3.4(13)	8.4(18)	4.0(13)	8.76(47)
	3.78(84)	8.8(12)	3.99(91)	8.94(38)
	4.3(14)	9.1(20)	4.9(15)	9.53(50)
	4.0(12)	8.8(16)	3.9(12)	8.72(45)
toluene	3.41(64)	7.74(90)	3.11(77)	7.53(34)
	3.72(69)	7.94(95)	3.42(79)	7.76(34)
	3.01(27)	7.55(37)	3.02(26)	7.56(15)
Alcohols				
diphenylmethanol	2.08(27)	8.36(38)	2.03(28)	8.33(16)

Table 18. B3LYP (6-31G) calculated transition states for hydrogen abstraction from a) toluene and b) triphenylmethane by *t*-BuO•**

a) Toluene + *t*-BuO•	b) Triphenylmethane + *t*-BuO•
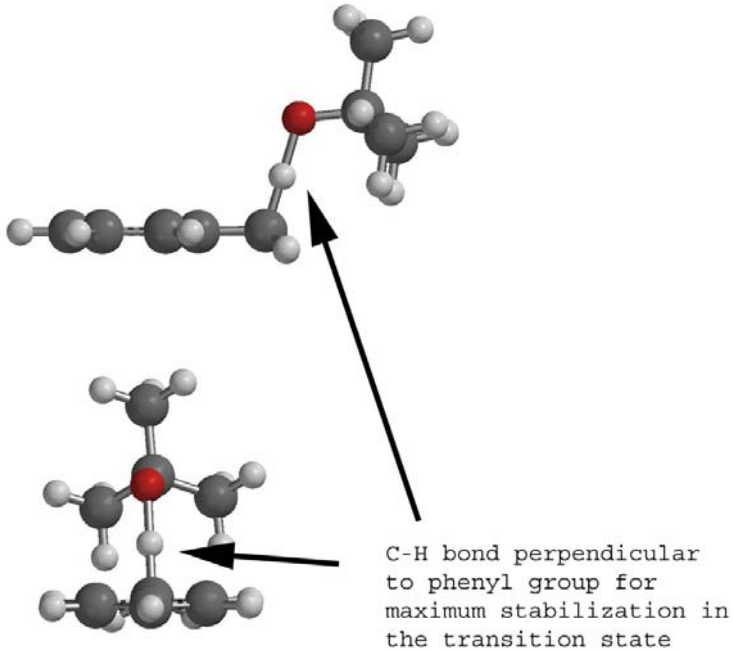	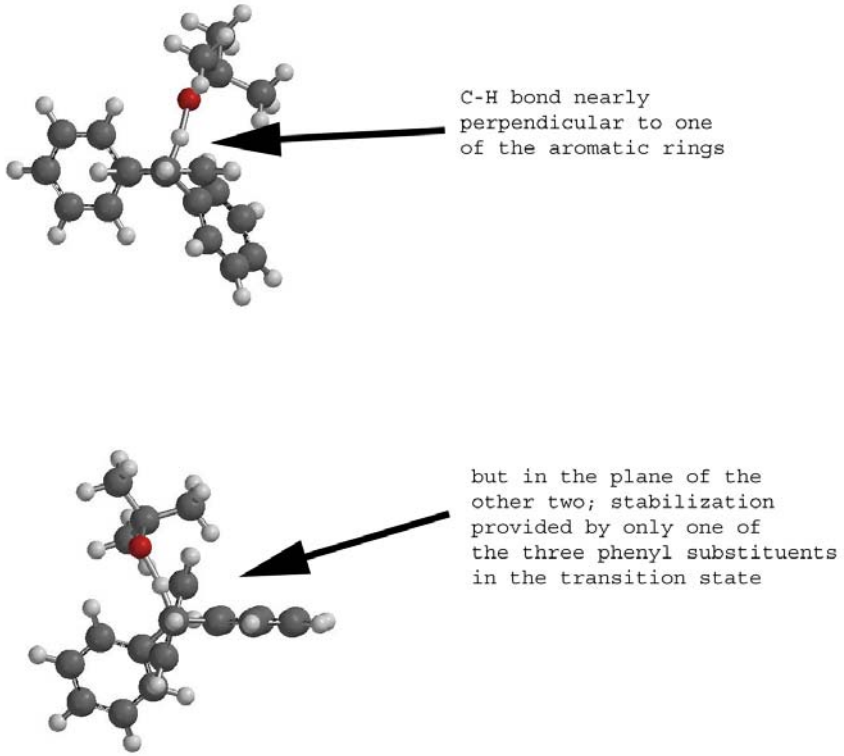

APPENDIX B. SPECTRA AND ARRHENIUS PLOTS FOR RADICAL ANIONS

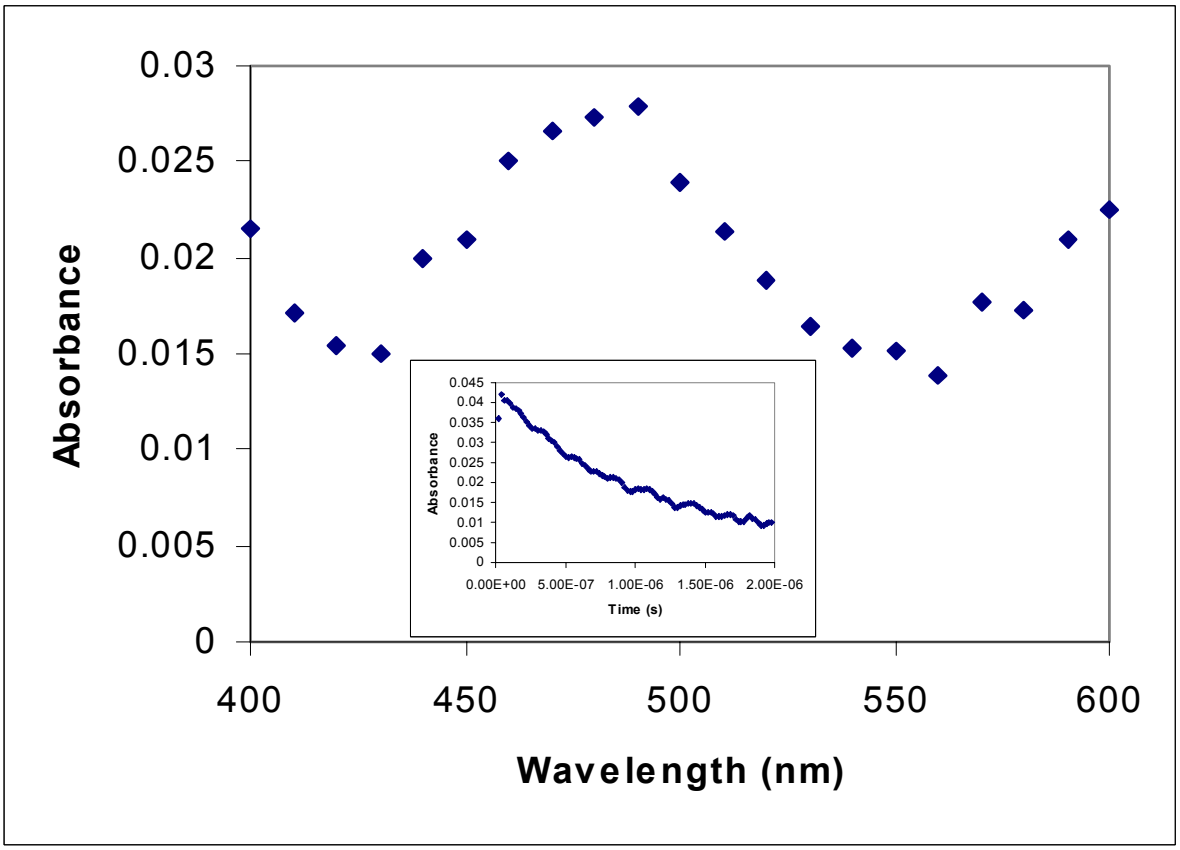

Figure 1. **Spectrum and Transient Signal for the Decay of the *t*-Butyl Phenyl Ketone Radical Anion at 490 nm Generated by the Excitation of 0.00551 M *t*-Butyl Phenyl Ketone with 0.0004 M DMS and 0.01 M Tetrabutylammonium Azide in Acetonitrile**

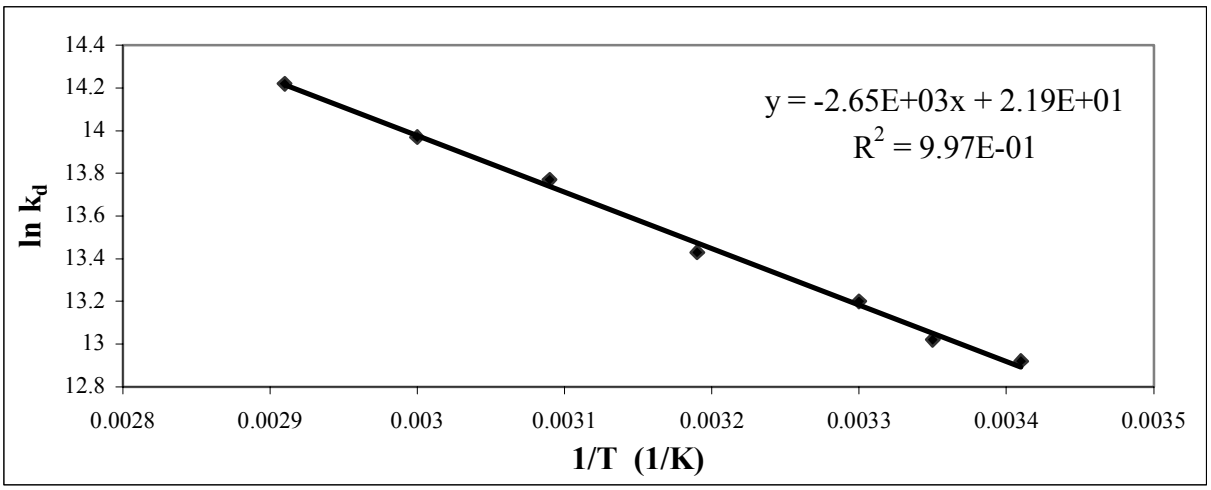

Figure 2. **Arrhenius Plot of *t*-Butyl Phenyl Ketone Radical Anion Generated by the Excitation of 0.00551 M *t*-Butyl Phenyl Ketone with 0.0004 M DMS and 0.01 M Tetrabutylammonium Azide in Acetonitrile**

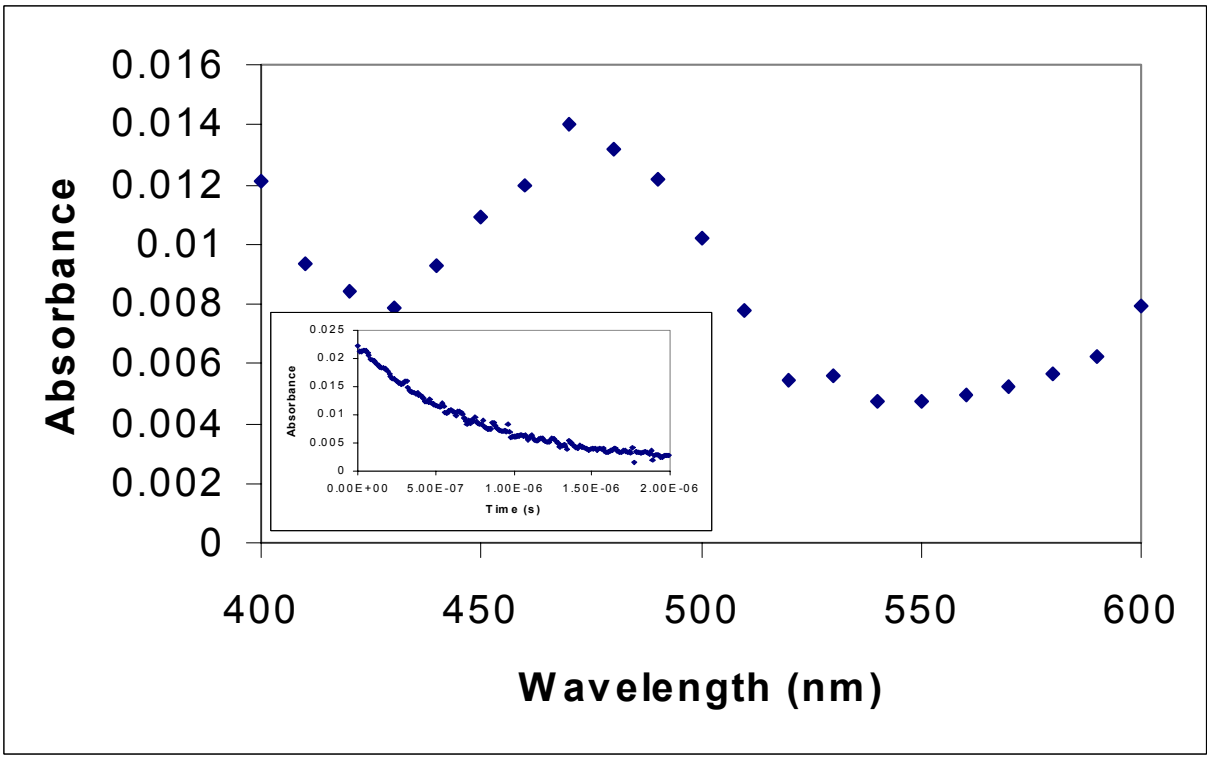

Figure 3. **Spectrum and Transient Signal for the Decay of the Cyclopropyl Phenyl Ketone Radical Anion at 480 nm Generated by the Excitation of 0.00654 M Cyclopropyl Phenyl Ketone with 0.0003 M DMS and 0.01 M Tetrabutylammonium Azide in Acetonitrile**

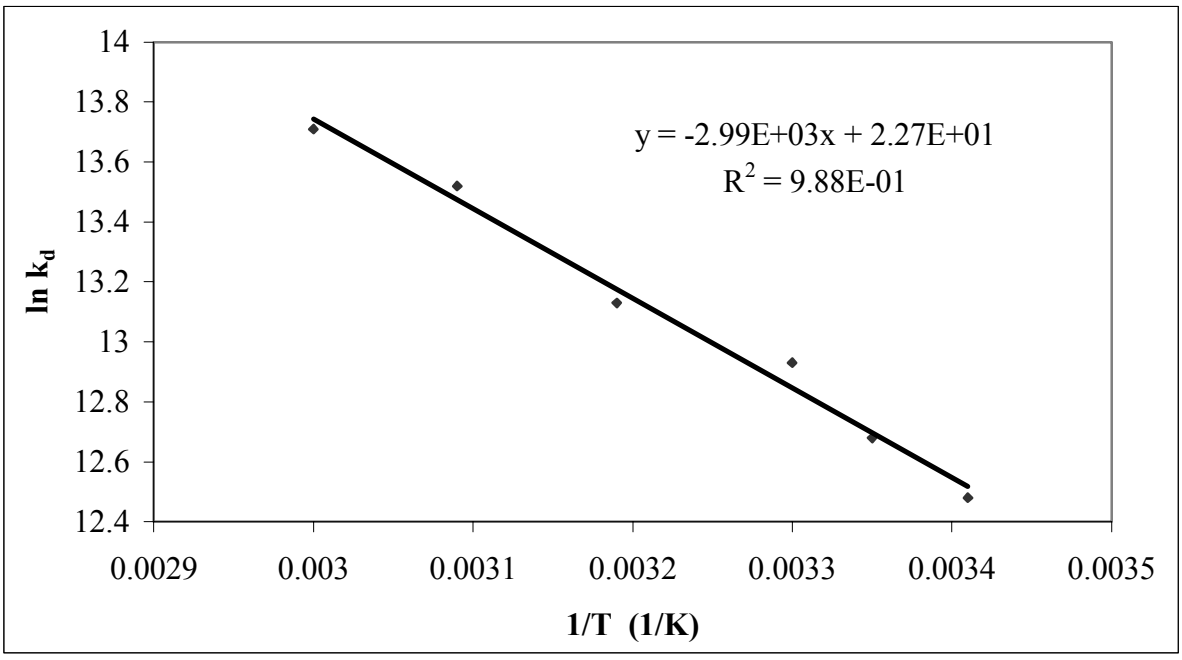

Figure 4. **Arrhenius Plot of Cyclopropyl Phenyl Ketone Radical Anion Generated by the Excitation of 0.00654 M Cyclopropyl Phenyl Ketone with 0.0003 M DMS and 0.01 M Tetrabutylammonium Azide in Acetonitrile.**

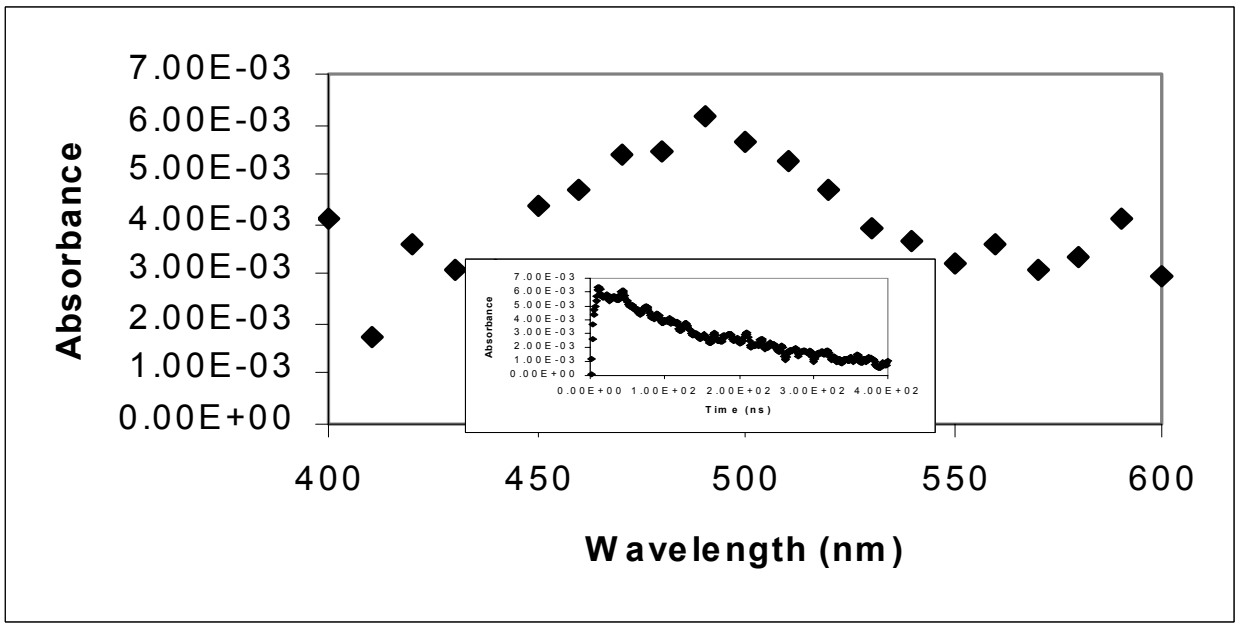

Figure 5. **Spectrum and Transient Signal for Decay of the *p*-Tolyl Cyclopropyl Ketone Radical Anion at 490 nm Generated by the Excitation of 0.00541 M *p*-Tolyl Cyclopropyl Ketone with 0.00033 M DMS and 0.01 M Tetrabutylammonium Azide in Acetonitrile**

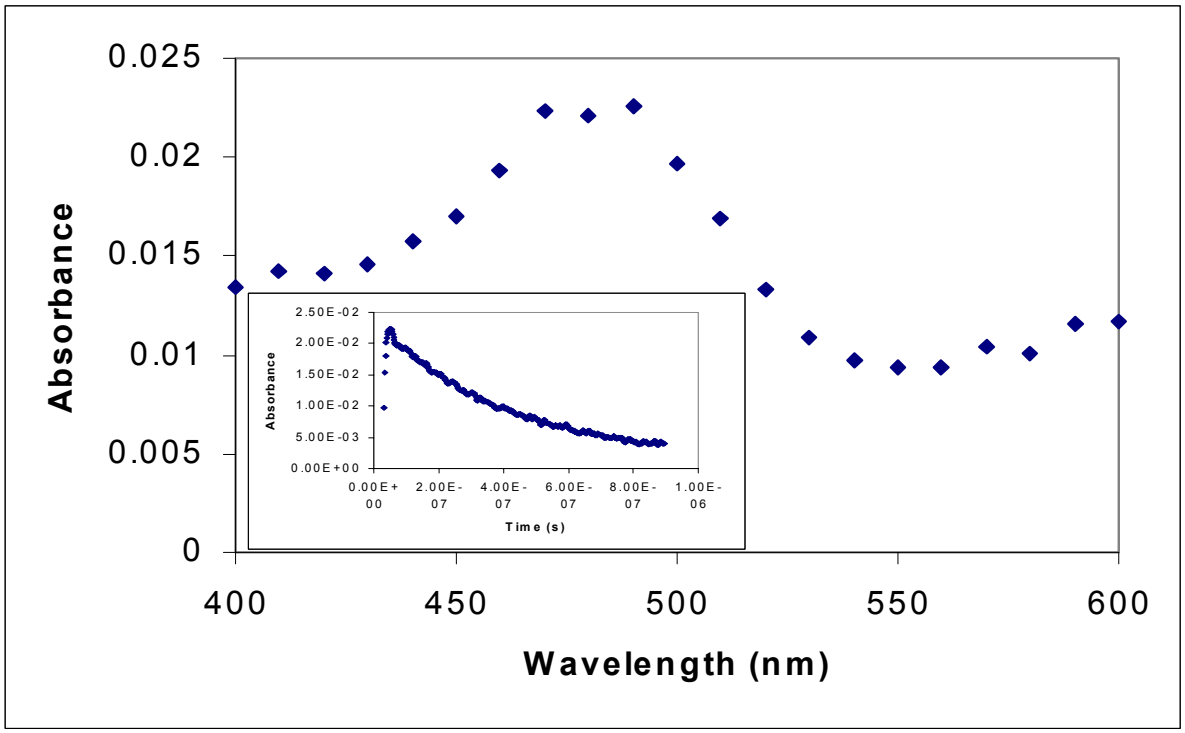

Figure 6. **Spectrum and Transient Signal for the Decay of the *trans*-1-Benzoyl-2-Methyl Cyclopropane Ketone Radical Anion at 470 nm Generated by the Excitation of 0.00601 M *trans*-1-Benzoyl-2-Methyl Cyclopropane with 0.00031 M DMS and 0.01 M Tetrabutylammonium Azide in Acetonitrile**

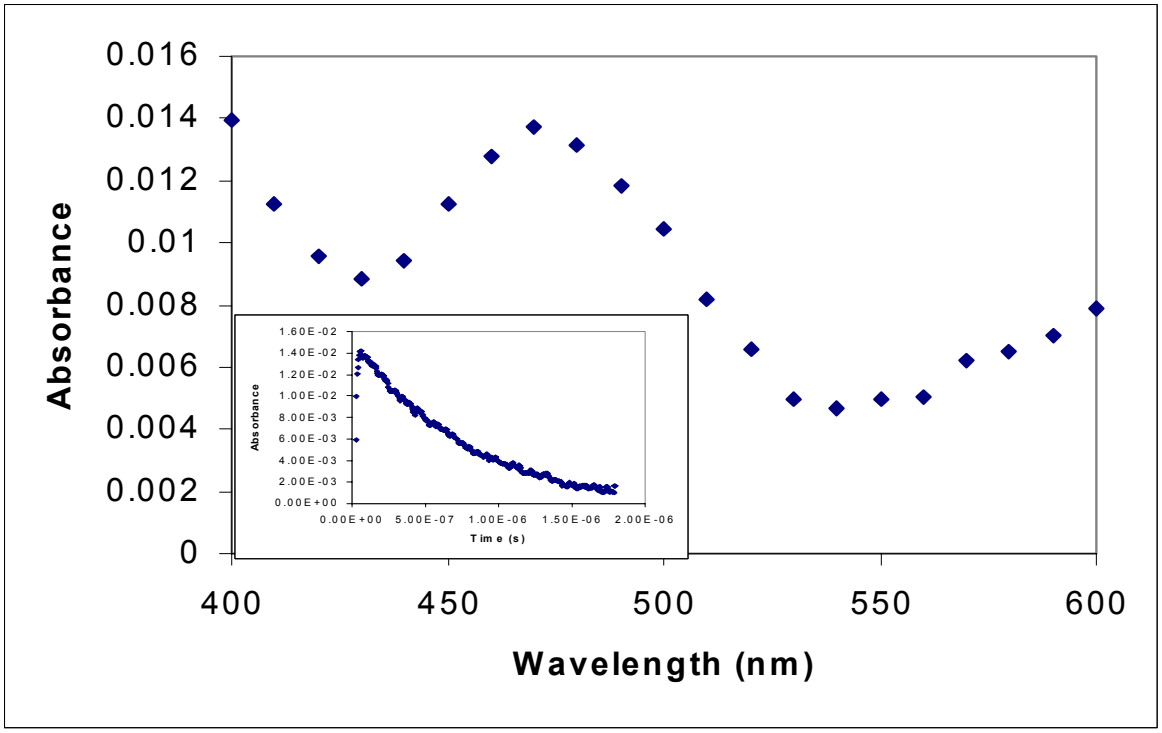

Figure 7. **Spectrum and Transient Signal for the Decay of the 1-Benzoyl-2,2-Dimethyl Cyclopropane Ketone Radical Anion at 470 nm Generated by the Excitation of 0.00582 M 1-Benzoyl-2,2-Dimethyl Cyclopropane with 0.00028 M DMS and 0.01M Tetrabutylammonium Azide in Acetonitrile**

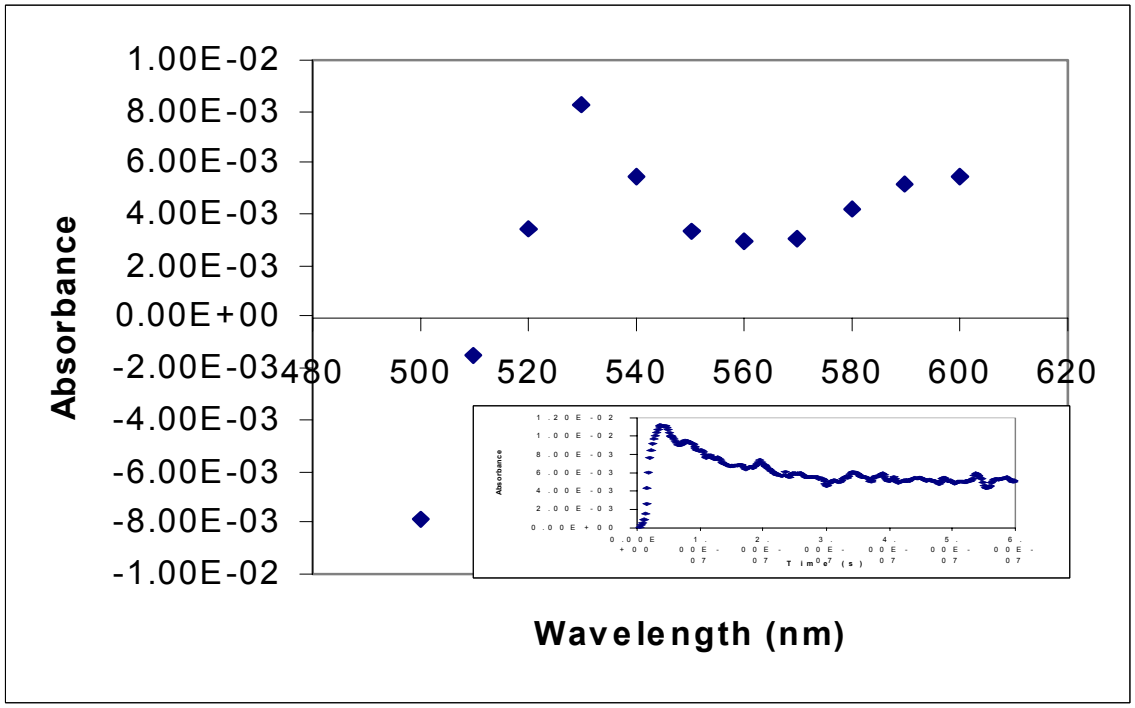

Figure 8. **Spectrum and Transient Signal for Decay of the *trans*-1-Benzoyl-2-Phenylcyclopropane Ketone Radical Anion at 530 nm Generated by the Excitation of 0.00531 M *trans*-1-Benzoyl-2-Phenylcyclopropane with 0.00023 M DMS and 0.01 M Tetrabutylammonium Azide in Acetonitrile**

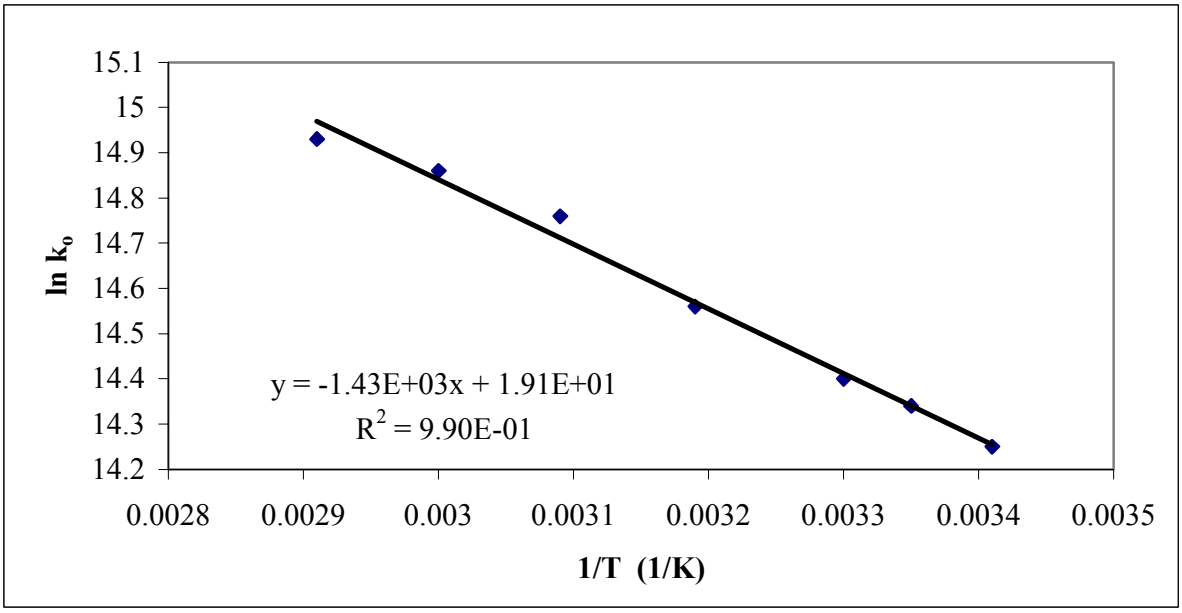

Figure 9. **Arrhenius Plot of *trans*-1-Benzoyl-2-phenylcyclopropane Radical Anion Generated by the Excitation of 0.00519 M *trans*-1-Benzoyl-2-phenylcyclopropane with 0.00031 M DMS and 0.01 M Tetrabutylammonium Azide in Acetonitrile.**

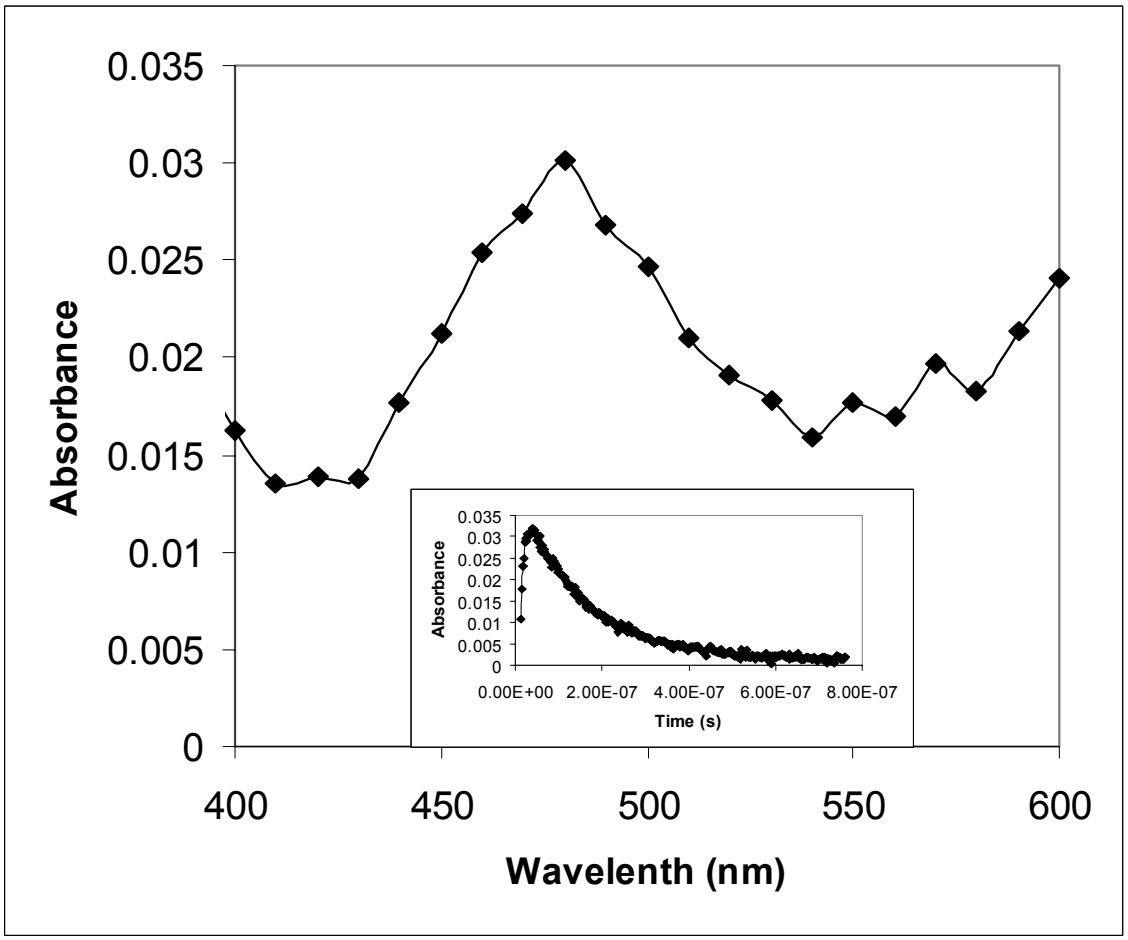

Figure 10. Spectrum and Transient Signal for Decay of the 2,3-epoxy-1-phenyl propan-1-one Radical Anion at 480 nm Generated by the Excitation of 0.0089 M 2,3-epoxy-1-phenyl propan-1-one with 0.0003 M DMS and 0.01 M Tetrabutylammonium Azide in Acetonitrile

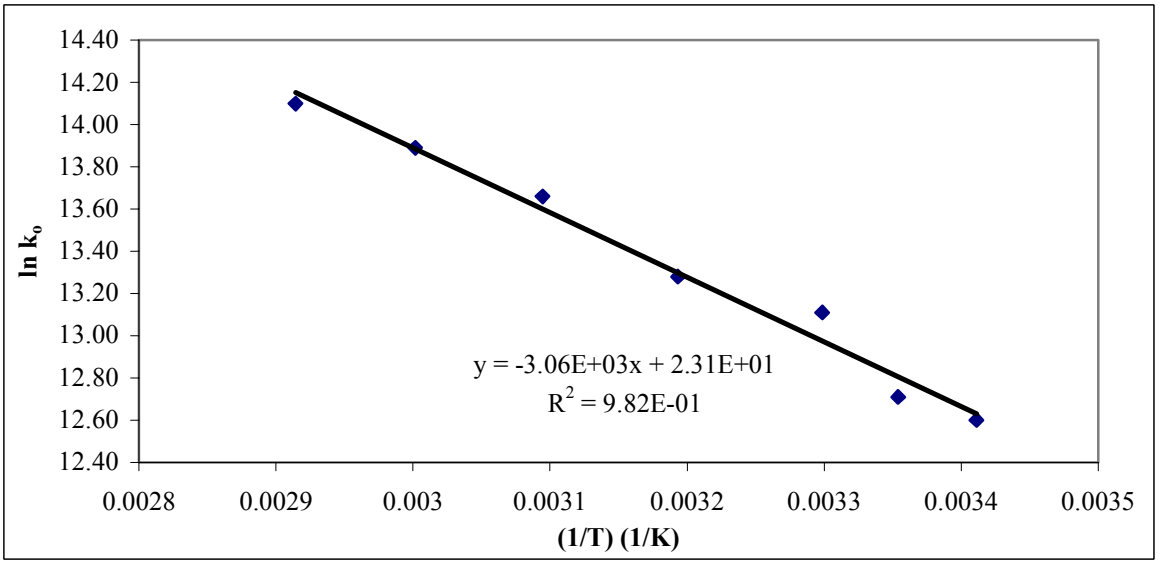

Figure 11. **Arrhenius Plot of 2,3-Epoxy-1-phenyl-1-propan-1-one Radical Anion Generated by the Excitation of 0.006 M 2,3-Epoxy-1-phenyl-1-propan-1-one with 0.0003 M DMS and 0.01 M Tetrabutylammonium Azide in Acetonitrile.**

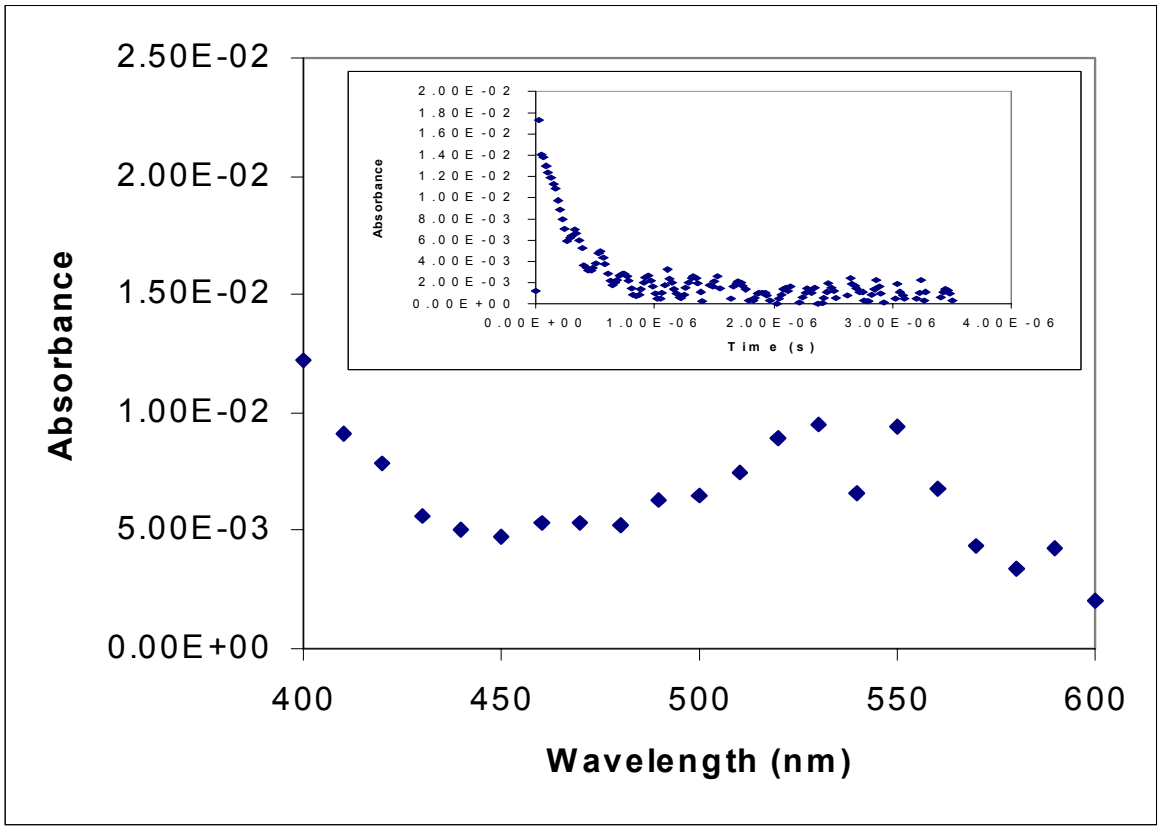

Figure 12. **Spectrum and Transient Signal for the Decay of the 2,3-Epoxy-1,3-diphenyl-1-propan-1-one Ketone Radical Anion at 530 nm Generated by the Excitation of 0.00565 M 2,3-Epoxy-1,3-diphenyl-1-propan-1-one with 0.00033 M DMS and 0.01 M Tetrabutylammonium Azide in Acetonitrile.**

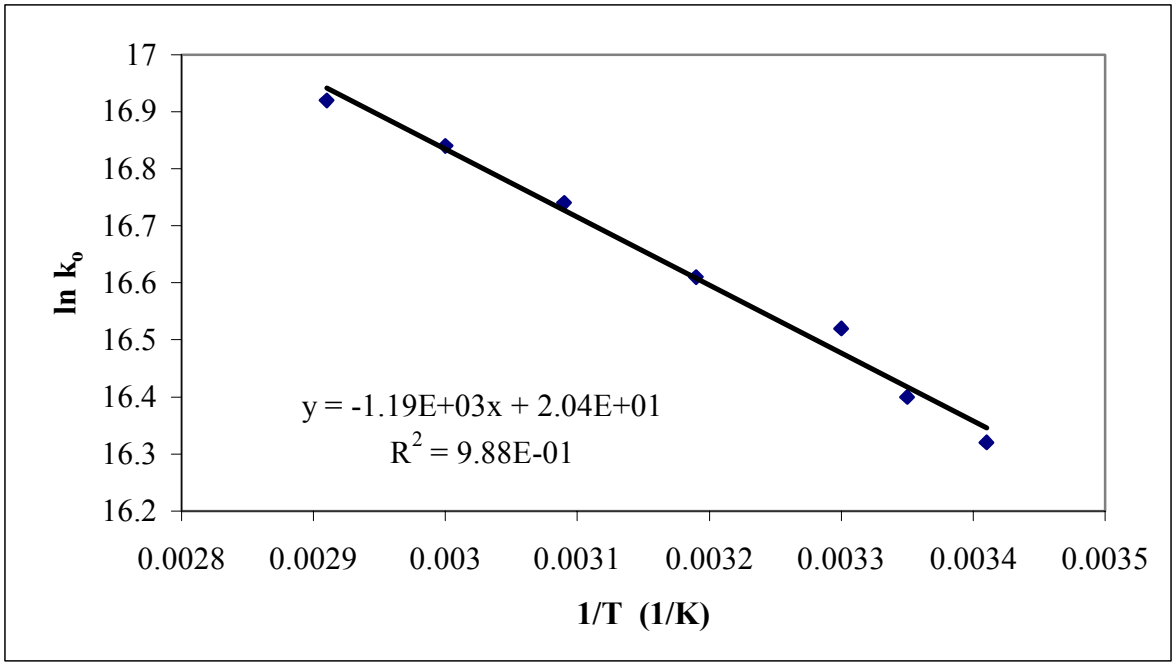

Figure 13. **Arrhenius Plot of 2,3-Epoxy-1,3-diphenyl-1-propan-1-one Radical Anion Generated by the Excitation of 0.006 M 2,3-Epoxy-1,3-diphenyl-1-propan-1-one with 0.0003 M DMS and 0.01 M Tetrabutylammonium Azide in Acetonitrile.**

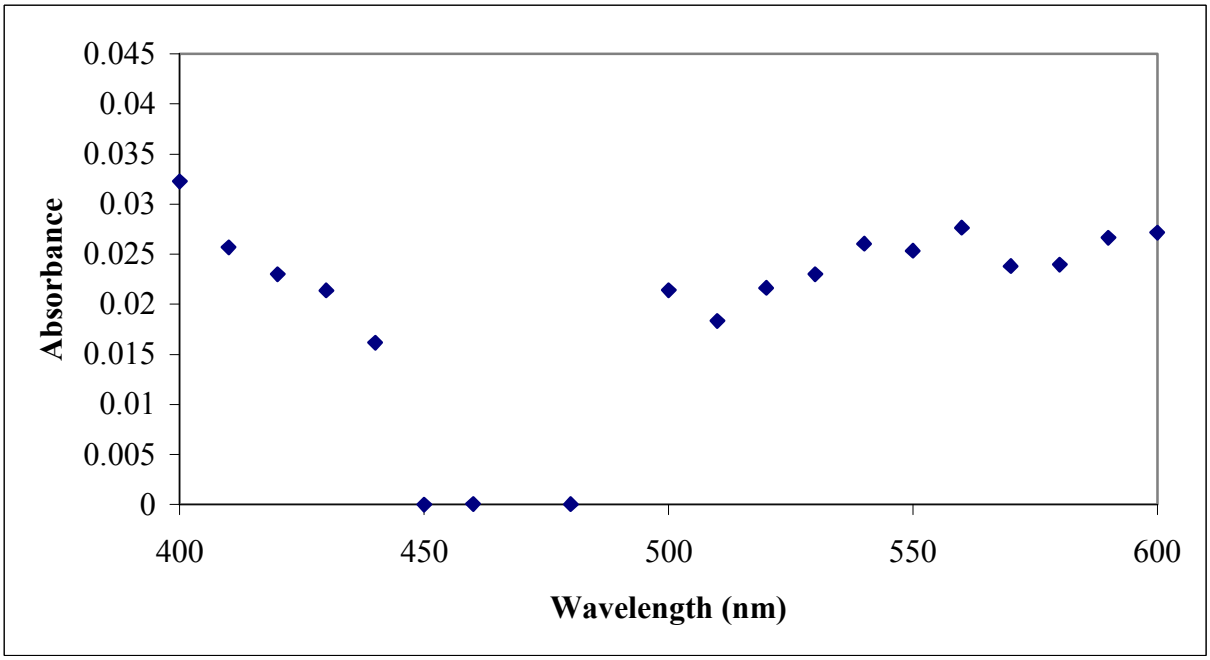

Figure 14. **Spectrum and Transient Signal for the Decay of the trans-1,2-Dibenzoyl Cyclopropane Radical Anion at 560 nm Generated by the Excitation of 0.005 M *trans*-1,2-Dibenzoyl Cyclopropane with 0.0003 M DMS and 0.01 M Tetrabutylammonium Azide in Acetonitrile.**

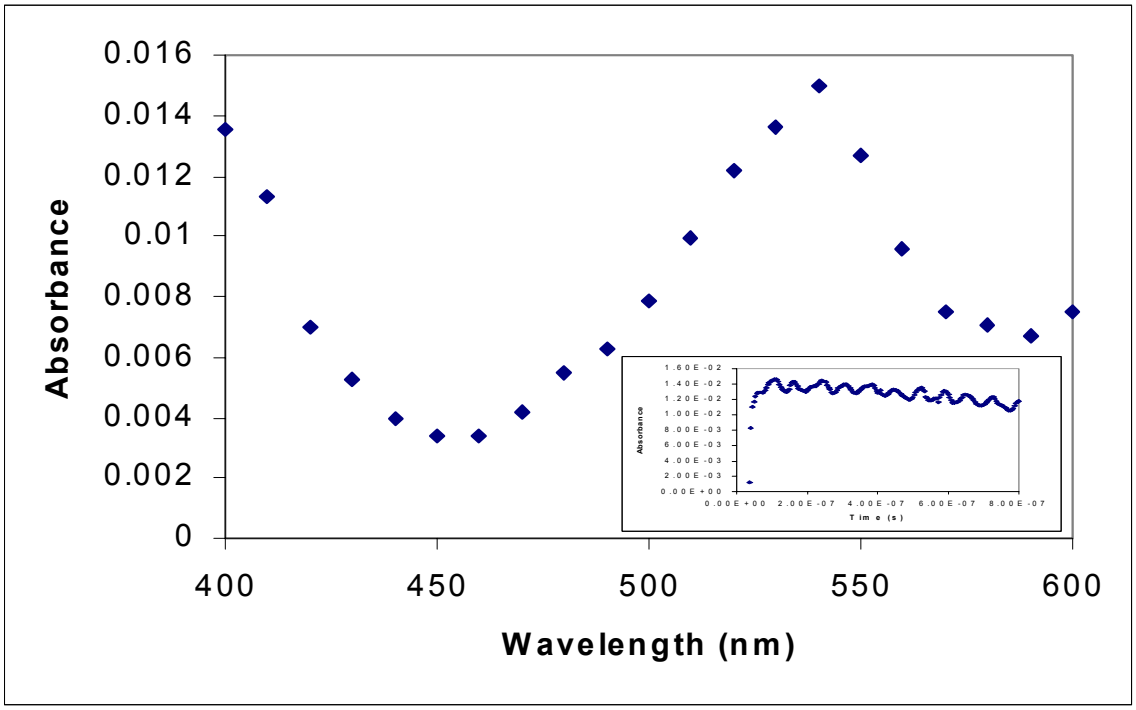

Figure 15. **Spectrum and Transient Signal for the Decay of the 10-Spirocyclopropyl-9-anthracenone Radical Anion at 540 nm Generated by the Excitation of 0.003 M 10-Spirocyclopropyl-9-anthracenone with 0.0003 M DMS and 0.01 M Tetrabutylammonium Azide in Acetonitrile.**

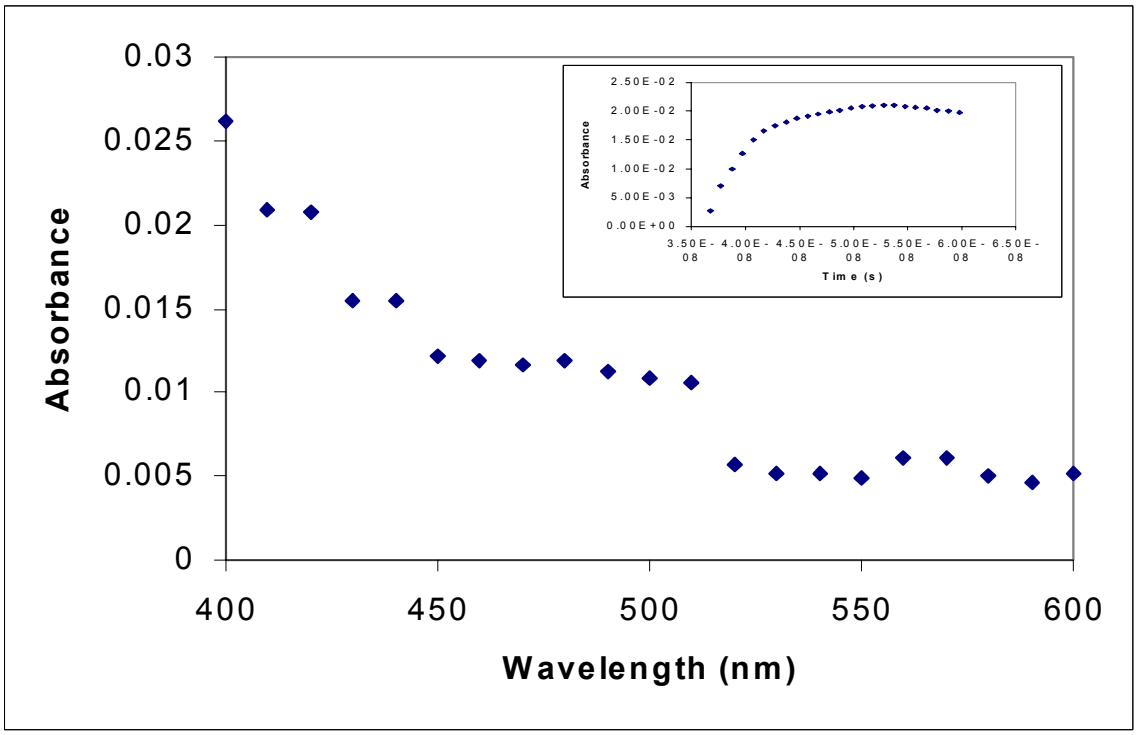

Figure 16. **Spectrum and Transient Signal for the Decay of the 5,7-Di-*tert*-butylspiro[2.5]octa-4,7-dien-6-one Radical Anion at 400 nm Generated by the Excitation of 0.005 M 5,7-Di-*tert*-butylspiro[2.5]octa-4,7-dien-6-one with 0.0003 M DMS and 0.01 M Tetrabutylammonium Azide in Acetonitrile.**

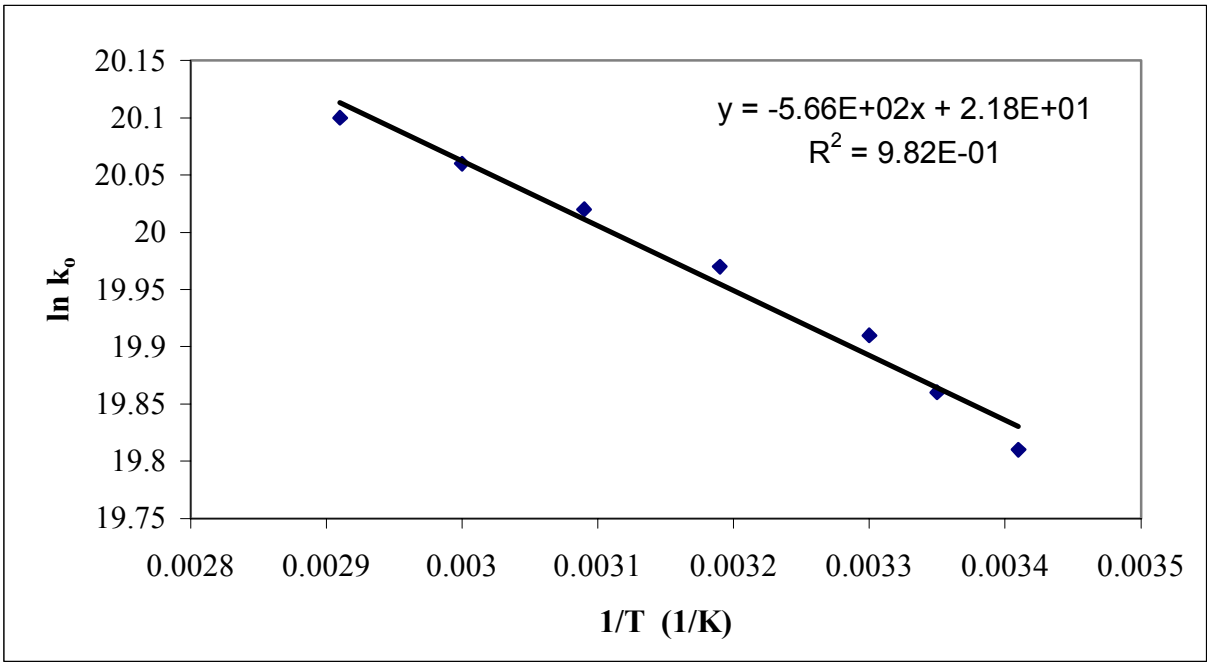

Figure 17. **Arrhenius Plot of 5,7-Di-*tert*-butylspiro[2.5]octa-4,7-dien-6-one Radical Anion Generated by the Excitation of 0.005 M 5,7-Di-*tert*-butylspiro[2.5]octa-4,7-dien-6-one with 0.0003 M DMS and 0.01 M Tetrabutylammonium Azide in Acetonitrile.**

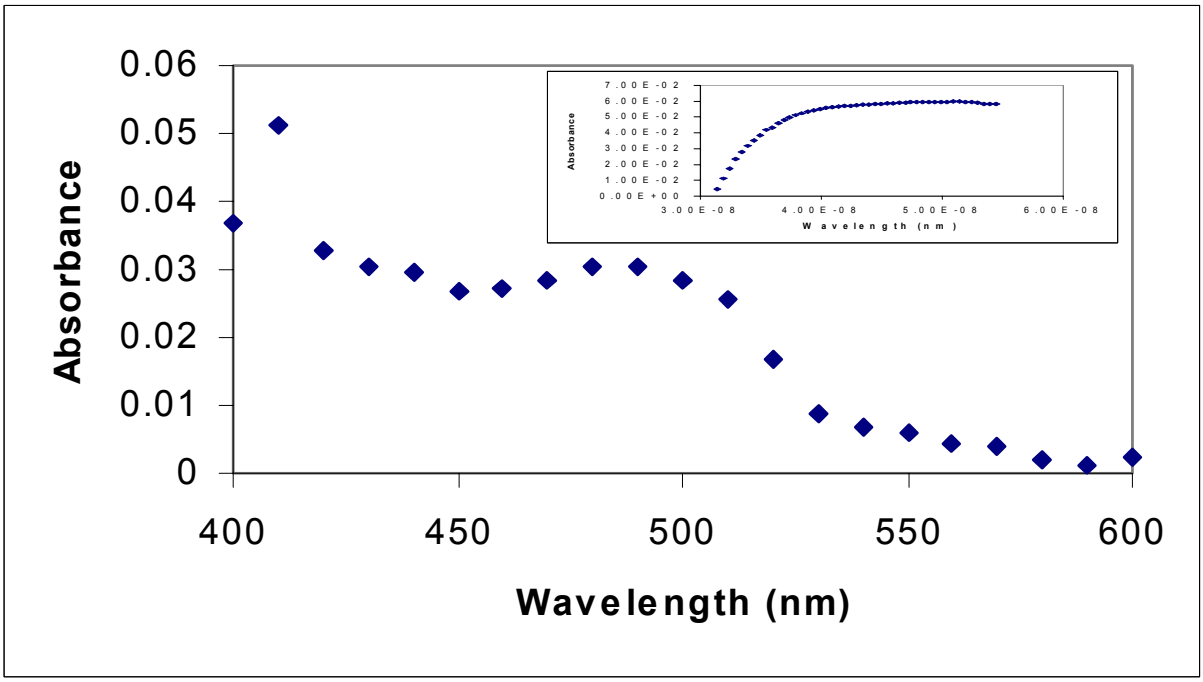

Figure 18. **Spectrum and Transient Signal for the Decay of the 1,1-dimethyl-5,7-di-*tert*-butylspiro[2.5]octa-4,7-dien-6-one Radical Anion at 410 nm Generated by the Excitation of 0.005 M 1,1-dimethyl-5,7-di-*tert*-butylspiro[2.5]octa-4,7-dien-6-one with 0.0003 M DMS and 0.01 M Tetrabutylammonium Azide in Acetonitrile.**

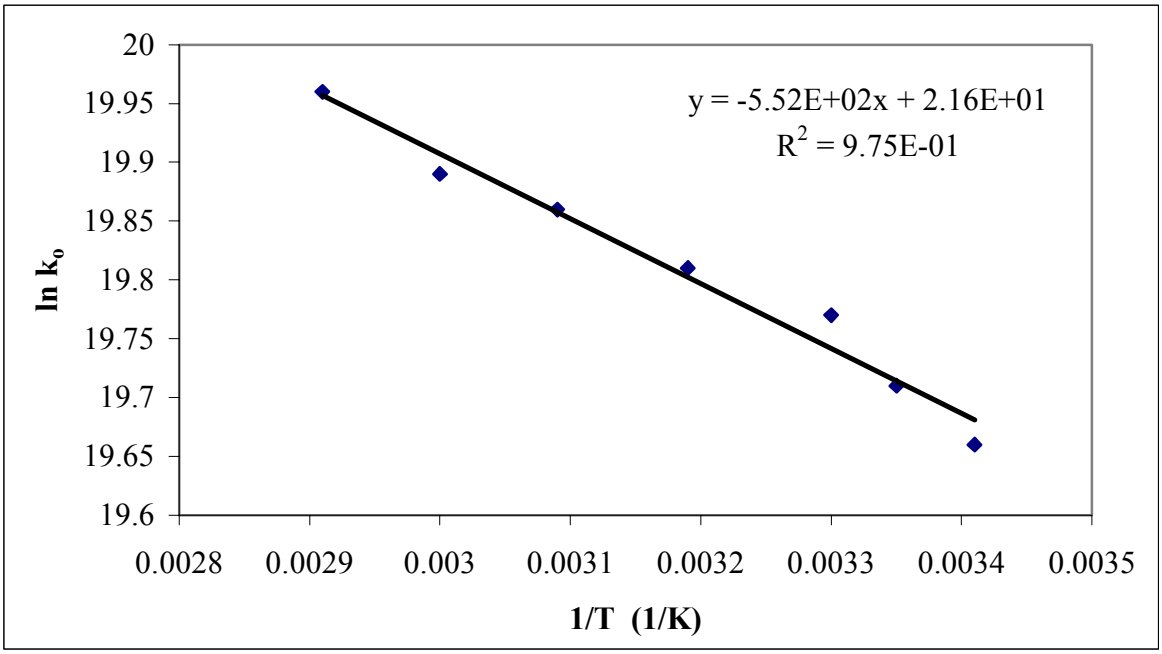

Figure 19. Arrhenius Plot of 1,1-dimethyl-5,7-di-*tert*-butylspiro[2.5]octa-4,7-dien-6-one Radical Anion Generated by the Excitation of 0.005 M 1,1-dimethyl-5,7-di-*tert*-butylspiro[2.5]octa-4,7-dien-6-one with 0.0003 M DMS and 0.01 M Tetrabutylammonium Azide in Acetonitrile

VITA

Robert Alan Friedline was born on August 8th, 1977 in Pittsburgh, Pennsylvania to Paul Alan and Donna Jean Friedline. He graduated high school from Mars Area High School in Mars, Pennsylvania in 1995. In the fall of 1995, he began his undergraduate education at Washington and Jefferson College in Washington, Pennsylvania. Plans of medical school took a slight detour during his second year and lead him down his pathway towards graduate school.

In the fall of 1999, he entered the doctoral program at Virginia Polytechnic Institute and State University where he worked in the area of physical organic chemistry under the leadership of Dr. James M. Tanko. During his years in graduate school, he taught as a general chemistry instructor for VPI and as an instructor at Radford University. He received a Doctor of Philosophy in Chemistry in May 2004 from VPI & SU. He shall commence his career working in pharmaceuticals and consumer products in the chemical industry.